CARBON CAPTURE IN METAL-ORGANIC FRAMEWORKS

Mehrdad Asgari and Wendy L. Queen

Laboratory of Functional Inorganic Materials, Ecole Polytechnique Federale de Lausanne, Sion, Switzerland

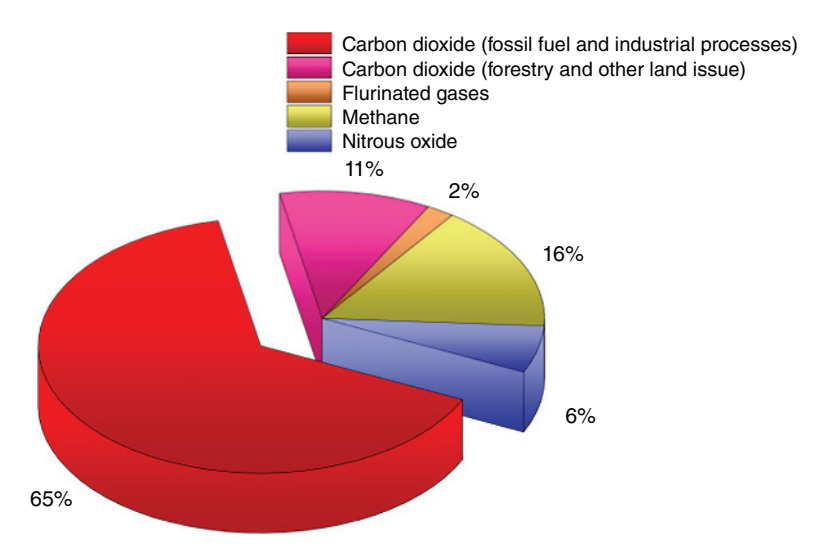
1.1 INTRODUCTION

1.1.1 The Importance of Carbon Dioxide Capture

Carbon dioxide, an important chemical gas found in the atmosphere, is critical for the continuation of life on earth. This molecule is required for photosynthesis that fuels plants, which serve as the main source of food for all humans and animals and further produce oxygen that is essential for human respiration [1]. Studies have shown that a small accumulation of CO_2 in the atmosphere is necessary to warm earth to a level where glaciation is inhibited, producing an environment where plant and animal life can thrive [2]. However, there is recent evidence that human activity related to energy production is generating an abundance of CO_2 in the atmosphere that can no longer be balanced by earth's natural cycles, an act that is expected to confront mankind with serious environmental problems in the future. Since CO_2 is the most abundantly produced greenhouse gas (Figure 1.1) [3], it is directly

Materials and Processes for CO₂ Capture, Conversion, and Sequestration, First Edition. Edited by Lan Li, Winnie Wong-Ng, Kevin Huang, and Lawrence P. Cook.

^{© 2018} The American Ceramic Society. Published 2018 by John Wiley & Sons, Inc.



<u>Figure 1.1</u> The contribution of different constituent in the greenhouse gas emission. Source: Victor et al. 2014 [3].

implemented in global warming. It is predicted that if the negligent release of CO_2 persists, it could have detrimental effects on our environment that include melting ice caps, rising sea levels, strong changes in weather patterns, ocean acidification, ozone layer depletion, poor air quality, and desertification; all of these things could lead to the potential demise of the human, plant, and animal life, making CO_2 mitigation an urgent need [4, 5].

Eighty percent of the world's energy is currently supplied by the combustion of carbon-based fossil fuels [6], an anthropogenic activity that has led to steady increase in atmospheric CO₂ levels. Since the beginning of the industrial revolution in the 1750s, atmospheric CO₂ concentration has increased from 280 ppm [7] to above 400 ppm in March 2015 [8, 9]. While the best remediation method is to transition from traditional carbon-based fuels to clean energy sources, like wind and solar, energy transitions are historically slow [9]. As such, it is projected that the use of fossil fuels will continue for years to come, requiring the development of materials that can remediate the effects of CO₂ through direct carbon capture and sequestration (CCS) and/or conversion of this greenhouse gas into value-added chemicals and fuels. While CO₂ capture directly from air is considered to be an unfeasible task, carbon capture from large point sources, such as coal- or gas-fired power plants, could be realized. Currently, 42% of the world's CO₂ emissions come from production of electricity and heat [10] and it is anticipated that approximately 80-90% of these emissions could be eliminated with the implementation of adequate CCS technology [11]. CCS is a multi-step process that includes the capture of CO₂ and its transport to sites where it is subsequently stored. While the processes of storage and transport INTRODUCTION 3

are well-developed technologies, the actual implementation of capture process on a global scale is still constrained by the development of an adequate gas separation technology. Thus, the discovery of new materials with high separation ability is a pertinent obstacle that must be overcome.

1.1.2 Conventional Industrial Process of Carbon Capture and Limitations: Liquid Amines

The most mature capture technology, which has been around since the 1930s, includes aqueous alkanolamine-based scrubbers [12]. These chemical absorbents feature an amine functionality that undergoes a nucleophilic attack on the carbon of the CO₂ molecule (Figure 1.2) to form either a carbamate (in the case of primary or secondary amines) or a bicarbonate species (in the case of tertiary amines) [13]. While amine scrubbers are highly selective in the capture of CO₂ relative to other components in a gas stream, operate well at low partial pressures, and can be readily included into existing infrastructure at power plants, they have several limitations that inhibit their implementation on scales large enough for post-combustion carbon capture [14]. The materials are quite corrosive to sources of containment requiring their dilution with water to concentrations ranging from 20 to 40 wt% of the amine [15]. The high heat capacities of the aqueous amine solutions combined with high

(a)
$$\begin{bmatrix}
O & R' \\
C & + NH
\end{bmatrix} + H_2^+N R$$

$$\begin{bmatrix}
O & R' \\
C & + NH
\end{bmatrix} + H_2^+N R$$

$$\begin{bmatrix}
O & R' \\
H_2O
\end{bmatrix} + H_1^+N R + HN R$$
(b)
$$\begin{bmatrix}
O & R' \\
H_2O
\end{bmatrix} + H_2^+N R + HN R$$

$$\begin{bmatrix}
O & R' \\
H_2O
\end{bmatrix} + H_1^+NH R$$

$$\begin{bmatrix}
O & R' \\
H_2O
\end{bmatrix} + H_1^+NH R$$

$$\begin{bmatrix}
O & R' \\
H_2O
\end{bmatrix} + H_1^+NH R$$

$$\begin{bmatrix}
O & R' \\
H_2O
\end{bmatrix} + H_2^+NH R$$

$$\begin{bmatrix}
O & R' \\
H_2O
\end{bmatrix} + H_1^+NH R$$

$$\begin{bmatrix}
O & R' \\
H_2O
\end{bmatrix} + H_1^+NH R$$

<u>Figure 1.2</u> Reaction scheme for carbon dioxide with a (a) primary, secondary, or (b) tertiary amine.

adsorption enthalpies of CO₂, approaching -100 kJ mol⁻¹, creates a large parasitic energy cost for the subsequent release of CO₂. While the strength of CO₂ binding can be tuned to some degree with amine substitution ($1^{\circ} > 2^{\circ} > 3^{\circ}$, i.e., monoethanolamine, diethanolamine, or triethanolamine) [13], the regeneration process typically requires temperatures that range from 120°C to 150°C [16–18]. The instability of the materials at these temperatures leads to a slow decomposition and hence a decrease in the materials' performance with subsequent absorption cycles. Given all of these problems, this technology, which has already been employed in hundreds of plants worldwide for CO₂ removal from natural gas, hydrogen, and other gases, requires that approximately 30% of the energy produced from a power plant be put back into the carbon-capture process [12]. It is projected that solid adsorbent materials with lower heat capacities might cut the energy consumption assumed from the current carbon-capture technology considerably [19]. For this to be realized, much further work is required to design porous solid adsorbents that show (i) high stability in the presence of various components in the gas stream, particularly water, (ii) high selectivity and adsorption capacity, (iii) low cost, (iv) reversibility, and (v) scale ability [20]. To date, there are several classes of porous adsorbents studied for applications related to carbon capture including zeolites, activated carbons, and covalent organic frameworks; however, all of these materials suffer quite significantly from a minimal adsorption capacity and/or low selectivity [19, 21–25].

1.1.3 Metal-Organic Frameworks and Their Synthesis

One materials solution to the aforementioned carbon-capture problem is a relatively new class of porous adsorbents known as metal-organic frameworks (MOFs), which are constructed by metal ions or metal-ion clusters linked together by organic ligands (Figure 1.3) [26, 27]. Since the discovery in the late 1990s that these materials can exhibit permanent porosity [28], they have rapidly moved to the forefront of materials research. Looking at publications related to carbon dioxide adsorption in MOFs, one can see a significant increase in the number since 2005, with over 500 publications in 2015 alone [29]. This is in part due to their unprecedented internal surface areas, up to 7000 m² g⁻¹ [30], which allows the adsorption of significant amount of guest species. Further, the molecular nature of the predefined organic linkers offers a modular approach to their design (Figure 1.3). Through judicious selection of the building blocks, MOF structures can be chemically tuned for a variety of environmentally relevant applications such as gas storage and separation, sensing, and catalysis [31-39]. MOFs have become particularly attractive due to recent reports of materials with high capacities and selectivities for the adsorption of various guest molecules [40, 41]. Currently, MOFs hold several world records related to small molecule adsorption that include (i) surface area [30], (ii and iii) room-temperature hydrogen [42] and methane storage [43], and (iv) carbon dioxide storage capacity [44]. The facile chemical tunability of MOFs is their primary advantage relative to other more traditional porous adsorbents such as activated carbons and zeolites. INTRODUCTION 5

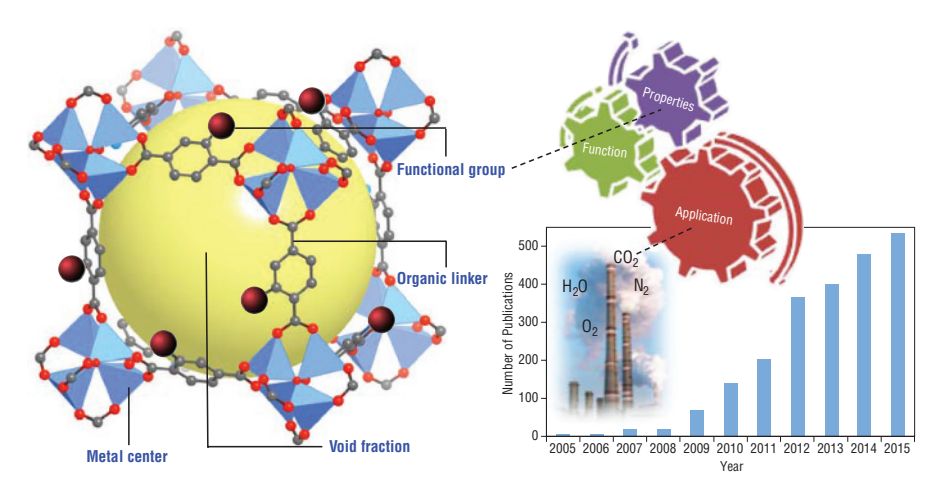


Figure 1.3 (Left) Ball-and-stick model of an MOF, MOF-5 or Zn₄O(1,4-benezendicarboxylate)₃ [27], showing the modular nature of the frameworks, which can be used to tune MOF properties for the selective binding of gas molecules, making the materials of particular interest in applications related to carbon capture. *Source:* Li et al. 1999 [27]. Reproduced with permission of Nature Publishing Group. (*Right*) The number of publications related to "CO₂ adsorption" and "metal–organic frameworks" increased significantly from 2005 to 2015. *Source:* Gallagher et al. 2016 [29]. Reproduced with permission of Royal Society of Chemistry.

Further, their highly crystalline nature combined with a non-homogenous van der Waals potential energy landscape on the internal MOF surface dictates that incoming guest molecules bind in well-defined positions and orientations; this allows diffraction techniques to be used to readily unveil their site-specific binding properties. Understanding the structure function relationship allows one to tune the properties of existing materials or rationally design new materials with specified function.

MOFs are typically synthesized using a combination of metal salts and ligands via standard hydrothermal or solvothermal methods; reactions are usually carried out inside of sealed vessels or using Schlenk line techniques with reaction times that range from hours to days. The aforementioned methodologies are typically limited to small-scale reactions, from milligram to gram size yields, making them only suitable for standard laboratory-based characterization. To reduce the energy requirements associated with these traditional procedures, recent efforts have been made to search for reaction conditions necessary to produce MOFs at room temperature; however, many of these methods involve non-aqueous solvents such as DEF, DMF, and ETOH [45]. Given this, more recent efforts have been made to develop MOF syntheses in water, an effort that makes industrial production of these materials more feasible [46, 47]. Other research has abandoned the more traditional forms of laboratory-based techniques and moved toward more innovative methods to assist

in materials scale-up; some examples of non-traditional techniques include microwave [48], mechanochemical methods [49, 50] (such as solvent-free neat grinding or extrusion), continuous flow reactions [51, 52], and spray drying [53]. Of these techniques, the highest space time yields (STY, kg per m³ per day), a process parameter that is used to determine industrial profitability, are reported for the mechanochemical extrusion methods developed by James et al.; these methods have remarkable STY values that range between 1 and 3 orders of magnitude greater than those for other methods, a result of the absence or near absence of solvent and high reaction rates. Further, it should be noted that the reported surface areas and pore volumes for the as-prepared materials are similar to those produced on small scales [50, 51]. The latter is an important note because many reports show that surface areas and CO₂ adsorption properties suffer quite significantly in the scale-up procedure [54].

While industrial scale synthesis of MOFs is currently limited to a handful of iconic frameworks, it is expected to become a developing trend as companies like BASF have shown proof of concept for the production of MOFs on large scales [55-57] using green synthetic methods (in aqueous media). These materials, targeted for applications related to on-board storage in natural gas and hydrogen powered vehicles, are currently available under the trade name Basolite® and include a few eminent frameworks such as HKUST-1 (Basolite C300 or [Cu₃(1, 3,5-benzenetricarboxylate),]), MIL-53 (Basolite A100 or [Al(OH)(1,4-benzenedicarboxylate)]), ZIF-8 (Basolite Z1200 or [Zn(2-methylimidazole)₂]), and Fe-BTC (Basolite F300 or [Fe(1,3,5-benzenetricarboxylate)]), and MOF-177 (Basolite 7377 or $Zn_4O(1,3,5$ -benzenetribenzoate)₂]) [58–60]. The most critical parameters that must be considered for the industrial scale-up of MOFs have been recently identified as the following: (i) the cost of raw material per kg of obtained MOF, (ii) the amount of MOF produced per m³ of reaction mixture per day, (iii) conditions required for reaction agitation during synthesis, (iv) length of time required and amount of solvent required for sample filtration, and (v) washing conditions necessary for drying (activating) prepared solids [61].

1.1.4 CCS Technologies and MOF Requirements

Growing energy demands related to continued population growth and the industrialization of developing countries, like China, imposes the need for the continued combustion of fossil fuels, including coal, natural gas, and oil [62, 63]. Considering that carbon capture from air is not a feasible task, capture at large point sources is certainly one of the best-case scenarios to significantly reduce global CO₂ emissions despite the tremendous effort that is required. It is projected that global reserves of coal, which has the highest carbon content and is responsible for 43% of CO₂ emissions from fuel combustion [64], will last over 110 years at the current production rate [65]. For comparison, oil reserves are projected to exist for the next 40–55 years [65–67].

Currently, there are three existing chemical processes used for the combustion of fossil fuels at large point sources such as coal and gas-fired power plants. These

INTRODUCTION 7

three processes, which include (i) post-combustion capture, (ii) pre-combustion capture, and (iii) oxy-fuel combustion capture, result in the need for a collection of separation materials capable of operating at different temperatures and pressures and offer selective adsorption for several different gas mixtures (Table 1.1). The three processes are briefly described below.

(i) Post-combustion capture at a coal-fired power plant (Figure 1.4a) involves the separation of CO₂ from flue gas (1 bar) that consists primarily of CO₂ (13–15% by volume), N₂ (73–77%), H₂O (5–7%), O₂ (3–4%), and other minor contaminates like SO_x and NO_x. Flue gas is generated after the combustion of fuel in air [78]. The high N₂ content in air lends to flue gas mixtures with low partial pressures of CO₂; as such, the selectivity for CO₂/N₂ is one of the most critical factors considered in the selection of a separation material. As in the case of the liquid amine-based scrubbers, finding a balance between CO₂ selectivity and binding affinity in MOFs

TABLE 1.1 Typical composition of gas for three carbon capture technologies

Molecules and conditions	Post-combustion ^a [23, 62, 68–73] by volume		Pre-combustion ^a [23, 74, 75] by volume		Oxyfuel ^a [76, 77] by volume
	Natural gas	Coal	Nautral gas	Coal	Air purification ^b
CO ₂	3–9%	13-15%	15-25%	26-34%	400 ppm
N_2	70–76%	73-77%	Trace	0.3 - 2.2%	78%
H_2O	7-18%	5-7%	_	18-38%	_
H_2	_	_	70-80%	35-45%	0.5 ppm
CH_4	_	_	3-6%	_	_
O_2	2-15%	3-4%	_	_	21%
H_2S	_	_	Trace	0.1 - 0.2%	_
SO_2	_	800 ppm	_	_	_
SO_3	_	10 ppm	_	_	_
HCl	_	100 ppm	_	_	_
Hg	_	1 ppb	_	_	_
CO	200-300 ppm	20-50 ppm	1-3%	0.5 - 0.6%	_
NO_x	10-300 ppm	500 ppm	_	_	0.3 ppm
Ne	_	_	_	_	18 ppm
Kr	_	_	_	_	1 ppm
Xe	_	_	_	_	0.087 ppm
Ar	_	_	_	0.04%	0.9%
Temperature	40-75°C	40-75°C	40°C	40°C	25°C
Pressure	1 bar	1 bar	5–40 bar	5–40 bar	1 atm

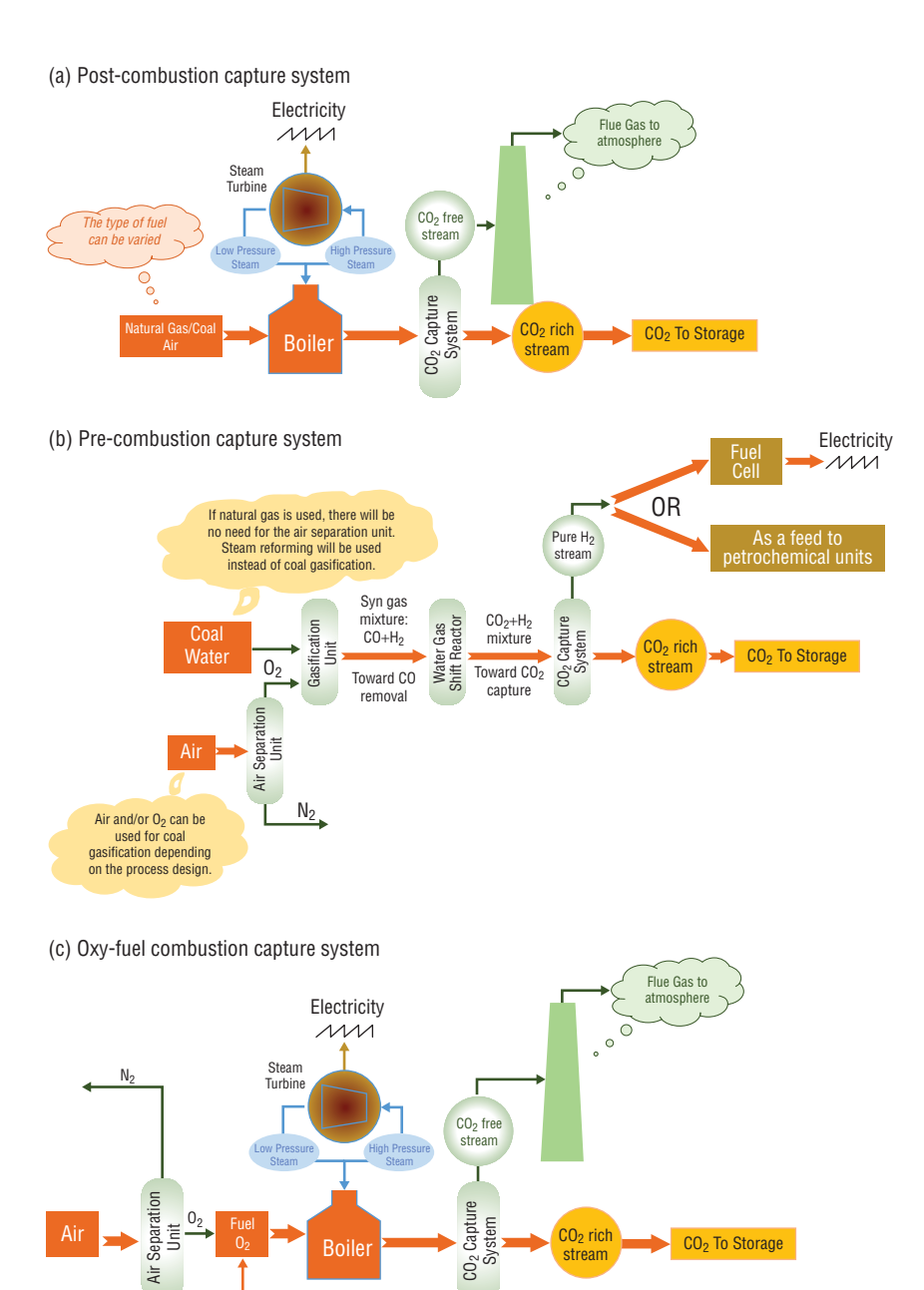
^aThe values are from some references reporting typical values for these streams. Although the values for other power plants may slightly differ from each other, they will be in the same range.

^bThis value is for the dry air.

- is necessary. Very high CO₂ binding energies on the sorbents affords high regeneration energies significantly reducing power plant efficiency [79].
- (ii) Pre-combustion capture (Figure 1.4b) involves the separation of CO₂ from H₂ prior to the combustion process and hence zero carbon emission afterward. In this process, coal undergoes gasification to produce a syngas that typically consists of CO, CO₂, H₂, and H₂O. Afterward, the syngas is reacted with steam in a process called the water-gas shift reaction to form CO_2 (26–34%), H_2 (35–45%) with small amounts CO_2 , H_2S_2 , and N_2 . It should be noted that there is also a significant amount of water present in the flue gas stream after the water-gas shift reaction. However, much of the water could be removed using existing technologies. From this point, the separation is carried out to remove CO₂ producing a nearly pure H₂ fuel that is then combusted to form water. This separation is significantly easier, relative to post-combustion capture, due to the higher partial pressures and concentrations of CO₂, approximately 5–40 bar and up to 34% CO₂, respectively, making the consideration for the separation medium a bit more versatile to include solid adsorbents, liquid absorbents, and membranes [80, 81].
- (iii) As the final alternative, rather than using air for the combustion of fossil fuels, oxy-fuel combustion (Figure 1.4c) involves a separation of O₂ from air before the combustion process. Post-separation this technology involves a nearly pure feed of O₂ (purity usually >95%) that is then used in the combustion step, eliminating the need for the separation of CO₂ and N₂ later. The problems with this separation is that it is currently limited to energetically unfavorable distillation as most adsorbents designed to date, such as lithium-containing zeolites, only show limited selectivity of N₂ over O₂ giving rise to gas mixtures with inadequate purity levels [82]. After combustion, the final gas mixture has CO₂ (72–85%) with some amount of water (6–7%) that can easily be condensed giving rise to CO₂ capture rates higher than 95%, a feat not yet achieved by pre-combustion and postcombustion capture separations. Compared with aforementioned processes utilizing N₂-rich air for combustion, the formation of NO_x is largely inhibited due to the initial removal of N₂; this will allow for a significantly smaller NO_x removal than in typical power plants.

For the aforementioned carbon-capture cases, there are three potential processes for regeneration after adsorbent bed saturation including (i) temperature swing adsorption (TSA), pressure swing adsorption (PSA), and vacuum swing adsorption (VSA). TSA is a process where the temperature of the bed will be increased (likely using heat from the power plant) post saturation allowing desorption of the small molecules from the surface of the adsorbent. The resulting pressure increase drives the adsorbate out of the bed, and once no further desorption is observed at the target temperature, a purge gas can additionally be run through the bed to push out

INTRODUCTION 9



<u>Figure 1.4</u> Schemes for the three different carbon capture technologies including (a) post-combustion capture, (b) pre-combustion capture, and (c) oxy-fuel combustion capture.

additional adsorbate. Subsequently, the bed can be cooled and additional adsorption cycles can be run. On the other hand, PSA and VSA processes entail lowering the pressure from which adsorption takes place to permit removal of the surface-bound guests. For PSA, the inlet valve, where high-pressure gas is allowed to flow into the bed, is simply closed allowing the pressure inside the bed to approach atmospheric pressure. Albeit similar, VSA entails lowering the bed pressure below atmospheric. The low partial pressure of CO₂ in post-combustion capture makes TSA the most plausible method for bed regeneration, as it would be energetically unfeasible to expand the bed or pull vacuum on such a large volume of gas. Considering precombustion capture involves high-pressure flue gas, it is much more feasible to employ PSA for the regeneration method.

Considering the parameters for these capture technologies and their subsequent regeneration methods are not easily modified, it is necessary to design adsorbents with all of these parameters in mind. As MOFs are the most chemically tunable adsorbent available, they offer unmatched opportunity to find the necessary balance between various parameters such as binding energies and densities of adsorption sites, capacities, and selectivities, which influence the ability to achieve high working capacities and low regeneration energies. The final decision related to which adsorbent should be applied to the carbon-capture process should be taken after a detailed evaluation of the technical performance and assessment of economic feasibility. Such an evaluation is imperative for implementation of carbon-capture processes on a global scale.

1.1.5 Molecule Specific

The elevated temperature at which carbon capture is carried out, combined with low boiling points (Table 1.2) of many of the small molecules in flue gas and air, makes cryogenic distillations, carried out on scales large enough for CCS, energetically unfeasible; hence, large energy savings could be realized with the use of solid adsorbents that function at much higher temperatures. When working to design adsorbent materials capable of separating gases, one must first consider the differences in the physical properties of the molecules of interest. The similarities in the kinetic diameters for most of the molecules in flue gas or air make separations dependent on size exclusion difficult; this makes thermodynamic-based separations that are dictated by the nature of the adsorptive interactions between the guest molecules and internal framework surface more feasible. For physisorptive-type interactions, the separation process relies on guest molecules having small disparities in their physical properties that include polarizability, quadrupole moment, and dipole moment. For most of the components in flue gas and air, the values for these aforementioned physical properties are listed in Table 1.2. While some important differences exist for instance between CO₂ and N₂, regarding the nature of their intermolecular interactions and their chemical reactivity, these differences are minimal and necessitate the careful design of carbon-capture materials that exhibit strong, molecule-specific chemical interactions on their internal surface.

Molecules	Normal boiling point (K)	Kinetic diameter ^a [62]	Quadrapole moment ^a [62]	Dipole moment ^b	Polarizability ^c [40]
CO_2	216.55	3.3	43.0	0	29.1
N_2	77.35	3.64	15.2	0	17.4
H_2O	373.15	2.64	_	18.5	14.5
H_2	20.27	2.89	6.62	0	8.04
CH_4	111.66	3.76	0	0	25.9
O_2	90.17	3.46	3.9	0	15.8
H_2S	212.84	3.62	_	9.78	37.8
SO_2	263.13	4.11	_	16.3	37.2
HCl	188.15	3.34	38.0	11.1	26.3
CO	81.66	3.69	25.0	1.1	19.5
NO	121.38	3.49	_	1.59	17.0
NO_2	302.22			3.16	30.2
Ne	27.07	2.82	0	0	3.96
Kr	119.74	3.66	0	0	24.8
Xe	165.01	4.05	0	0	40.4
Ar	87.27	3.54	0	0	16.4

TABLE 1.2 Chemical properties of small molecules involved in carbon capture

1.2 UNDERSTANDING THE ADSORPTION PROPERTIES OF MOFS

There are a variety of techniques used to assess MOFs for CO₂ capture applications. These include single-component adsorption isotherms, breakthrough analysis, multicomponent adsorption and a host of *in situ* techniques. Several studies have shown that pairing many characterization methods, particularly adsorption, with *in situ* characterization can provide molecular-level insight into the adsorption process giving direct evidence of the structural components that give rise to enhanced or diminished properties [83]. There is hope that in-depth experimental efforts like these can provide the insight necessary for the eventual deliberate design of new MOF for energetically favorable carbon-capture technologies.

1.2.1 Single-Component Isotherms

Nitrogen adsorption isotherms, collected at 77 K and up to 1 bar, are typically used to first assess the pore volume, pore size distribution and surface area of as-prepared MOF materials. Subsequently, adsorption isotherms can also be used to further assess a materials performance related to carbon-capture processes. For this, the isotherms are collected using carbon dioxide (or other small molecules) as probes. These experiments are typically carried out using commercially available equipment

^aThe numbers are expressed with the following unit: 10⁻²⁷ esu⁻¹ cm⁻¹.

^bThe numbers are expressed with the following unit: 10⁻¹⁹ esu⁻¹ cm⁻¹.

^cThe numbers are expressed with the following unit: 10⁻²⁵ cm³.

at temperatures ranging from 25°C to 40°C and from low pressures up to 50 bar. It should be noted that these measurements provide insight into a materials (i) adsorption capacity, (ii) selectivity, and (iii) enthalpy of adsorption [84]. These three metrics will be briefly discussed below.

1.2.1.1 Adsorption **Capacity** Adsorption capacity expressed gravimetrically or volumetrically as the amount of adsorbed CO₂ per unit volume or mass of adsorbent, respectively. While reports of gravimetric capacity are more predominate throughout the literature, it is equally important to look at the volumetric properties of materials as it dictates the required volume of the adsorbent bed and both parameters also influence the efficiency with which the materials can be regenerated. It was recently shown that MOF-177, a high surface area adsorbent (BET surface area >4500 m² per gram of adsorbent), exhibits a volumetric capacity at room temperature and 35 bar of 320 cm³ (STP) per cm³, a value that is over nine times larger than the quantity of CO₂ that can be stored in the same empty container without the MOF [85]. More often than not, high surface areas lend to high capacities in the high-pressure regime, while low-pressure adsorption measurements <1 bar are more strongly impacted by the strength and density of the binding sites (Figure 1.5). It should be noted that high-pressure CO₂ adsorption isotherms are important for pre-combustion capture while low-pressure, typically not higher than 1 bar, are more relevant for post-combustion capture.

1.2.1.2 Small Molecule Selectivity Selectivity can be kinetic in nature, based on size exclusion of molecules of varying size, or thermodynamic in nature, based on significant differences in interaction energies on the internal MOF surface. It can be seen from Table 1.2 that the kinetic diameters of the small molecules of interest for carbon capture, CO₂/N₂, CO₂/H₂, and O₂/N₂, are all less than 4 Å. Considering these issues and that MOF pore sizes are more often than not above 4 Å, kinetic-based selectivities become problematic. Instead, the gas separations are based on thermodynamics. Therefore, chemists must take other physical and chemical characteristics into consideration when designing separation materials.

The selectivity factor (S), is simply calculated using the following equation (1.1), where q represents the amount adsorbed of each gas and p represents the partial pressure of each gas. While this factor is a good way to compare different materials, it is not real selectivity because it is calculated from single-component isotherms where the gas molecules are not actually competing for adsorption sites.

$$S = \frac{q_1/q_2}{p_1/p_2} \tag{1.1}$$

Another method commonly used for predicting selectivities from single-component isotherms is using the ideal adsorbed solution theory (IAST) developed by Meyers and Prausnitz [86]. For this method, single-component isotherms are

used to predict the adsorption equilibria for gas mixtures. The adsorption isotherms are collected for two gases at the relevant temperature and they are mathematically fit to extract the mole fraction of each species in the adsorbed phase. While the method is not extensively reviewed here, it is becoming more visible throughout MOF literature due to the difficulty in acquiring multicomponent adsorption isotherms [87]. The validity of IAST estimations for the systems of CO₂/CH₄, CO₂/ H₂, CH₄/H₂, and CO₂/N₂ mixtures in a variety of MOFs (MgMOF-74, MOF-177, and BTP-COF) and zeolites (FAU, LTA, MFI, and CHA) has been established in literature [88–91]. While it is true that IAST theory can be utilized in many cases to give a relatively accurate estimation of the selectivity of different compounds relative to each other, there are some cases where the accuracy of estimated selectivities is questionable. A recent study of Cessford et al. investigated the applicability of IAST to a variety of MOFs with varying structural features and also to a variety of small molecules with differing sizes, shapes, and polarities. The results, which were directly compared with GCMC (grand canonical Monte Carlo) simulations, showed that IAST has difficulty in predicting accurate selectivities when the adsorbates have large differences in size and shape or the MOF framework exhibits heterogeneities such as large variations in cavities or pore sizes [92].

1.2.1.3 Isosteric Heat of Adsorption Isosteric heat of adsorption $(-Q_{\rm st})$ is an important parameter that gives an indication of the affinity of an MOF toward a specific small molecule. Often defined as the average enthalpy of adsorption at constant coverage, it can give further insight into the energy required for the molecule's subsequent release, a crucial point to be considered for lowering the overall energy consumption in carbon-capture processes. Although a high isosteric heat implies stronger binding of the guest molecule to the surface, large values also indicate a larger amount of energy for the subsequent release of the guest molecule upon regeneration of the adsorbent. And so, chemists are constantly striving to find a balance where a small molecule binds strong (and selectively) enough to give large amounts of high purity gas after the separation, but weak enough so that the materials can be easily regenerated.

To calculate the isosteric heat, first single-component adsorption isotherms are collected for at least two temperatures (or more) usually within 10 to 15 K of one another. These isotherms are then fit using a high order polynomial or other more physically meaningful mathematical models such as the single or dual site Langmuir model to formulate an expression representative of the adsorption isotherm [93, 94]. Then the ($\ln P$) is plotted as a function of 1/T.

$$(\ln P)_N = -(Q_{st}/R)(1/T) + C$$
 (1.2)

From the Claussius Clapeyron [95] equation (1.2) (where P = pressure, R = universal gas constant, T = temperature, and C = a constant), the isosteric heat of adsorption can be determined.

Another mathematical model for determining the isosteric heat is using a virial-type equation (1.3) shown below, which is first used to again model the adsorption isotherm. Afterward, the isosteric heat can be extracted using equation (1.4) [95].

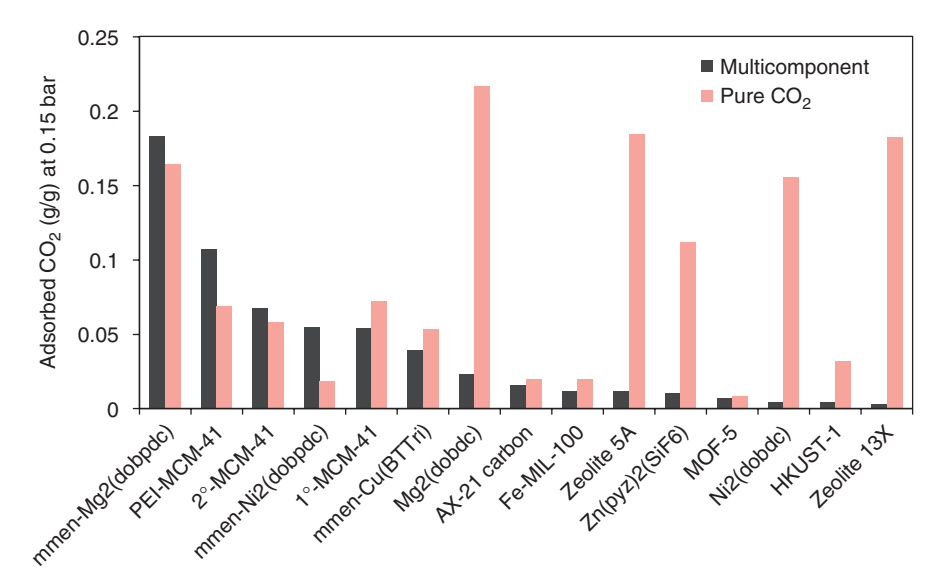
$$\ln P = \ln(n) + (1/T) \sum_{i=0}^{m} a_i n^i + \sum_{i=0}^{k} b_j n^i$$
 (1.3)

$$Q_{\rm st} = -R \sum_{i=0}^{m} a_i n^i \tag{1.4}$$

The biggest advantage of this mathematical model lies in the fact that the isosteric heat can be obtained by the direct derivation of the equation (1.3). However, it should be noted that the dual site Langmuir model is particularly good for accurately fitting data that have a combination of both strong and weak adsorption sites. Without a proper fit to the adsorption isotherm, which meaningfully models the physics of the adsorption of interest, inaccurate determination of isosteric heats will likely be the result. This is apparent throughout the literature where the same MOF can have markedly different reported values for isosteric heats. A few examples include HKUST-1 whose isosteric heats range from 15 to 35 kJ mol⁻¹ [96, 97] and Mg₂(dobdc) whose isosteric heats range from 39 to 47 kJ mol⁻¹ [98, 99]. This inconsistency in reported results could be related to improper activations, varied sample quality, or issues regarding the method chosen to determine the low-coverage isosteric heat. In these cases, theory capable of accurately determining enthalpies of adsorption can be quite useful for experimentalists to gauge the quality of their results [83].

1.2.2 Multicomponent Adsorption

A more realistic, yet somewhat experimentally intractable method to assess the performance of a material for carbon-capture applications is through multicomponent adsorption isotherms. While single-component isotherms are readily accessible using commercially available equipment, multicomponent adsorption measurements are time-consuming, require customized equipment, and pose challenges regarding data analysis. Binary adsorption measurements in MOFs were first carried out in 2009 by Férey et al. [100] who measured the co-adsorption in a mixture of CO₂/CH₄ in a flexible framework known as MIL-53(Cr) [101] (also known as Cr(OH)(1,4-BDC) where 1,4-BDC = 1,4-benzenedicarboxylate, MIL = Material des Instituts Lavoisier). Since this time, other studies have been limited to a few other systems [102] exposed to binary mixtures and none of these reports assess CO_2/N_2 mixtures. However, in 2015, Mason et al. reported multicomponent adsorption carried out in ternary mixtures of CO₂/N₂/H₂O at temperatures of 298 and 313 K in 15 iconic frameworks that include MOFs, zeolites, activated carbons, and mesoporous silica [87]. The amount of CO₂ adsorbed in these materials in the CO₂/N₂/H₂O mixtures at 40°C can be seen in Figure 1.5. This gas mixture was meant to assess materials performance in a mixture of the main components found in post-combustion flue gas. It can be seen that the amount of CO₂ adsorbed in the single (pure)-component



<u>Figure 1.5</u> Comparison of CO_2 adsorption in 15 different framework materials in a single-component isotherm, (pure CO_2) or a multicomponent mixture consisting of CO_2 , N_2 , and H_2O . Experiments were carried out at 40°C and at equilibrium. The pressures for the multicomponent mixture include N_2 between 0.679 and 0.698 bar, CO_2 between 0.113 and 0.178, and H_2O between 0.01 and 0.029 bar with the total pressures ranging from 0.821 to 0.890 bar. For the equilibrium pressure, refer to Reference [87]. *Source:* Mason et al. 2015 [87]. Reproduced with permission of American Chemical Society.

isotherms varies quite significantly from the multicomponent measurements, likely due to water competing for CO_2 adsorption sites in the series of materials. For these measurements, Mason et al. used a custom built high-throughput analyzer capable of measuring 28 different samples and as many as 8 different gases including $\mathrm{H}_2\mathrm{O}$. This instrument is the first reported to be capable of performing high-throughput multicomponent adsorption measurements at equilibrium [87].

1.2.3 Experimental Breakthrough

Considering post-combustion capture will consist of flue gas flowing through a packed bed of adsorbent, breakthrough measurements are a good way to prove the feasibility of MOFs' performance in more application-relevant environments. A typical breakthrough apparatus consists of a gas mixing system, a column where the sample is packed, and a detector, which usually consists of a gas chromatograph and/or mass spectrometer. A known gas mixture is flowed through the fixed adsorbent bed and the detector is used to monitor the downstream gas composition as a function of time. As the gas flows through the bed, certain components in the gas stream will break through the bed at different times. The idea is that the gases with the lowest affinity for the MOF surface passes through the bed more rapidly. As

such, from a practical point of view, the best adsorbent is the one that exhibits a long breakthrough time for the small molecule of interest, while exhibiting a short breakthrough time for the other components in the gas stream. In this case, the adsorption bed will have longevity, passing undesired gases through very quickly, while capturing the component of interest. At some point, once the adsorbent bed becomes saturated with the targeted molecule, the composition of the effluent downstream will match the initial composition of the gas feed.

Typically, breakthrough experiments are carried out at room temperature and slightly above [103, 104]. Thus far in the MOF literature, several MOFs have been studied in multicomponent streams, such as CO₂/N₂ [105], CO₂/N₂/H₂O [106–108], CO₂/H₂O [109], and CO₂/N₂/O₂ [110]. Most of the reported studies are only relevant to post-combustion carbon capture or natural gas sweetening applications. While breakthrough experiments are relatively straightforward, due to variations in the MOF particle size, the density of the packed bed, and flow rates of the gas mixture, there are often difficulties in using this method to get an accurate comparison between different materials. As such, breakthrough curves are often instead simulated [111].

1.2.4 In Situ Characterization

As in the case of carbon capture, most practical applications for MOFs are reliant on interactions with guest species. Knowing the nature of these interactions is essential to interpret the properties of existing frameworks, and this knowledge can be used to inform the design of new materials with specified function. As such, a number of in situ techniques including single-crystal and powder diffraction [63, 112, 113], infrared spectroscopy (IR) [114], Raman spectroscopy [115, 116], nuclear magnetic resonance (NMR) [117-119], X-ray absorption spectroscopy (XAS) [120], inelastic neutron scattering (INS) [93, 121–123], and quasielesctic neutron scattering (QENS) [124, 125] have been employed to investigate the static and dynamic properties of various small molecules in MOFs. These techniques can be used to provide pertinent information on how and where guest molecules bind, on the nature of the electronic environment around the adsorption site, and also how the molecules move throughout the material. As an example, a powder X-ray diffraction cell and single-crystal X-ray diffraction cells are shown in Figures 1.6 and 1.7. For most in situ experiments, customized gas cells are integrated with a gas-dosing manifold that is able to deliver a predetermined amount of gas to an activated sample, which is then heated or cooled to the temperature regime of interest. For measurements focused on obtaining static structural information, usually temperatures below 100 K are used in order to eliminate dynamic disorder associated with the surface-bound molecules. For spectroscopic measurements used to unveil dynamic properties like diffusion, researchers typically work at higher temperatures where these dynamic modes are activated [118]. Recent work has also focused on studying materials under more application-relevant environments at higher pressures and temperatures and many of these studies are intent on unveiling information related to mechanical stability or framework flexibility [126].

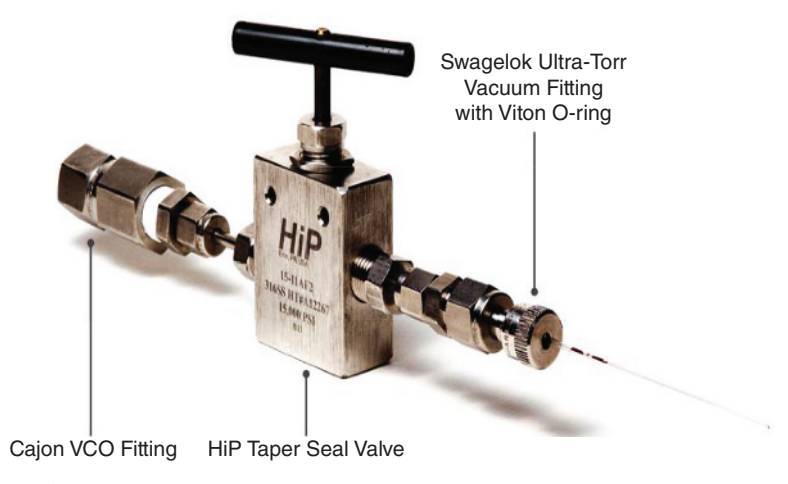
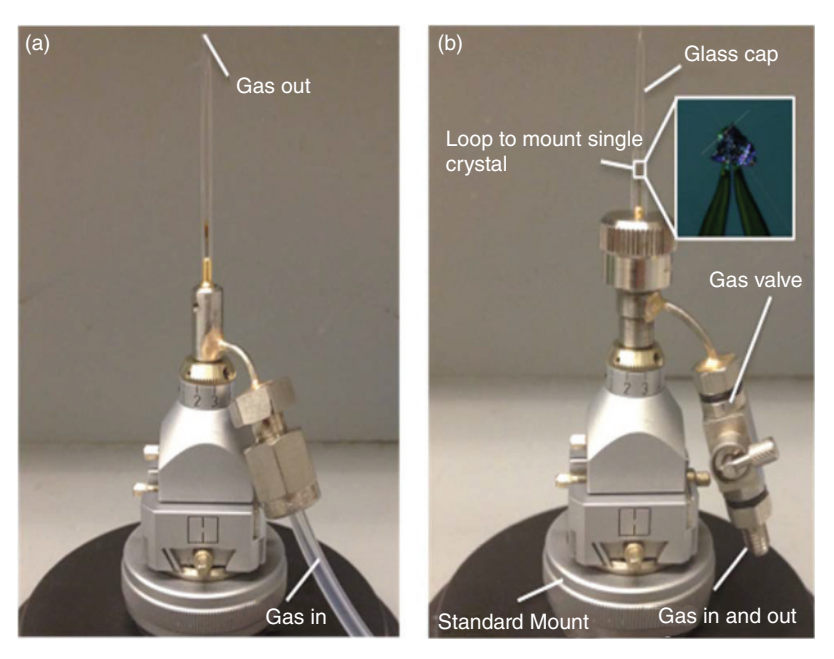


Figure 1.6 Custom built *in situ* gas cell used for synchrotron powder X-ray diffraction.

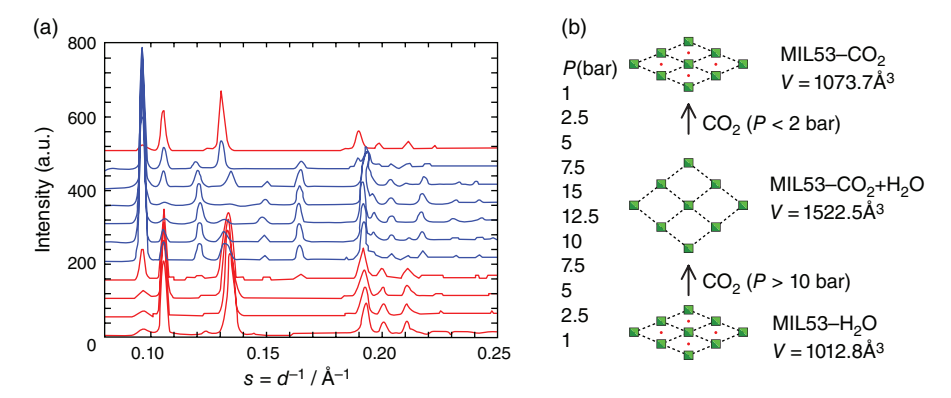
The most predominate forms of characterization throughout the MOF literature are briefly reviewed in sections 1.2.4.1 and 1.2.4.2. While all of these techniques have their limitations, when combined, they can provide a complete experimental picture of the adsorption process and its effect on the structure of the materials.



<u>Figure 1.7</u> A customized gas cell designed for Single-crystal X-Ray Diffraction (SXRD). The cells can be used for (a) flow through or (b) gas dosing.

1.2.4.1 Crystallographic Techniques Due to their crystalline nature, MOFs have a non-homogeneous van der Waals potential energy landscape that dictates how incoming guest molecules arrange themselves on the internal framework surface. This makes diffraction the most direct way to probe static site-specific binding properties of MOFs, and it is a particularly powerful tool when paired with adsorption isotherms. In addition to providing the location and orientation of surface-bound guest species, diffraction techniques can be used to unveil a host of information such as the relative difference in binding energy between neighboring adsorption sites. The latter is done through sequential dosing-type experiments, where diffraction data are collected after the sample has been dosed with increasing amounts of gas, allowing one to see an increasing number of sites populated with higher gas doses. Of course, this information is gained under the assumption that sites with the strongest binding energy are populated first. Further, diffraction is used to probe the structural response of materials under more application-relevant environments with varying pressures and temperatures that are required for various gas storage and separation applications, providing information on the framework flexibility and mechanical stability [127]. Last, this technique can provide valuable insight in the nature of host–guest interactions [128]. While most MOFs are dominated by weak van der Waals interactions and typically exhibit host-guest distances above 3 Å, many reports have shown that the presence of highly reactive, electron-deficient open metal coordination sites (OMCs) can create strong electrostatic-type interactions with small guest molecules; these are often depicted by shorter framework-guest distances ranging from 2.0 to 3.0 Å. In some instances, there are much stronger chemisorptive-type interactions where there is charge transfer between the MOF and guest species, lending to structural changes at the adsorption site and/or small molecule [82]. For chemisorptive interactions, diffraction data usually reveal very short distances between the host framework and guest species. Further, when compared to those of the unbound species, small molecule activation can give rise to significant changes in bond distances and/or angles that can easily be seen in diffraction data [82]. All of this information cannot easily be determined from in situ spectroscopic techniques, which do not easily provide a direct visualization of surface-bound guest species. Crystallographic investigations of a variety of small molecules, such as CO [129], N₂ [82], CO₂ [63, 113, 130, 131], H₂O [132], O₂ [82, 133, 134], NO [135], and H₂ [133, 136, 137], have been carried out for a number of MOFs of interest for carbon-capture applications.

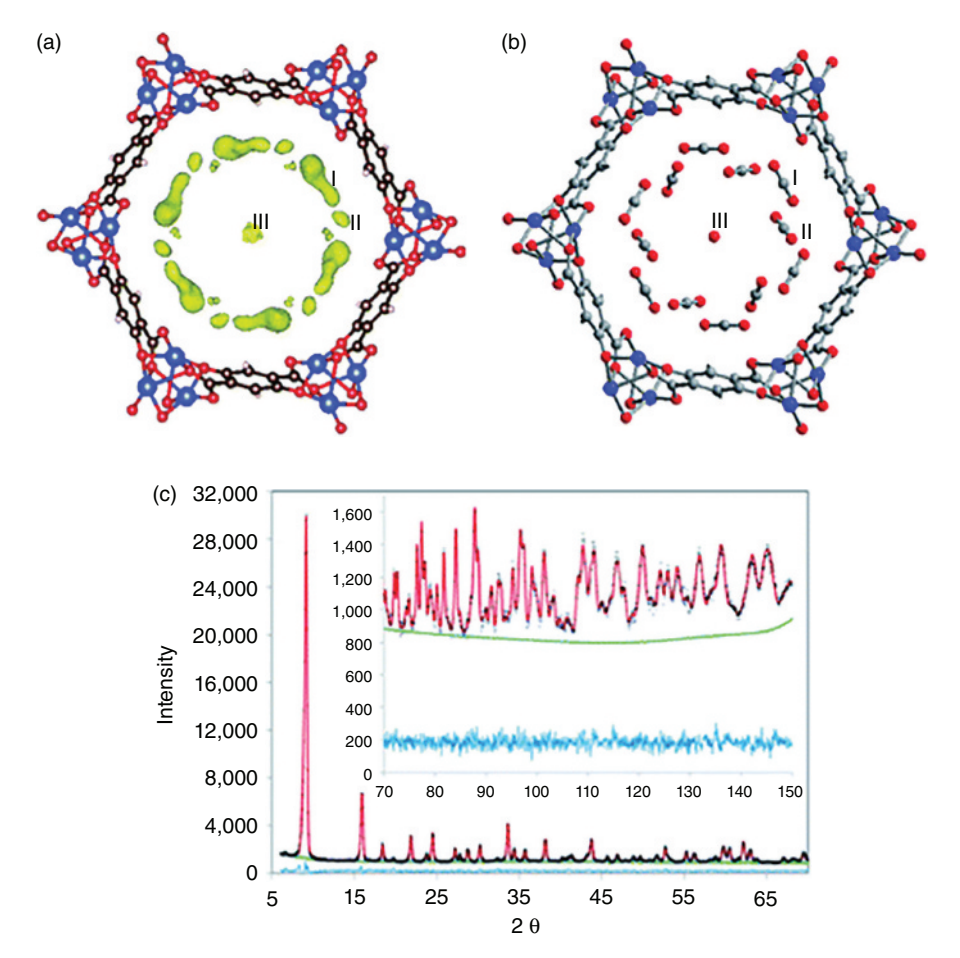
One of the first crystallographic studies of CO₂ adsorption in an MOF was carried out on a breathing framework known as Cr-MIL-53 [101] that is made up of Cr(III)O₆ nodes with 1,4-benzodicarboxylic acid struts. The framework pores undergo expansion and compression as a function of changing pressure. *In situ* powder diffraction carried out on the hydrated-MIL-53 under various CO₂ pressures was used to understand the structural evolution (Figure 1.8a) [131, 138]. Prior to the introduction of CO₂, the material exhibits a narrow pore phase [139], which is maintained up to a pressure of approximately 5 bar, where there is co-existence of both a narrow pore and large pore phase. At 15 bar, there is complete conversion to the



<u>Figure 1.8</u> (a) The illustration of structural change of hydrated MIL-53(Cr) unveiled using *in situ* X-ray powder diffraction carried out as a function of CO₂ pressure. (b) Schematic diagram of corresponding breathing behavior of MIL-53(Cr) as a function of pressure. *Source:* Llewellyn et al. 2006 [140]. Reproduced with permission of John Wiley & Sons.

large pore phase (Figure 1.8b). In this structural transition, the unit cell increases by over 30% from 1012.8 Å³ for the hydrated analog to 1522.5 Å³ after CO_2 loading. While the narrow pore material adsorbs minimal CO_2 , the structural phase transition opens up a significant amount of accessible surface area depicted as a step in the CO_2 adsorption isotherm [140].

Most crystallographic reports in the MOF literature include either neutron or X-ray powder diffraction [141, 142], while only a few studies have used single-crystal methods [63]. Although the data obtained by single-crystal diffraction are more complete and hence can give more structural detail, the technical aspects of the experiment is more difficult. MOF single crystals often experience a decrease in the quality with sample activation. There are also inherent limitations in MOF chemistry, due to weak coordination-type bonding that renders metal-ligand interactions quite labile, which can inhibit the growth of sizeable single crystals for structural analysis. Hence, there is a bottleneck in the field related to isolating the reactions conditions necessary for single crystal growth. Further, due to the extremely small sample size, very minor leaks in gas dosing equipment can cause contamination and hence problems in the final data refinement. This is particularly a problem for MOFs with OMCs, which typically bind water relatively strong compared to CO₂ and other small molecules of interest for postcombustion carbon capture. As such, in situ neutron or synchrotron X-ray powder diffraction, which requires significantly larger samples sizes (gram or milligram scale for neutrons an X-rays, respectively), is more straightforward. For powder neutron or X-ray experiments, activated samples are loaded into either a vanadium sample can or glass/ kapton capillary (Figure 1.6). After data collection, Fourier difference analysis, followed by subsequent Rietveld refinement is used to elucidate CO₂ locations and orientations (Figure 1.9a) [63]. Figure 1.9b shows three adsorption sites identified in $Cu_2(dobdc)$ (dobdc⁴⁻ = 2,5-dioxido-1,4-benzenedicarboxylate) with site I bound at the OMC as determined by neutron powder diffraction. The plot of the diffraction data (Figure 1.9c) shows an excellent match with the final structural model [63].



<u>Figure 1.9</u> (a) Fourier difference map revealing excess scattering density in Cu₂(dobdc) that results from CO₂ adsorption in the framework channel. (b) A ball-and-stick model of the finalized structure of Cu₂(dobdc) showing three CO₂ adsorption sites (determined from Rietveld analysis). (c) NPD data from Cu₂(dobdc) (10 K) after dosing with 0.5 CO₂ per Cu²⁺. The green line, crosses, and red line represent the background, experimental, and calculated diffraction patterns, respectively. The blue line represents the difference between experimental and calculated patterns. *Source:* Queen et al. 2014 [63]. Reproduced with permission of Royal Society of Chemistry.

While crystallographic tools have been used in the characterization of a number of MOF systems, there are also a few limitations to be considered. The time and position averaged diffraction data can suffer from static or dynamic disorder that inhibits the elucidation of fine structural detail associated with small molecule bond distances and angles [63]. Further crystallographic problems can arise due to poor crystalline quality and improper sample handling or activation.

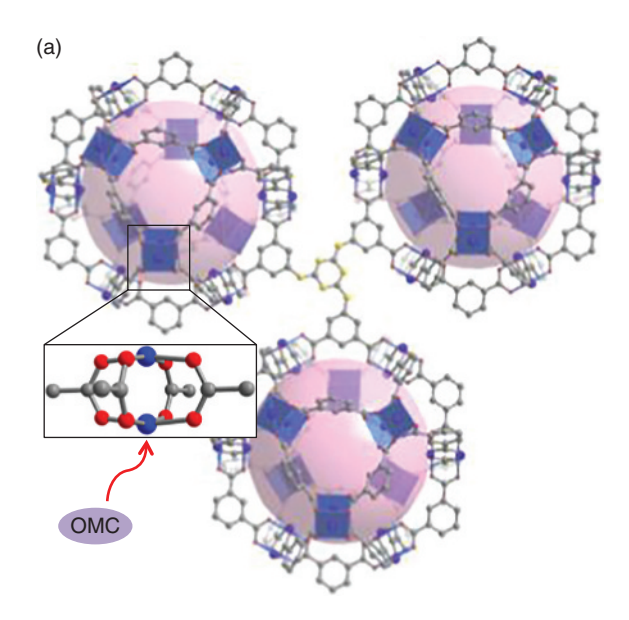
1.2.4.2 Spectroscopic Techniques

IR, RAMAN, AND INS While PXRD can be used to probe the static structure of materials, IR, Raman, and INS are often used to look at local vibrations and rotations of guest species throughout MOF materials. These spectroscopic tools are highly sensitive to molecular interactions in the frameworks. As such, they can also be used to indirectly probe binding configurations, binding enthalpies, and loading levels. However, this information is usually extracted from peak shifts, broadening, or intensities and so interpretation should proceed with caution. There are many false assumptions throughout the literature that peak shifts, which are very sensitive to the coordination environment around the adsorption site, are directly correlated with the adsorption enthalpy. Last, the integrated spectral intensities are often assumed to correlate with loading level. While this can hold true in some instances, sometimes intermolecular interactions can strongly influence the peak intensities as highlighted in a recent study $\rm H_2$ adsorption in $\rm Mg_2(dobdc)$, which was published by Nijem et al. [143]. They found that high $\rm H_2$ loadings resulted in a counterintuitive decrease in IR intensity due to a decrease in the effective charge of $\rm H_2$ at the OMC.

There are three vibrational modes associated with CO₂, the asymmetric stretching mode, $v_3 = 2349 \text{ cm}^{-1}$ and bending $v_2 = 667 \text{ cm}^{-1}$, mode are IR-active, while the symmetric stretching mode, $v_1 = 1388 \text{ cm}^{-1}$, is IR-inactive [144, 145]. If there is significant polarization of the surface-bound molecules, as in the case of OMCs, the IR-active modes offer a way to probe the nature of the CO₂ framework interaction. Dietzel et al. carried out one of the earliest in situ IR studies on Ni₂(dobdc) framework to unveil the nature of the CO₂ interaction with the Ni²⁺-OMC [113]. They observed several bands associated with the CO2 adsorption that were assigned to the CO₂ in an end-on orientation at the OMC, an observation that agreed well with in situ diffraction experiments. The v^3 mode was slightly red shifted by 8 cm⁻¹ with respect to the gas phase, a result of the charge transfer between the lone-pair of electrons on the CO₂ to the OMC. They additionally observed a combination mode of ν_3 + $\nu_{\text{M-O}}$, where $\nu_{\text{M-O}}$ is the stretching mode of the Ni²⁺-(O)CO₂ adduct. The position of ν_{M-O} was determined to be 67 cm⁻¹, a value that is comparable to the expected value of approximately 70 cm⁻¹. Further, there was observation of the aforementioned bending mode. While it is expected to be doubly degenerate, a doublet was instead observed at 659 and 651 cm⁻¹. This observation was used to support bending of the CO₂ molecule at the OMCs observed in the diffraction data. It should also be noted that the CO₂ angle found in the diffraction studies carried out in this work was $162(3)^{\circ}$ [113], a huge deviation from the expected linear geometry. Later studies showed that this unexpected bending was due to a misinterpretation of the time and position averaged diffraction data and that the CO_2 angle should not deviate greatly from 180° [63].

Since this initial work, IR and Raman have both become highly active tools for the characterization of many MOFs. Valenzano et al. used variable temperature IR data to obtain the enthalpy and entropy of adsorption for CO₂ adsorbed at the OMC in Mg₂(dobdc). The calculated enthalpy of adsorption was estimated to be -47 kJ mol⁻¹, which agreed very well with previously reported values obtained from adsorption isotherms [146]. An additional in situ IR study of CO₂ adsorption was carried out in the rht-type MOF known as Cu-TDPAT [147] (Cu-TDPAT = $[Cu_3(TDPAT)(H_2O)_3]\cdot 10H_2O\cdot 5DMA$ and TDPAT = 2,4,6-tris(3,5-dicarboxylphenylamino)-1,3,5-triazine), a framework that consists of Cu paddlewheel clusters and triazine ligands (Figure 1.10a). CO₂ adsorption studies show not only high carbon dioxide uptake (0.072 grams of CO₂ per gram of MOF at 0.15 bar and 298 K) [148], but also high CO₂ to N₂ selectivity (34.2 determined via IAST). An in situ IR study carried out on the Cu-TDPAT framework, which exhibits both Lewis acidic OMCs and Lewis basic amine functionality on the triazine linker, gives evidence of two strong adsorption sites [149]. A follow up study of Lockard et al. monitored certain Raman-active vibrational frequencies associated with the metal-containing building unit, the ligand, and surface-bound CO₂ (Figure 1.10b) [150]. They were able to monitor a Cu-Cu stretching mode in the paddlewheel, revealing that the Cu-Cu interaction became stronger with dehydration and with CO₂ loading, implying a shorter Cu-Cu distance. Additional Raman active modes were used to show a rearrangement of the linker configuration to become more planar and hence less strained upon activation, which was verified using DFT simulations of the Raman spectra. Further, the Raman-active CO₂ vibrational modes gave additional insight into the presence of two strong adsorption sites, one associated with the metal and one associated with the triazine linker. After poisoning the OMC with the addition of water, and effectively blocking that adsorption site, the linker reverts back to a non-planar configuration, enhancing the Lewis basicity of the linker. The latter, in turn, enhances the CO₂ interaction with the Lewis base functionality, an observation that is consistent with theoretical work that predicts that the selectivity for CO₂ over N₂ will be enhanced in wet gas streams [147].

In situ DRIFTS (diffuse reflectance infrared Fourier transform spectroscopy) studies were utilized to study CO_2 adsorption in mmen-CuBTTri (Cu-BTTri = $H_3[(Cu_4Cl)_3(BTTri)_8(mmen)_{12}]$ [151] and mmen: N_1N_0 -dimethylethylenediamine) [152, 153]. The idea was to mimic the chemical reactivity observed in liquid amine scrubbers through the appendage of alkyl amines to the OMC on the internal MOF surface. After dosing the mmen-CuBTTri framework with CO_2 , there is disappearance of a peak at 3283 cm⁻¹, which is related to the N–H stretching mode. There is also



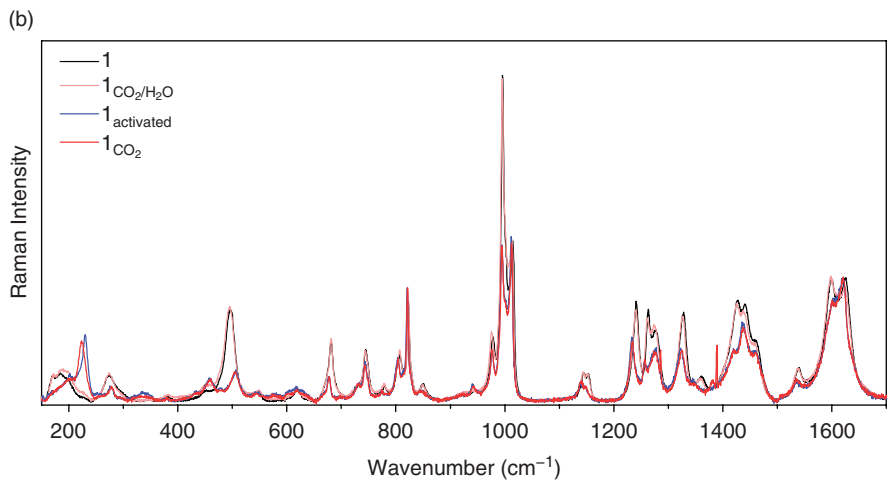
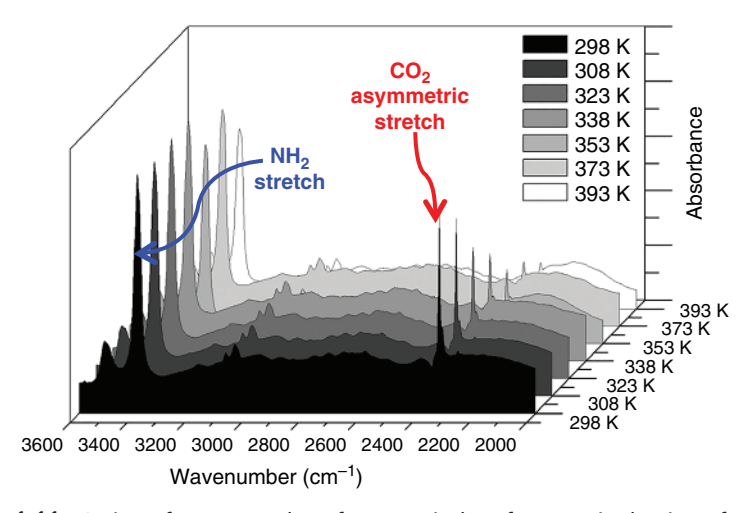


Figure 1.10 (a) Ball-and-stick model of Cu-TDPAT that shows interconnected cuboctahedral building units, consisting of Cu-paddlewheels and isophthalate ligands. The pink balls represent void space. Cu, C, O are represented by blue, grey, and red spheres, respectively. (b) Full Raman spectra of as-synthesized Cu-TDPAT (black), Cu-TDPAT treated with H_2O -saturated CO_2 (pink), activated Cu-TDPAT (blue), and activated Cu-TDPAT treated with pure CO_2 gas (red). Source: Chen et al. 2015 [150]. Reproduced with permission of Royal Society of Chemistry.

an emergence of several other peaks that were unobserved before the introduction of CO₂. These significant changes in the spectrum have been attributed to the formation of zwitterionic carbamates or carbamic acid, which are the expected species via chemisorption of CO₂ to the amine functional groups.

Last, recent work of Wright et al. showed that synchrotron-based IR microspectroscopy with polarized IR light could be used to determine the orientation of adsorbed CO₂ molecules, the CO₂ loading level, and the enthalpy of adsorption in single crystals of a small pore amine-containing MOF, $Sc_2(BDC-NH_2)$ (BDC-NH₂ = 2-amino-1,4-benzenedicarboxylate) [154]. The measurements, collected during CO, uptake at partial pressures 0.025-0.2 bar at 298-393 K (Figure 1.11), have 100-fold higher photon flux density relative to lab sources. Further, this technique yields a large improvement in the signal-to-noise ratio so that high-quality direction-dependent polarized IR spectra can be measured for anisotropic crystals. As such, in this study, measurements could be done at extremely low CO₂ coverage of ~0.1 mmol g⁻¹ which is equivalent to a site occupancy of 1.5%. This value is within the error of what can be measured by diffraction experiments and certainly outside the regime of what can be seen with most other *in situ* techniques. While it was not shown in this study, due to the high rate of CO₂ diffusion at the temperatures probed, it is suggested that the technique could be used to elucidate CO₂ diffusivities. This can be done by following the temporal and spatial variations over a single crystal [154].



<u>Figure 1.11</u> Series of spectra taken from an isobar from a single site of a single $Sc_2(BDC-NH_2)_3$ crystal. As temperature increases, the magnitude of the adsorbed CO_2 asymmetric stretch (red arrow) at 2335 cm⁻¹ wavenumbers decrease relative to the NH_2 stretching modes, one of which is shown with a blue arrow. *Source:* Greenaway et al. 2014 [154]. Reproduced with permission of John Wiley & Sons.

It should be noted that while Raman and IR have been used extensively due to their sensitivity to CO₂ and several other small molecules of interest, INS, a technique that does not suffer from selection rules, rarely has been used to study materials for carbon-capture applications. The reason is that the incoherent scattering cross sections for C, O, and N are weak relative to those of H [155]. As such, these studies require long measurement times. Further, for INS measurements, data are first collected for the activated framework. This is followed by data collection for the framework loaded with gas, and the spectrum of the bare framework is then subtracted from the spectrum obtained for the CO₂ loaded sample. Given the data subtraction, when possible, frameworks should be deuterated in order to lower the contribution of the framework H atoms in the background spectrum. Further, in cases where CO₂ binds very strongly and causes significant changes in the unit cell parameters, this can shift the framework phonon frequencies. These two problems were highlighted in an INS study of CO₂ adsorption in Mg₂(dobdc). Despite framework deuteration, Queen et al. could still see no convincing indication of vibrational modes associated with framework adsorbed CO2. The difference spectrum instead revealed negative and positive intensities, indicating significant shifts in the framework modes upon CO₂ adsorption. This was further verified by neutron powder diffraction, which showed a significant reduction in unit cell volume from the bare framework to the CO₂ dosed one. Both softening and hardening of the vibrational modes are observed, likely due to the inverse effect CO₂ adsorption has on the lengths of the a/b and c-axes, as supported by the diffraction data [63].

NMR In situ NMR, a powerful technique that can be used to complement diffraction studies, locally probes the nuclear spins present in the sample, and hence the local environment around each atom. This technique, which does not require any long-range order, can provide binding configurations, information on adsorptioninduced framework flexibility, as well as the dynamic properties of imbibed guest molecules throughout the frameworks (in the millisecond regime). While the number of studies is growing, in situ NMR experiments reported to date for the elucidation of host-guest interactions are few in number. To the best of our knowledge, in situ studies have been carried out with the following adsorbates including Xe [156], CO₂ [118, 157], H₂ [158–160], H₂O [158, 161], NH₃ [162], and hydrocarbons [163, 164]. It is thought that the lack in utilization of in situ NMR is due to the lack of accessible instruments, difficulty in data interpretation, and probe restrictions. It has been shown that CO₂ adsorption in frameworks can result in anisotropic or restricted motions of CO₂. As such, the ¹³C NMR signals exhibit characteristic line shapes that in turn allow determination of information pertaining to the motion of the adsorbed molecules [165], such as rotational axes of surface-bound CO₂. These characteristic line shapes were observed in in situ ¹³C NMR spectra of CO₂ adsorbed in Ni₂(2,6-ndc)₂(dabco) or DUT-8 (2,6-ndc = 2,6-naphthalenedicarboxylate, dabco = 1,4-diazabicyclo[2.2.2]octane) [166] (Figure 1.12), an should be a MOF that exhibits a gate opening effect at a characteristic pressure of 5 bar. Below this pressure, the only signal observed in the NMR is from unbound CO₂ at 335 ppm; however,

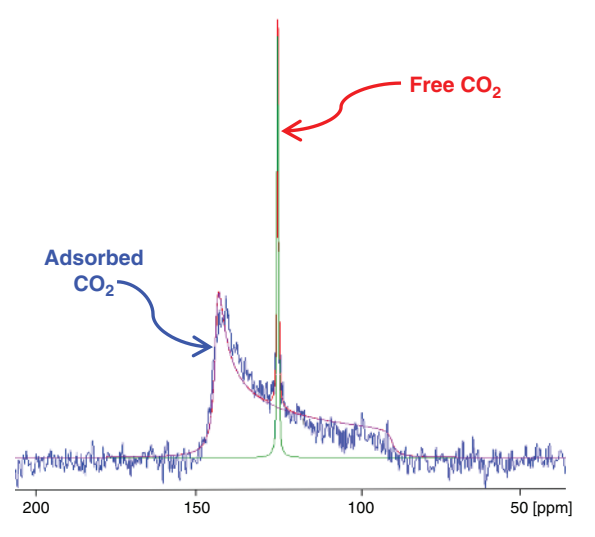


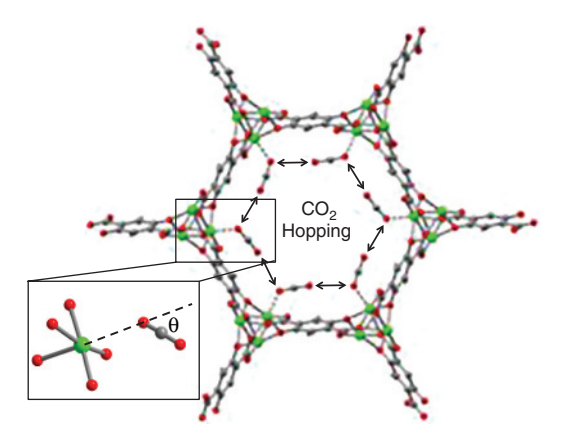
Figure 1.12 ¹³C NMR spectrum of DUT-8(Ni) pressurized with 9.5 bar carbon dioxide measured at 237 K. Note that the initially closed structure opens during the adsorption experiment at the temperature-dependent gate-opening pressure (~5 bar at 237 K) whereas it remains open during desorption down to 1 bar (hysteresis). (Blue: experimental spectrum, green: simulated gas phase signal, magenta: simulated signal of adsorbed CO₂; red: Sum of the simulated signals.). *Source:* Hoffmann et al. 2012 [167]. http://www.mdpi.com/1996-1944/5/12/2537/htm. Licensed under CC BY 4.0.

at higher pressures, the framework pops open and a broad signal is observed with a characteristic shape due to chemical shift anisotropy, Δav of 52 ppm. From these data, the tilt angle, θ , defined as the angle between the symmetry axis and the rotational axis, can be calculated using the following equation:

$$\Delta av = \Delta \left(\frac{3\cos^2 \theta - 1}{2} \right) \tag{1.5}$$

The tilt angle determined for DUT-8(Ni) was calculated to be 49(2)° [167]. Following this study, a similar effort was made by Kong et al. to elucidate the CO_2 adsorption behavior in Mg_2 (dobdc) [118]. This study is briefly described in the next section; however, an image showing the determined θ value for CO_2 in Mg_2 (dobdc) is shown in Figure 1.13.

QENS Quasielastic neturon scattering (QENS), often combined with molecular dynamics simulations, has on several occasions been used to understand diffusive properties of small molecules in MOFs. One thing to note for QENS is that the incoherent scattering cross section is minimal for many elements other than H and so in the case of CO₂, collective motions of molecules are measured rather than



<u>Figure 1.13</u> Ball-and-stick model of Mg_2 (dobdc) with CO_2 adsorbed at the open metal site, as determined by NPD. The arrows represent the CO_2 -hopping mechanism proposed by molecular simulations used to interpret NMR data. The higher-magnification view represents the fixed rotation angle, θ . The green, red, and grey spheres represent Mg, O, and C, respectively. *Source:* Lee et al. 2015 [83]. Reproduced with permission of John Wiley & Sons.

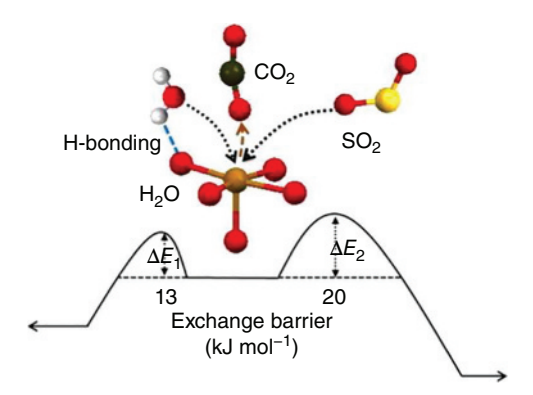
diffusivities of individual molecules that can be measured for some small molecules like H₂ and CH₄, for instance [125, 168, 169]. Most QENS studies are used to extract three parameters, the self-diffusivity (D_s) , which describes the diffusion of individual molecules, the transport diffusivity (D_i) , which describes the mass transport that is induced in the presence of a gradient, and the corrected diffusivity (D_0) which is related to the transport diffusivity via a thermodynamic correction factor that is calculated from the experimental adsorption isotherm. When looking at many industrial applications regarding separations, particularly membrane separations, where there might be mass transport in non-equilibrium environments, the transport diffusivity becomes very important and so it is necessary to assess these terms separately. Because the scattering from CO₂ is coherent in nature, the transport diffusivity is probed. Compared to NMR, QENS measures fast diffusive motions on time scales ranging from 10¹⁰ to 10¹³ sec⁻¹. Further, the distances over which the diffusive properties are observed are well defined and variable: typically, for QENS, the distances range from 2 to 100 A, while in NMR the time scales and distances are longer compared to QENS. Time scale for NMR is normally in the millisecond regime and the distances are normally in the microns range.

One of the first QENS studies of CO_2 adsorption in an MOF was carried out by Maurin et al. in MIL-47(V) or VO(1,4-BDC) (1,4-BDC = 1,4-benzenedicarboxylate) [170] to extract the aforementioned three diffusivity parameters over a wide range of loadings. They found that while D_s and D_o decrease as functions of loading, D_t shows a non-monotonous response that is rationalized to be the result of intermolecular CO_2 interactions that deviate from the behavior expected for an ideal gas.

They show that through coupling QENS with molecular dynamics simulations (QENS-MD), transport diffusivity in MOFs can be directly probed, and hence can be applied to understand the dynamics associated with industrially relevant gas mixtures [170]. Since this time, the diffusivity of H₂ and CO₂ in the small pore Zr-based MOF MIL-140A(Zr) has been evaluated using the QENS-MD technique to determine the self-diffusivities of H₂, and the corrected and transport diffusivities of CO₂ as single components and also in a binary mixture. Of these two guests, H₂, with its smaller kinetic diameter, was shown to diffuse through the narrow triangular channel of MIL-140A(Zr) at a significantly faster rate than CO₂ at the same temperature. In the binary mixture, H₂ is still faster, but it shows a slightly slower self-diffusivity, while CO₂ gets a bit faster. Despite these slight changes, there is still a significant difference in the observed diffusivities in the binary mixture, suggesting that this material might be a good candidate for kinetic-based separations of CO₂ and H₂ [171, 172].

COMPUTATIONAL AID FOR DATA INTERPRETATION While spectroscopic tools are generally accepted as a means to assess small molecule interactions in MOFs, because of the aforementioned reasons, data interpretation should proceed with caution. When relevant, it is helpful to utilize theoretical tools capable of incorporating vdW interactions to reduce error in data interpretation. There are several examples throughout the literature where computational tools have proven essential to interpret spectra. This was highlighted by the work of Lin et al. [119] who used molecular simulations to reproduce chemical shift anisotropy (CSA) powder patterns of ¹³C NMR, work that was proven to be essential for the interpretation of diffusive motions of CO₂ in Mg₂(dobdc). In this study, the NMR measurements of CO₂-adsorbed Mg₂(dobdc) [118] revealed a distinct CSA powder pattern, which at the time was interpreted to be the result of a uniaxial rotation with a fixed rotation angle θ that ranged from 56° to 69° (at temperatures from 200 to 400 K). However, a more recent study used molecular simulations to probe the free-energy landscape of CO₂ in Mg₂(dobdc) under conditions similar to those used in the NMR study. The Monte Carlo simulations indicated that NMR signature was instead the result of a molecular-hopping motion between metals within the crystallographic ab plane (Figure 1.14). This study implies that the dynamics of CO₂ within Mg₂(dobdc) were more complex than originally expected [119].

X-ray absorption spectroscopy (XAS), an element-specific technique used to probe changes in the electronic environments with the adsorption or desorption of guest species, is highly sensitive yet difficult to interpret without the help of theory. Near edge X-ray absorption fine structure (NEXAFS) was used to probe the Mg K-edge first in the activated Mg₂(dobdc), and then again with the DMF and CO₂ bound to the open Mg²⁺ site. Spectra were simulated using DFT and then compared with the experimental spectra. This theoretical analysis proved necessary to understand the variations in the local electronic environment around the OMC from the activated MOF to the one with surface-bound molecules [120]. Using *in situ* XAS (X-ray absorption spectroscopy), a similar study was carried out to study CO₂ adsorption



<u>Figure 1.14</u> Ball-and-stick model of the OMC in M_2 (dobdc) with CO_2 being displaced by either H_2O or SO_2 and their energy barriers to activation. M^{2+} , O, C, H, and S are represented by orange, red, great, white, and yellow spheres, respectively. *Source:* Tan et al. 2015 [173]. Reproduced with permission of American Chemical Society.

around the OMC in Cu-TDPAT [150]. The constant edge position at 8990 eV has confirmed the oxidation state of the Cu²⁺ throughout the adsorption and desorption process. In addition, the activated framework was exposed to both water and carbon dioxide, and due to the fact that the edge feature intensity for the CO₂ dosed framework was between that of H₂O loaded and activated one, it has been concluded that the interaction of the OMC with the CO₂ molecule is not as strong as that of water, giving a strong indication that in a competitive environment, water would preferentially bind over CO₂.

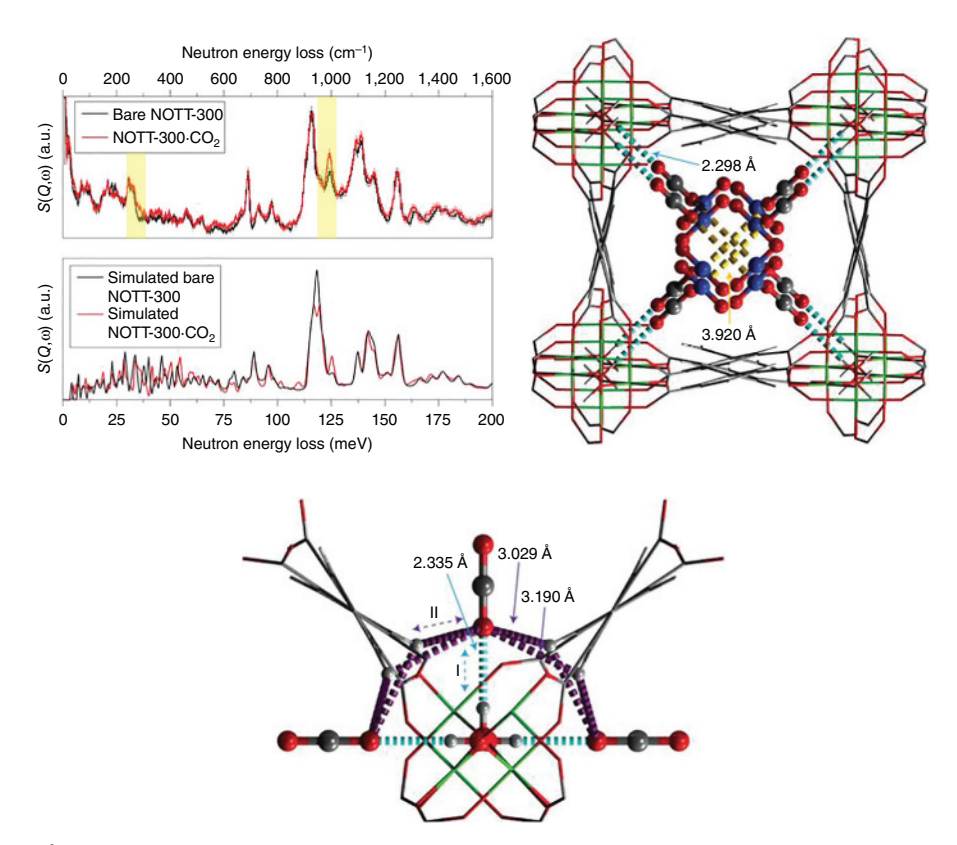
More recently, Chabal et al. used *in situ* IR combined with *ab initio* simulations to investigate competitive binding of small molecules in M_2 (dobdc) where M = Mg, Co, and Ni [173]. They investigated the displacement of CO₂ with several molecules including H₂O, NH₃, SO₂, NO, NO₂, N₂, O₂, and CH₄. They found, despite the higher binding energy of SO₂, NO₂, and NO (~70-90 kJ mol⁻¹), that H₂O and NH₃ (~60-80 kJ mol⁻¹) are the only molecules able to sufficiently displace the CO₂ (38–48 kJ mol⁻¹ for the three metals). They used DFT simulations to evaluate the energy barrier associated with CO₂ displacement by H₂O and SO₂. They found the energy barrier to be approximately 13 and 20 kJ mol⁻¹, for H₂O and SO₂, respectively. The calculations revealed that, instead of differences in binding energies, the kinetic barrier for this exchange is dictated by the interaction of the second guest molecule (in this case H₂O or SO₂) with the MOF ligands. Hydrogen bonding between the H₂O and oxygen on the organic linker facilitate the positioning of the oxygen atom of the water molecule toward the metal center (Figure 1.14). These interactions reduce the exchange barrier for the CO₂ displacement by H₂O. In contrast, the SO₂ instead interacts with the benzene ring that is more distant from the metal center, an occurrence that hinders the exchange process. To the best of our knowledge, this is the first in situ work that provides insight into competitive co-adsorption [173].

Due to the aforementioned problems with negligible incoherent scattering cross sections of many of the elements of interest for CO₂ capture, many INS studies actually pair DFT-based calculations to aid in understanding of the hostguest interactions. For instance, Al₂(OH)₂(bptc) (where bptc = biphenyl-3, 3', 5,5'-tetracarboxylate alternatively known as NOTT-300), shows relatively high CO₂ uptake with a value of 2.64 mmol per gram of MOF at 0.15 bar and 298 K and minimal uptake of CH₄, N₂, Ar, O₂, or H₂ [174]. INS, paired with DFT-derived simulations of the INS spectrum, was used as the primary method for characterization of the surface-bound CO₂, a process that was then validated via powder X-ray diffraction. The sample was loaded with 1.0 CO₂ per formula unit, and the INS data revealed an increase in the intensity of two peaks located at 30 meV and 125 meV. Further, peaks above 100 meV were shifted to higher energy indicative of a hardening of the framework modes with CO₂ adsorption (Figure 1.15a). The DFTderived INS spectrum showed very good agreement with the experimental one and indicated that the preferential CO₂ adsorption site was located in an end-on orientation approximately 2.33 Å from the framework hydroxyl group. This implies that moderate H-bonding interactions were responsible for the observed CO₂ adsorption properties (Figures 1.15b and 1.15c). The low energy peak in the INS spectrum was assigned to a wagging mode of the -OH that was induced by the presence of CO₂, while the higher energy peak was assigned to the wagging mode of four aromatic C-H bonds that are found adjacent to the surface-bound CO₂. This work shows that pairing DFT and INS made it possible to visualize the binding mechanism of CO₂ and gain necessary insight into the high CO₂ absorption capacities of the framework at low pressures. Additionally, the low H₂ uptake for this material was rationalized using the same methodology [174].

1.3 MOFs FOR POST-COMBUSTION CAPTURE

1.3.1 Necessary Framework Properties for CO₂ Capture

Maximizing the framework adsorption capacity (both volumetric and gravimetric) and selectivity of CO_2 at low pressures and in the presence of other components in the flue gas stream is of principal importance to post-combustion carbon capture. As shown in Table 1.1, this process is carried out at a pressure of ≈ 1 bar with CO_2 volumes that range from 3% to 15% depending on the fuel source and at temperatures between 40°C and 75°C. As such, absorbents used for post-combustion capture must show high CO_2 adsorption capacity at partial pressures less than 0.15 bar, a property that can be positively influenced by designing frameworks with high densities of strong adsorption sites. Other properties required for post-combustion capture include the ease of regeneration (likely to occur between 100°C and 200°C in a TSA



(a) Experimental and simulated INS spectra for the CO₂-loaded Figure 1.15 Al(OH), (bptc). The yellow bars highlight the position of peak I and II. (b) Wire view of the Al(OH)2(bptc) obtained using PXRD analysis. The two identified CO2 adsorption sites in the pore channel are represented by a ball-and-stick model. Site I (with the grey carbon) was determined by INS/DFT and verified via powder x-ray diffraction, and site II (with a blue carbon) was determined by powder x-ray diffraction. The dipole interaction between neighboring CO₂(I,II) molecules is highlighted in orange. (c) Detailed view of the interactions between MOF -OH and -CH groups with CO2 molecules in a pocket-like cavity (determined by DFT simulation). The modest hydrogen bond between $O(\delta^-)$ of CO₂ and H(δ ⁺) from the Al-OH moiety is highlighted in cyan. The weak cooperative hydrogen-bond interactions between $O(\delta^-)$ of CO_2 and $H(\delta^+)$ from –CH are highlighted in purple. Each $O(\delta^-)$ center therefore interacts with five different $H(\delta^+)$ centers. Framework aluminium, carbon, oxygen, and hydrogen are represented by green, grey, red, and white, respectively. Source: Yang et al. 2012 [174]. Reproduced with permission of Nature Publishing Group.

process), rapid diffusion of gases through the adsorbent, and long-term stability of materials under application-relevant conditions. While it is considered difficult to design materials to meet all of these criteria, the facile structural tunability of MOFs offer an unprecedented opportunity to target new materials with tunable interactions for the energy-efficient capture of CO₂.

Due to the similarities in the kinetic diameter of the two most abundant molecules in the flue gas stream, CO₂ and N₂ (3.3 and 3.6 Å, respectively) size exclusion is difficult. As such, most of the focus is on carrying out this separation via physisoprtion or chemisorption methods. Knowledge of the fundamental differences in the physical properties and reactivity of CO₂ and N₂ has aided the design of multiple frameworks that exhibit strong CO₂ adsorption in the low-pressure regime that is of interest for post-combustion carbon capture [175]. For example, Table 1.2 shows that CO₂ has higher polarizability (CO₂ = 29.1 × 10⁻²⁵ cm³; N₂ = 17.4 × 10⁻²⁵ cm³) and quadrupole moment (CO₂ = $43.0 \times 10^{-27} \text{ esu}^{-1} \text{ cm}^{-1}$; N₂ = $15.2 \times 10^{-27} \text{ esu}^{-1} \text{ cm}^{-1}$) compared to N₂. As such, the introduction of structural components that exhibit high charge densities on the framework surface can be used to polarize incoming CO₂ molecules and hence manipulate both the selectivity and the adsorption capacity at low pressures [176]. As an alternative, CO₂ is also known to be susceptible to attack by nucleophiles as demonstrated with the aforementioned liquid amine-based scrubbers. Chemisorptive interactions, achieved via Lewis base functionality appended on the internal MOF surface, are also becoming a common trend in MOF chemistry [177–180].

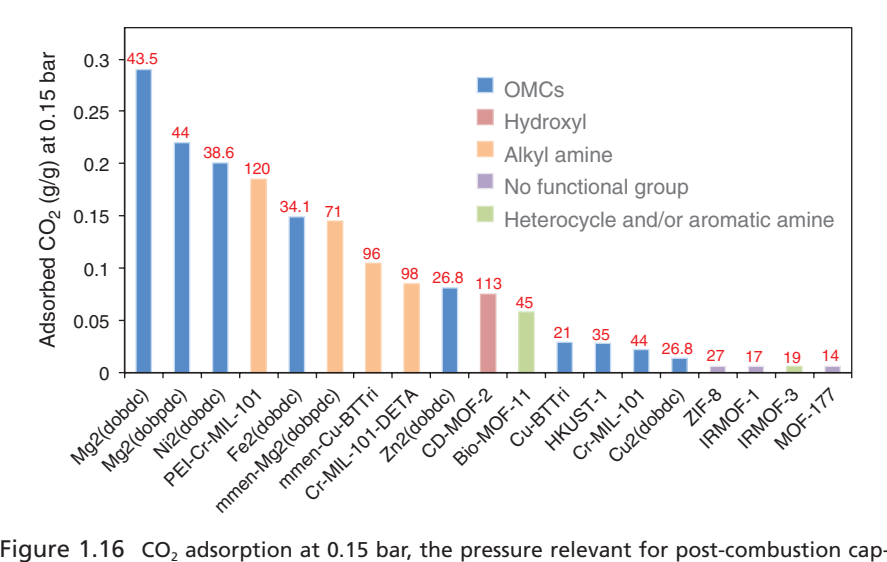
1.3.2 Assessing MOFs for CO₂/N₂ Separations

The most common method to assess applicability of MOFs in post-combustion flue gas capture is through the assessment of CO₂ and N₂ single-component isotherms collected between 293 and 313 K at pressures up to 1 bar [23]. From extraction of isosteric heats obtained from variable temperature adsorption data and analysis of the CO₂ uptake in the low-pressure regime, one can gain immediate insight into the materials affinity for CO₂, its potential regarding adsorption capacity, and the potential ease of regeneration. It should be noted that, compared to many reports in the literature, flue gas will be introduced to the adsorbent at temperatures ranging from 50°C to 75°C and then released at temperatures that range from 100°C to 200°C. As such, there is a clear need in the literature for materials assessment at significantly higher temperatures. This fact was highlighted in a recent report by Mason et al. which show assessment of CO₂ and N₂ adsorption in two MOF frameworks, Mg₂(dobdc) and MOF-177, at temperatures ranging from 20°C to 200°C [62]. With this work, they report a methodology to assess the performance of materials in a likely scenario using temperature swing adsorption.

Given the partial pressures of CO_2 and N_2 in the flue gas of a coal-fired power plant, MOF selectivities reported in the literature for CO_2 over N_2 are usually calculated using the molar ratio of the CO_2 uptake at pressures of 0.15 bar over the

 N_2 uptake at 0.75 bar. It should be considered that the significantly larger quadrupole moment of CO_2 over N_2 will lead to an overestimated N_2 adsorption in MOFs that contain highly polarizing adsorption sites because CO_2 will preferentially bind to strong adsorption sites and hence reduce the actual amount of adsorbed N_2 in a binary mixture. While this molar ratio method is the simplest way to calculate selectivity, it has been shown in a recent report by Mason et al. that the obtained values cannot be taken too literally. In assessment of CO_2 adsorption isotherms of CO_2 dobdc) between 40°C and 60°C, they show an unrealistic increase in selectivity for CO_2 over N_2 demonstrating the importance of using IAST [181] to calculate the selectivities for MOFs containing strong adsorption sites [111].

One very important metric for assessing a material for post-combustion carbon-capture applications is the isosteric heat of adsorption, $-Q_{\rm st}$. The $-Q_{\rm st}$ at low coverage is indicative of the strength of binding of the strongest adsorption site and strongly influences the low-pressure adsorption capacity and selectivity of MOFs and further influences their ability to undergo regeneration [182, 183]. Figure 1.16 shows the CO_2 adsorption capacity and isosteric heats for a number of frameworks in the low-pressure regime of interest for post-combustion capture [63, 96, 111, 114, 152, 184–191]. It should be noted that because the density of adsorption sites is not taken into account in this image, the strength of



<u>Figure 1.16</u> CO₂ adsorption at 0.15 bar, the pressure relevant for post-combustion capture. It should be noted that all for the data presented were obtained from isotherms collected at 298 K with the exception of HKUST-1, Cr-MIL-101, and Cr-MIL-101-DETA, which were collected at 293 and 296 K, respectively. The values in red represent the low-coverage experimental isosteric heats of adsorption, $-Q_{\rm st}$ [63, 96, 111, 114, 152, 184–191].

the adsorption site does not correlate very well with the low-pressure capacity. However, for the high surface area materials with no polarizing surface functionality, such as MOF-177, the adsorption capacity is only 6 mg of CO_2 per gram of adsorbent and the isosteric heat is 14 kJ mol⁻¹, while $Mg_2(dobdc)$, a material with much stronger adsorption sites due to the presence of exposed metal cations (43.5 kJ mol⁻¹) and a modest BET surface area of only 1200 m² g⁻¹ of adsorbent, takes up 290 mg CO_2 per gram of adsorbent at 0.15 bar and 298 K. This shows that surface area has minimal impact on the low-pressure adsorption properties. Further, it can be seen in Figure 1.16 that the strongest binding sites for CO_2 (hence the highest $-Q_{\rm st}$ values) are related to frameworks with alkyl amine-based functionality or highly polarizing open-metal coordination sites (OMCs). These two structural components have been used quite extensively throughout MOF chemistry to enhance the overall low-pressure CO_2 adsorption properties.

1.3.3 MOFs with Open Metal Coordination Sites (OMCs)

In most reported MOFs, weak van der Waals (vdW) forces are the dominant interactions between the framework and incoming guests; however, recent work has shown that an effective strategy to increase the surface packing density of adsorbates is through the generation of MOFs that contain high concentrations of open metal coordination sites (OMCs) [192]. The incorporation of highly reactive, electron deficient OMCs into frameworks can also enhance both binding energy and selectivity and permit charge transfer between the framework and surface-bound guest species [82, 128], a property of much interest for the conversion of small molecules into other useable products. While many of the frameworks with OMCs have been discovered serendipitously [26], there are emerging methodologies for their controlled introduction including the incorporation of metalloligands [193] and using synthetic protocols where metal clusters containing OMCs are used ab initio [98]. In all of these cases, the frameworks form with solvent remaining in the channels and in the metal coordination sphere. Post-synthetic treatment of the materials with a combination of heat and vacuum, a process called activation, can liberate the solvent molecules from the framework, and if the MOF porosity is maintained, the newly generated OMCs are available for guest inclusion.

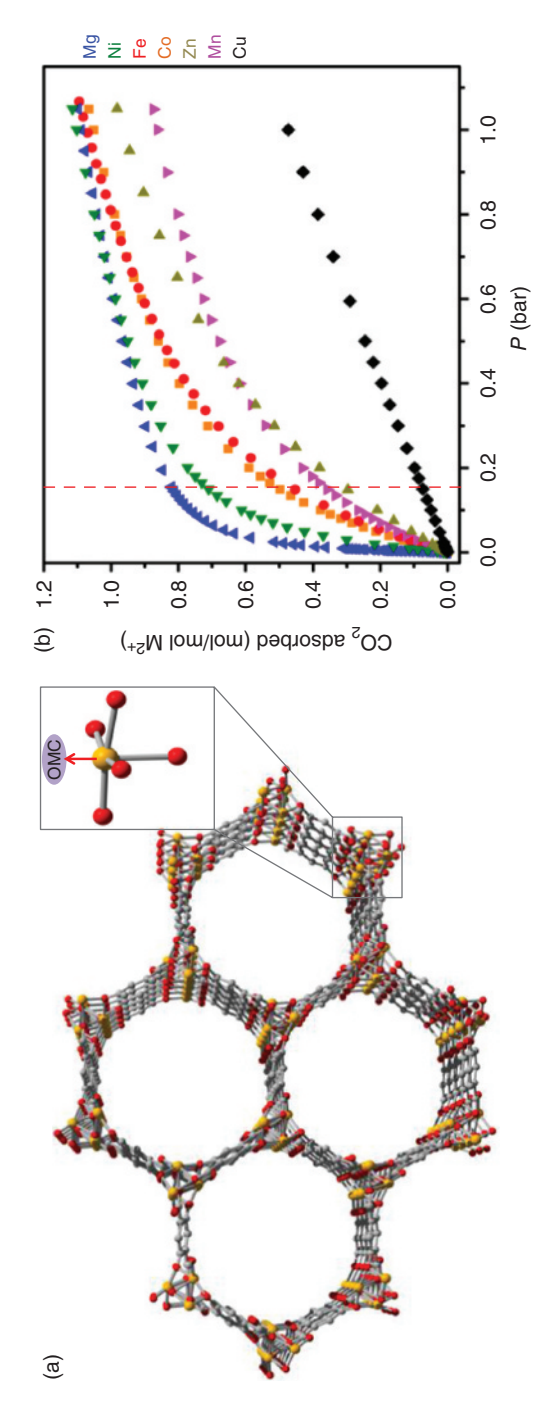
Figure 1.16 shows the low-pressure adsorption capacity for several MOFs at 0.15 bar and 298 K. Those highlighted in blue are the adsorption capacities for MOFs with OMCs while those highlighted in purple are frameworks dominated by weak vdW-type interactions [98]. It can easily be seen from this plot that the electron deficient OMCs, which strongly polarize incoming CO₂, lend to significantly higher adsorption at low pressures of interest for post-combustion carbon capture. It should also be noted that while OMCs provide strong interactions allowing CO₂ adsorption

at higher temperatures and lower pressures than typically used for energy-consuming cryogenic distillation processes, the adsorbate—adsorbent interactions are often weak relative to the formation of chemical bonds, providing facile release of the molecules during the regeneration step of a separation process [98].

One of the most well-studied OMC-containing MOFs to date is M_2 (dobdc), alternatively known as M-MOF-74, CPO-27-M, or M_2 (dhtp) where M = Mg, Mn, Fe, Co, Ni, Cu, or Zn and dobdc⁴⁻ = 2,5-dioxido-1,4-benzenedicarboxylate (Figure 1.17a) [99, 105, 112, 113, 135, 194–196]. The framework consists of one-dimensional honeycomb like channels that are constructed by metal oxide chains interlinked by dobdc⁴⁻ ligands. The significance of this framework is related to the interesting adsorption properties that derive from the existence of unique structural features. For instance, upon solvent removal, M_2 (dobdc) offers one of the highest densities of OMCs of any framework discovered to date. It also undergoes chemical substitution with a wide range of first-row transition metals. The extent of the metal substitution is only rivaled by a few MOF families such as M-BTT (BTT³⁻ = 1,3,5-benzenetristetrazolate), where M = Cr, Mn, Fe, Co, Ni, or Cu [133, 197–200], and M_3 (btc) $_2$ (btc 3- = 1,3,5-benzenetricarboxylate), where M = Cr, Fe, Ni, Cu, Zn, Mo, or Ru [201–206].

The high concentration of electron deficient OMCs in Mg₂(dobdc) leads to an unprecedented adsorption at low pressures of ≈0.29 g CO₂ per gram MOF (0.15 bar and 298 K) and an isosteric heat of -43.5 kJ mol⁻¹ [63]. The low-pressure adsorption is still the highest reported to date. Multiple in situ techniques including NMR, IR, EXAFs, and in situ diffraction have shown that the high-initial isosteric heat is directly related to the presence of OMCs [63, 118, 120, 143, 146]. Rietveld analysis of neutron powder diffraction data followed by subsequent Fourier difference analysis has revealed CO₂ bound to Mg²⁺ in an end-on orientation that is angled with respect to the framework surface, a direct result of secondary vdW interactions between the CO₂ and ligand atoms (Figure 1.13). The high isosteric heat is reflected in the ability of the CO₂ molecule to get close to the framework with short Mg-CO₂ distances approaching ≈2.3 Å [207]. Britt et al. also showed a facile release of CO₂ in Mg₃(dobdc) at a moderate temperature of 80°C [98]. Later, Mason et al. calculated the working capacity for the material to be approximately 17.6 wt% with a temperature swing process from 40°C (at 0.15 bar CO₂) to 200°C [98]. This value is much higher than MOF-177, a material without strong adsorption sites, which has a negative working capacity at all evaluated temperatures.

It has recently been demonstrated that chemical substitution of the framework metals offers tunability with regard to the CO_2 adsorption properties, Figure 1.17b. The low-coverage isosteric heats show the following trend: (Cu < Zn < Mn < Fe < Co < Ni < Mg) for the M_2 (dobdc) series, one that does not correlate with the expected ionic radii or Irving Williams series [63]. A first principles study of Yu et al. show that the trend is instead dictated by the effective nuclear charge



resent metals, oxygen, and carbon, respectively. (b) Excess CO₂ adsorption isotherms collected for the M_2 (dobdc) series at 298 K showing variability in the low-pressure adsorption properties with metal substitution. The red line, located at 0.15 bar, represents a pressure rele-Figure 1.17 (a) Ball-and-stick model of M_2 (dobdc) showing open metal coordination sites (OMCs). Orange, red, and grey spheres repvant to post-combustion flue gas capture in a coal-fired power plant. Source: Queen et al. 2014 [63]. Reproduced with permission of Royal Society of Chemistry.

seen by the CO_2 as it approaches the OMC [208]. Much additional theoretical work has been focused on predicting the structures and properties of this family of compounds. The wide range of chemical substitution and vast amount of experimental data provide a platform to test the efficacy and accuracy of developing computational methods in slightly varying chemical environments [83]. On the experimental side, in addition to metal substitution, recent efforts have been made to elongate the framework ligands to tune the pore size. Deng et al. have constructed an isoreticular series of MOFs that contain expanded versions of the linker with as many as 11 additional benzene rings giving rise to pore diameters as large as 98 Å [44].

Another iconic framework that has been the subject of a large number of CO₂ adsorption studies throughout the literature is Cu₃(BTC)₂ (alternatively known as HKUST-1 or Cu-BTC), which has a cubic structure that consists of copper-containing paddlewheels, Cu₂(COO)₄, interlinked by BTC³⁻ ligands. This material is shown to have an isosteric heat of -35.0 kJ mol⁻¹ with a modest CO₂ uptake of 4.56 wt% at 0.15 bar and 25°C [209]. This value is significantly lower than Mg₃(dobdc) due to a lower density of OMCs and the smaller charge density of the Cu²⁺ cation. This work was followed by Wade et al. performed CO₂ adsorption studies on the M3(BTC)2 analogs that are capable of maintaining their permanent porosity post-activation [206]. They found the following trend for isosteric heats of adsorption: Ni > Ru > Cu > Mo \approx Cr, which range from -36.8 to -26.7 kJ mol⁻¹. However, it should be noted that the OMC on the Ni analog is incapable of undergoing complete activation and instead is blocked by coordinated guest molecules including H₂O and MeNH₂. As such, it is thought that Coulombic interactions occurring between the surface-bound CO2 and guest molecules could be the culprit for the high isosteric heat [206]. This is further supported by a recent study of Snurr et al. that shows that slightly hydrated variations of Cu₃(BTC), show improvements in the low pressure CO₂ adsorption capacity and zero-coverage isosteric heats of adsorption when compared to the completely activated framework [123]. Framework families like the aforementioned ones that undergo a broad range of chemical substitution provide a mechanism for tuning the adsorption properties (Figure 1.17b) while retaining the same structural motif. These types of in-depth studies offer an unprecedented opportunity to gain insight into the structure-derived function of MOFs, knowledge that is necessary to understand how to design new candidates with optimized properties for post-combustion capture applications.

1.3.4 MOFs Containing Lewis Basic Sites

Much work has been focused on functionalizing the surface of MOFs with a variety of functional groups that, unlike the Lewis acidic OMCs, can additionally function as electron-donating Lewis bases. This work has primarily been focused on (i) the generation of framework ligands with strongly polarizing functional groups and/or

heterocycles and the (ii) appendage or infusion of MOFs with Lewis base containing substituents that lend to chemisorptive interactions. The nature of the framework –CO₂ interaction, whether it be physi- or chemisorption, respectively, is dictated by the type of the functional group.

(i) Strongly Polarizing Ligands for Physisorption. The quadrupole moment of CO₂ can become polarized by the existence of dipole moments from a variety of framework functionality. This dipole moment can be generated for instance by the introduction of heterocycles in the organic ligand or through direct functionalization of the ligand with a variety of chemical groups including amine, hydroxyl, thio, cyano, and halides. The idea is that the stronger polarizing the functionality, the stronger the interaction with CO₂. This effort is highlighted in the zeolitic imidazolate frameworks (ZIFs), a class of MOFs that have zeolite-based topologies; ZIFs are generally described by a formula, M(Im)2, that is similar to their zeolite counterparts Al(SiO₂) where the Si nodes and oxygen bridges are replaced by metal cations and imidazolate ligands, respectively. Due to their high porosity and chemical and thermal stability, they have been investigated for carbon-capture applications. A variety of ZIF topologies with varying functionalities on the imidazole ligands have been prepared. Figure 1.18a for instance shows the introduction of various functional groups into the RHO ZIF framework family reported by Yaghi and coworkers [210]. It is reported that the improved CO₂ adsorption of the amine functionalized ZIF-96 relative to the others (Figure 1.18b) is likely due to a combination of two effects: a large contribution arising from electrostatic interactions, due to the asymmetric functionalization, and strong vdW interactions arising from the polarizability of the functional groups. While this framework family shows some tunability in the CO₂ adsorption properties, the low-pressure adsorption is moderate, leaving little room for potential applications in post-combustion carbon capture. As a significant improvement, An et al. introduced Bio-MOF-11 (also known as $Co_2(ad)_2(CO_2CH_3)_2 \cdot 2DMF \cdot 0.5H_2O$ where ad = adeninate) whose structure consists of Co²⁺ paddlewheels capped with two acetate ligands and interlinked by two heterocyclic adeninate ligands, which have amine-based functionality [211]. This MOF has a high initial isosteric heat of adsorption of -45 kJ mol⁻¹ and an impressive selectivity of 75:1 for CO₂:N₂ calculated from the molar ratios of CO₂ and N₂ uptake at 298 K. While these values are very impressive, it should be noted that the isosteric heat drops off rapidly with higher loading and stabilizes around -35 kJ mol⁻¹, likely due to the rapid saturation of strong adsorption sites. As a result, the low pressure CO₂ adsorption has a modest value of ≈5.8 wt% at 0.15 bar. While this value is significantly improved from the aforementioned ZIFs and any reported framework containing aromatic amines, it is well-below many of the OMC-containing MOFs (Figure 1.16) and frameworks made with alkylamine functionality [211]. However, a follow-up study of Chen et al. report molecular simulation studies on Bio-MOF-11. They show that, relative to other nanoporous adsorbents including

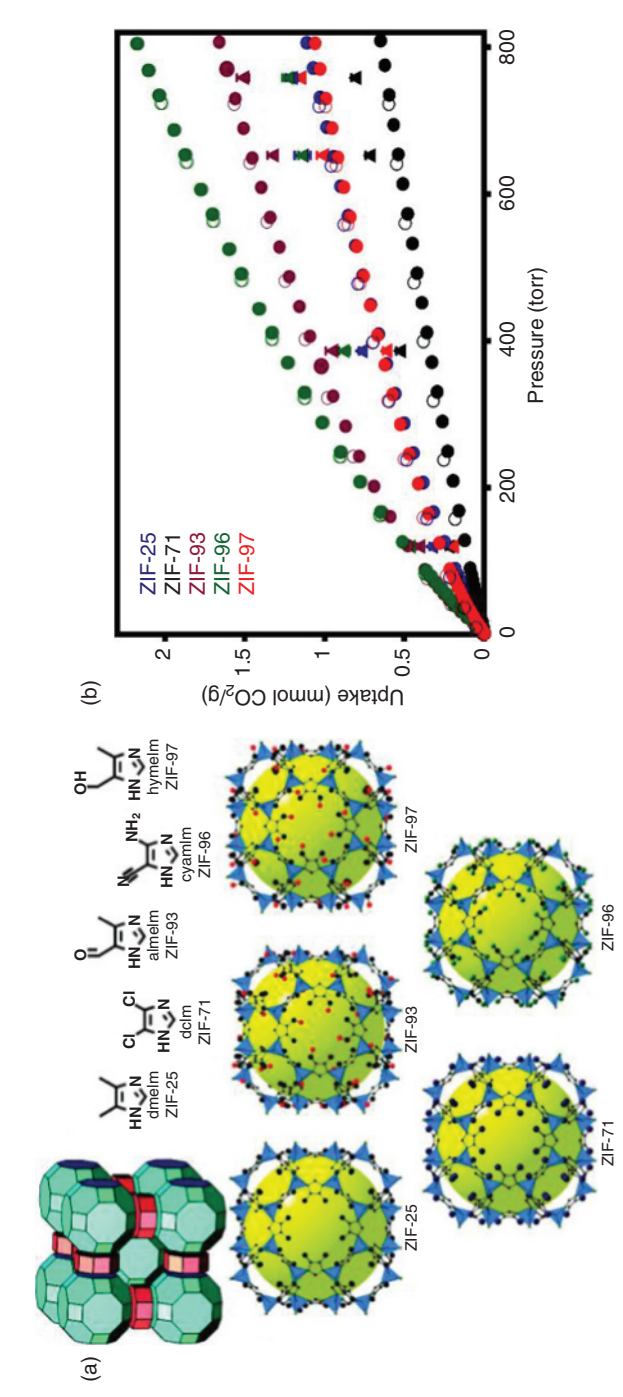


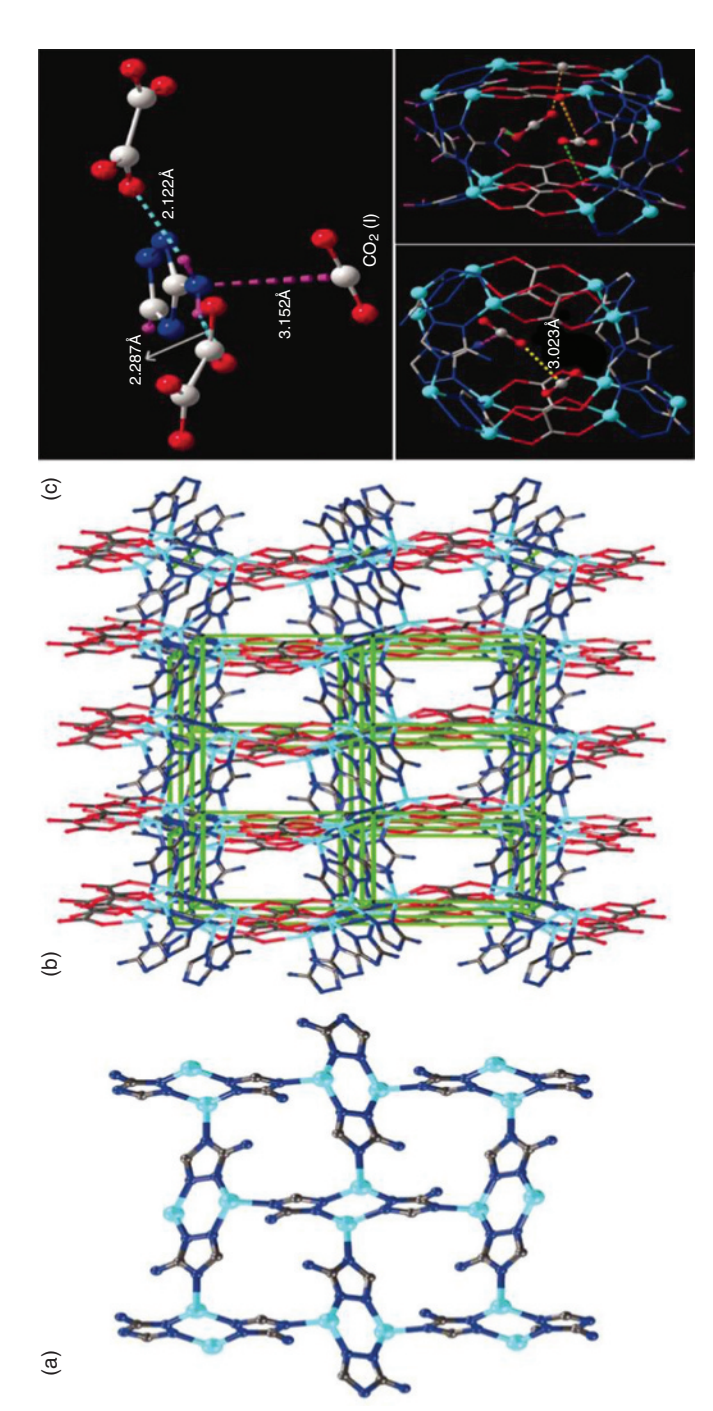
Figure 1.18 (a) Isotructural series of RHO Zeolitic Imidazolate frameworks with varying functionality and (b) experimental (circles) and theoretical (triangles) excess CO₂ adsoprtion isotherms collected at 298 K for the RHO ZIF series. Source: Morris et al. 2010 [210]. Reproduced with permission of American Chemical Society.

MOFs and zeolites, this framework has one of the highest CO_2/N_2 selectivities, and it is even slightly enhanced in the presence of water, a factor that makes the material of high interest for post-combustion capture applications. They further attribute the preferential adsorption of CO_2 to the presence of pyrimidine and amino Lewis basic adsorption sites [212].

More recently Woo and coworkers used *in situ* single-crystal diffraction to provide the first observation of CO_2 binding to an amine in $Zn_2(C_2O_4)$ ($C_2N_4H_3$)₂·(H_2O)_{0.5} (alternatively known as $Zn_2(atz)(ox)$ where atz = aminotriazole and ox = oxalate, Figure 1.19) [213], which features an isosteric heat of -40.8 kJ mol⁻¹ and low-pressure capacity of 13.6 at 0.15 bar and 22°C [214]. This MOF has two crystallographically distinct CO_2 adsorption sites. The first is located near the free amine group, while the second adsorption site is near the oxalate, both with distances above 3 Å. The intermolecular CO_2 distances imply strong intermolecular interactions. Using this experimental work combined with molecular simulation studies, they concluded that the observed CO_2 adsorption properties are a combination of appropriate pore size, strong interaction between CO_2 and functional groups on the pore surface, and intermolecular interactions between neighboring CO_2 molecules [213].

(ii) Lewis Bases for Chemisorption. Amines do not only polarize CO₂, in many instances they can strongly and selectively bind CO₂ via chemisorptive interactions. Considering the lower heat capacity of solid adsorbents compared to the liquid amine-based scrubbers, which are already implemented industrially for various CO₂ separations, it seems feasible that decorating the surface of MOFs with pendant alkylamines could lower regeneration energies, and hence give rise to an overall energy penalty that is closer to the projected thermodynamic minimum (projected to be about 11% energy penalty) [215]. Some recent work in the MOF field have been focused on either appending alkylamines to the internal surface of MOFs via OMCs or through impregnation of MOF frameworks with polymers, such as polyethyleneimine.

The first report of post-synthetic appendage of small molecules to OMCs was carried out by Hwang et al. who appended ethylenediamine to Cr^{3+} sites in the MIL-101 framework (alternatively known as $Cr_3O(1,4-BDC)_3(H_2O)_2X$, where $X = F^-$ or $NO3^-$) [216]. While the targeted application was Knoevenagel condensation catalysis, several works reported since are focused solely on post-combustion carbon capture. The first report of an amine-appended MOF for flue gas separation was by McDonald et al. in 2011. At 25°C mmen-CuBTTri (mmen = N,N'-dimethylethylenediamine and $H_3BTTri = 1,3,5$ -tri(1H-1,2,3-triazol-4-yl) benzene) adsorbs 0.105 g CO_2 per gram MOF with an IAST selectivity of 327,



structure of CO₂ binding in Zn₂(atz)(ox) at 173 K. (c) (Top) The amine group of Atz ligand is shown bound to CO₂(I). (Bottom) The H atoms Ball-and-stick model of the Zn₃(atz)(ox) structure formed from Zn-atz layers that are pillared by the oxalate units. (c) Single crystal x-ray of the amine group form H-bonds to the oxalate O atoms, directing the N lone pair toward the C atom of the CO, molecule. (Bottom) The CO₂ molecules are found in a cavity with short intermolecular distances (CO₂-I and CO₂-II). There are secondary interactions between Figure 1.19 (a) Partial structure showing Zn-atz layer that is made up of Zn₂ dimers rotated by 90° with respect to each other. (b) the CO₂-I and Ox (drawn in orange). Zn, N, O, C, and H are represented by cyan, blue, red, grey and purple spheres, respectively. So*urce*: Vaidhyanathan et al. 2010 [213]. Reproduced with permission of American Association for the Advancement of Science.

a direct result of the high isosteric heat of CO₂ adsorption, which was calculated to be -96 kJ mol^{-1} at zero coverage ($-Q_{\text{st}}$ for Cu-BTTri = 21 kJ mol⁻¹). In addition to this, in situ IR spectra gave evidence of the formation of a zwitterionic carbamate species indicative of a chemisorptive interaction. Despite the large initial isoteric heat of adsorption, the CO₂ uptake was also fully reversible and the framework could be easily regenerated at 50°C, enabling a cycling time of just 27 min and no loss of capacity over the course of 72 adsorption/ desorption cycles tested [152]. Later, Hu et al. appended several amines to the surface of Cr-MIL-101 and showed a threefold enhancement of the low pressure CO₂ adsorption properties compared to the bare framework (from 0.022 to 0.085 g CO₂ per gram MOF at 0.15 bar and 23°C). The isosteric heats of CO₂ adsorption increased from -44 [114] to -98 kJ mol⁻¹ and the selectivity of the aminebased analog again showed nearly no N₂ uptake at 296 K leading to a very high selectivity factor for CO₂/N₂ [186]. More recently, Lin et al. reported polyethyleneimine (PEI) infused Cr-MIL-101 [184]. Although the surface area and pore volume of MIL-101 decreased significantly with a 100 wt% PEI loading (BET surface areas range from 3125 to 608 m² g⁻¹), there is a dramatic enhancement in the CO₂ adsorption capacity at 0.15 bar that ranges from 0.0145 to 0.185 g CO₂ per gram MOF at 25°C, respectively (Figure 1.16). Further, at 50°C, a temperature more relevant to post-combustion capture, the adsorption capacity is still 0.150 g CO₂ per gram of 100 wt% PEI-Cr-MIL-101 [184].

In 2012, McDonald et al. reported mmen-appendage to Mg₂(dobpdc) (dob $pdc^{4} = 4,4'-dioxido-3,3'-biphenyldicarboxylate$) (Figures 1.20a and 1.20b), which showed 0.088 g CO₂ per gram MOF at 0.39 mbar (298 K) and 0.138 g/g at 0.15 bar (at 40°C), conditions relevant to CO₂ capture from air and flue gas, respectively [185]. The material also shows excellent performance in the presence of water [217]. Adsorption/desorption cycling experiments, carried out via TGA, demonstrate that mmen-Mg₂(dobpdc) can be repeatedly regenerated (at 150°C under N₂ flow) after many 15 min exposures to simulated flue gas. The working capacity, calculated to be 0.11 g CO₂ per gram of MOF, corresponds to a total CO₂ removal of 98% [185]. With DSC (differential scanning calorimetry), the authors further estimated that regeneration would require approximately 2.34 MJ of energy to release 1 kg of CO₂ from mmen-Mg₂(dobpdc) compared to the 3.6 to 4.5 MJ energy requirement for the state of the art MEA scrubbers [218–220]. Later, in 2015, this study was extended to append mmen onto the internal surface of multiple M₂(dobpdc) analogs (where M = Mg, Mn, Fe, Ni, Co, and Zn). They show significant tunability in the steep steps observed in the adsorption isotherm. Using a combination of IR, synchrotron X-ray diffraction, and computational studies they were able to reveal the origin of the sharp adsorption step in the isotherm (Figure 1.20c) is the result of a cooperative insertion process in which CO₂ molecules insert into metal-amine bonds, inducing a reorganization of the

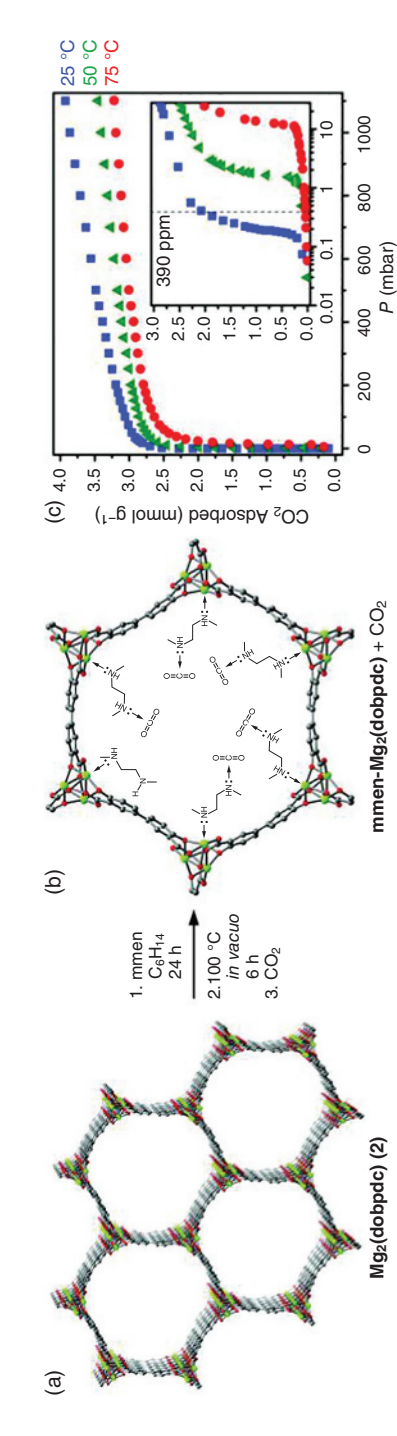


Figure 1.20 Ball-and-stick model of (a) Mg₂(dobpdc), (b) mmen-Mg₂(dobpdc), and (c) excess CO₂ adsorption isotherms for mmen-Mg₂ (dobpdc) at various temperatures showing a sharp step at 0.39 mbar (the partial pressure of CO₂ in air) that is shifted with temperature. Source: McDonald et al. 2012 [185]. Reproduced with permission of American Chemical Society.

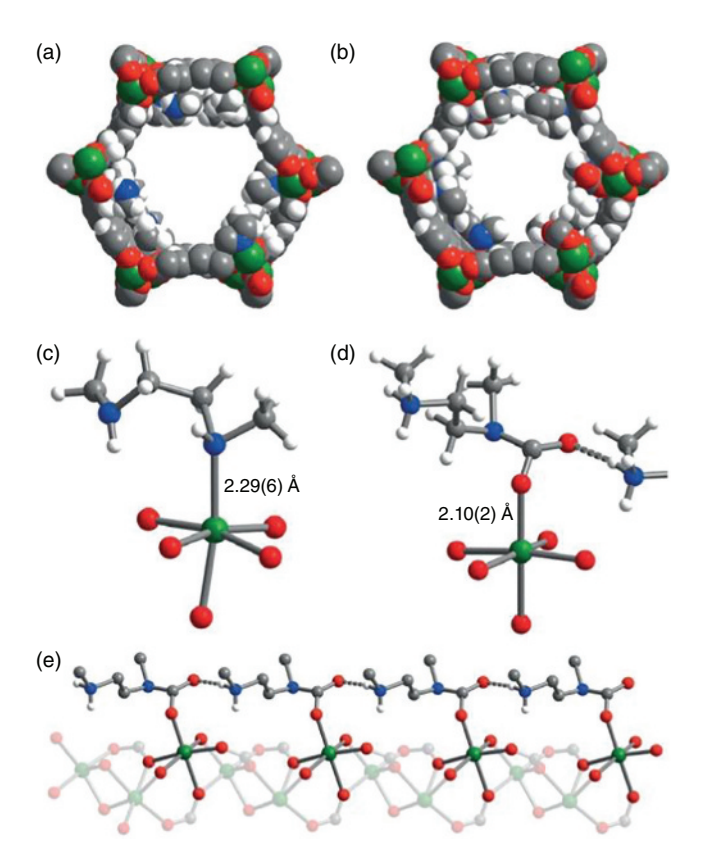


Figure 1.21 Space-filling models of the solid-state structures of (a) mmen-Mn₂ (dobpdc) and (b) CO_2 -mmen-Mn₂(dobpdc) at 100 K. Portions of the crystal structures for mmen-Mn₂(dobpdc) (c) before and (d) after CO_2 adsorption, as determined from synchrotron powder x-ray diffraction data. The latter shows CO_2 insertion between the amine and Mn metal. (e) A portion of the crystal structure shows the formation of an ammonium carbamate chain along the MOF pore. Green, grey, red, blue and white spheres represent Mn, C, O, N, and H atoms, respectively; some H atoms are omitted for clarity. *Source:* McDonald et al. 2015 [221]. Reproduced with permission of Nature Publishing Group.

amines into well-ordered chains of ammonium carbamate (Figures 1.21a–1.21e). As a consequence, large CO₂ separation capacities can be achieved with small temperature swings, and regeneration energies appreciably lower than achievable with state-of-the-art aqueous amine solutions become feasible [221].

Beyond alkyl amine-containing frameworks, there are few examples of other Lewis base functionality in MOFs that lend to chemisorptive-type interactions with CO_2 . Recently, Gassensmith and coworkers reported the synthesis of an MOF constructed by γ -cyclodextrin linked together by alkali metals such as Rb (CD-MOF-2) [157]. The ligand in this MOF, which is decorated with free hydroxyl groups, is a

natural product produced from starch. Further, the MOF can be prepared readily in green solvents such as water using slow evaporation methods. While this material was not assessed for room temperature N₂ adsorption, it shows extremely high uptake of CO₂ at very low partial pressures indicative of very strong binding. As such, solid-state cross-polarization magic-angle-spinning (CP/MAS) ¹³C NMR spectroscopy was used to monitor the material before and after exposure to CO₂. Upon introduction to CO₂, CD-MOF-2 shows a new peak at 158 ppm that was interpreted as the formation of carbonic acid functionality, due to a direct interaction between the CO₂ and surface hydroxyls. This additional resonance was also accompanied by chemical shifts of other signature peaks in the MOF supporting the hypothesis that a chemical reaction was occurring. Later, calorimetry revealed a zero coverage differential enthalpy of CO₂ adsorption equal to approximately -113.5 kJ mol⁻¹ at 25°C. This value quickly dropped to around -65.4 kJ mol⁻¹ binding event, which was attributed to less reactive hydroxyls and then another plateau at -40.1 kJ mol⁻¹ that was attributed to physisorptive-type interactions. It should be noted that the strongest binding sites appear to be irreversible; however, this only reduces the capacity slightly with cycling [222].

1.3.5 Stability and Competitive Binding in the Presence of H₂O

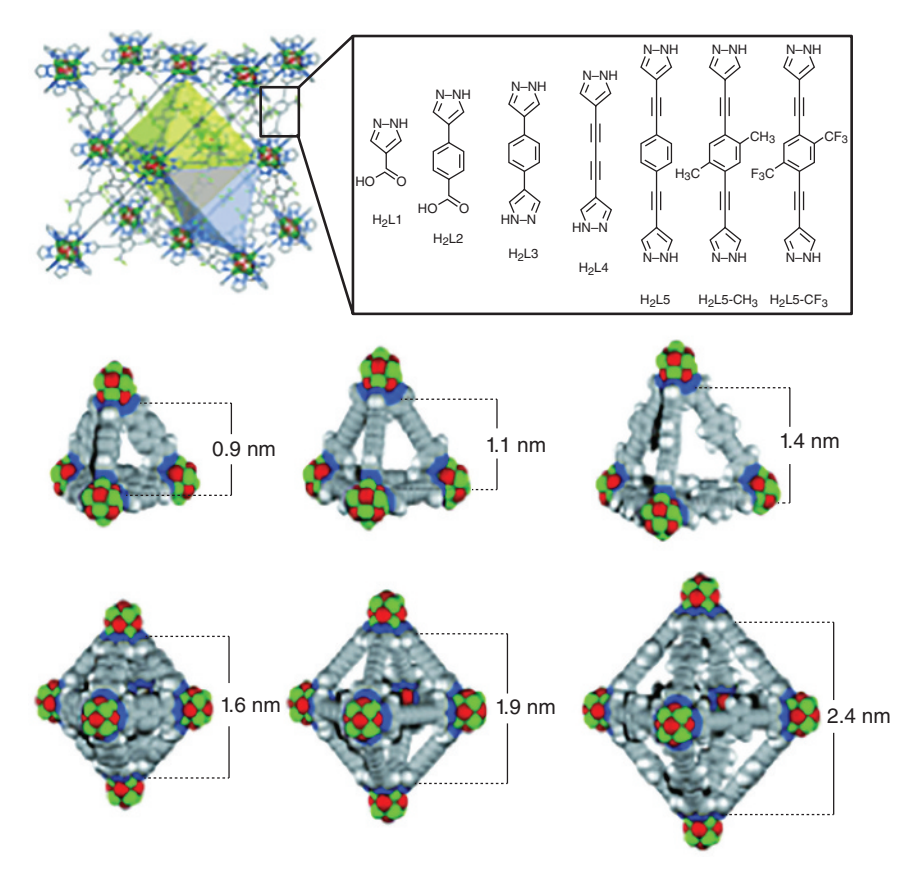
One of the major drawbacks for the utilization of MOFs in many applications is the widespread belief that they are unstable in the presence of water, a result of many reports that show frameworks that break down due to hydrolysis. While these materials do exhibit coordination-type bonding, that is considered to be weaker than that of their covalent counterparts, there have been many MOFs synthesized to date that exhibit water stability [223]. This effort has been driven by the need for materials that maintain high performance in wet environments, such as post-combustion flue gas separations. While the amount of water present in a flue gas stream could be reduced, it is energetically costly and complete removal is likely unfeasible [224]. As such, many synthetic strategies have been taken to provide water stable materials. These methodologies include the use of high oxidation state metals, multidentate ligands, metal nodes with large coordination numbers, MOF modification with hydrophobic ligands, guests or polymers, and the use of ligands with limited acidity, like pyrazoles and imidazoles [223, 225–232].

While many of the azole-based ligands can bind metals with similar geometries as carboxylates, the higher Lewis basicity creates stronger metal-ligand bonds improving both thermal and chemical stability. It is expected that MOF stability will increase with increasing pK_a to give the following stability trend: pyrazole > imidazole > triazole > tetrazole. A recent report of Long et al. reveals the synthesis of a new pyrazolate framework, $Ni_3(BTP)_2$ ($H_3BTP = 1,3,5$ -tris-1H-pyrazol-4-yl)benzene), which exhibits stability in boiling water for 14 days with varying pH levels that range from 2 to 14 [228]. Later, *in situ* IR studies revealed weak interactions of $Ni_3(BTP)_2$ with CO, CO₂, and H_2 . It is proposed that the pyrazolate ligand forces the Ni^{2+} into a diamagnetic low-spin state with a large energy barrier to transition from low spin to high spin of 75 kJ mol⁻¹, a value derived from *ab initio* molecular

modeling [233]. This low-spin state might also inhibit the interaction of the metal with water and hence add to the overall framework stability. While this study has focused on improving the strength of the metal-ligand bond other studies have added hydrophobic functionality to framework ligands such as $-CH_3$, $-CF_3$, and -F [234, 235]. A later study of Navarro et al. reports construction of an isoreticular series of MOFs denoted as $[Ni_8(OH)_4(H_2O)_2(L)_6]_n$ where L=a series of azolate ligands with increasing levels of hydrophobicity shown in Figure 1.22. Moreover, the length and functionalization of the linkers impact on the pore size as well as on the fine tuning of the surface polarity and the incorporation of trifluoroalkyl groups gives rise to a significant enhancement in the hydrophobicity and an overall improvement in hydrolytic stability. Although this study was mostly focused on overcoming problems related to the adsorption of harmful volatile organics in wet environments, these same principles can be applied to MOFs for various gas separation applications [236].

While the aforementioned studies worked to improve hydrolytic stability and hydrophobicity in the initial framework design, others have utilized post-synthetic modifications to manipulate these parameters. A recent report demonstrated that the encapsulation of HKUST-1 into polystyrene microspheres not only improved the hydrolytic stability of the framework, but additionally allowed retention of most of the CO₂ uptake capacity after exposure of the composite to 80% relative humidity at 27°C for 1 month [235]. This is a significant achievement considering that HKUST-1 readily decomposes in the presence of water, which coordinates to the Cu-OMC on the paddlewheel cluster, promoting hydrolysis of the metal–ligand bond and hence framework degradation [237].

For MOFs that exhibit highly charged functionality on their internal surface, such as OMCs, water will compete for adsorption sites with CO₂ and in most cases water will win this battle due to an existing dipole moment. As such, even if MOFs are deemed water stable, their separation performance must still be assessed in wet multicomponent streams or at minimum after exposure to water vapor. While Mg₂(dobdc) is currently the best-performing MOF at ambient pressure and dry conditions, it cannot be used for the capture of CO₂ under flue gas conditions due to diminished adsorption properties in the presence of water. In a study of Matzger et al., the breakthrough performance of a series of M_2 (dobdc) (where M = Zn, Ni, Co, and Mg) MOFs were evaluated in dry streams of CO₂:N₂ (0.16 bar and 0.84 bar, respectively) after exposure to relative humidity levels that range from 0% to 70%. For Mg₂(dobdc), after exposure to 70% RH and subsequent thermal regeneration, only about 16% of the initial CO₂ capacity was recovered. While the other metal-analogs experienced less of a performance decline, it is clear that in the event that water does not cause framework decomposition, it will be in competition for the OMCs and with further cycling the materials will become saturated [106]. Subsequent removal of water adsorbed at the OMCs can often be energy intensive, requiring high heat and vacuum. This work was additionally supported by a recent study of Mason et al., which carried out multicomponent adsorption studies of several MOFs in CO₂/N₂/H₂O mixtures. It was found that for every OMC containing MOF



<u>Figure 1.22</u> (a) The crystal structure of [Ni8(OH)4(H2O)2(L5-CF3)6]_n viewed as a combination of n octahedral (yellow polyhedron) and 2n tetrahedral (gray polyhedron) cavities. (b) Pyrazolate-based ligands used in the synthesis of the [Ni8(OH)4(H2O)2(L)6]_n MOFs. H2L1 = 1H-pyrazole-4-carboxylic acid; H2L2 = 4-(1H-pyrazole-4-yl)benzoic acid; H2L3 = 4,4'-benzene-1,4-diylbis(1H-pyrazole); H2L4 = 4,4'-buta-1,3-diyne-1,4-diylbis(1H-pyrazole); H2L5 = 4,4'-(benzene-1,4-diyldiethyne-2,1-diyl)bis(1H-pyrazole); and H2L5-R (R = methyl, trifluoromethyl). (c) View of the tetrahedral (top) and octahedral (tot) and octahedral (tot) and in the crystal structures of [Ni8(OH)4(H2O)2(L3)6]_n (tot), [Ni8(OH)4(H2O)2(L4)6]_n (tot), and [Ni8(OH)4(H2O)2(L5)6]_n (tot), and the corresponding metric descriptors. Ni, N, C, O, and F and H are depicted as green, blue, grey, red, and white spheres, respectively. Source: Padial et al. 2013 [236]. Reproduced with permission of John Wiley & Sons.

studied, that the low-pressure CO₂ adsorption capacity decreased significantly compared to the capacities in pure streams of CO₂ (Figure 1.5) [87]. To alleviate this problem, appending amines to the OMCs, which are known to preferentially bind CO₂, even in the presence of water, can be a useful solution. Given that the amine

appended frameworks are likely hydrophilic due to the high concentration of functional groups that readily form hydrogen bonding interactions, it also promotes water adsorption inside of the MOF that could inadvertently induce structural changes or simply decrease the overall capacity. As such, there is still a need to assess the separation ability of many amine-appended frameworks in wet streams [238]. However, it should be noted that the aforementioned study of Mason et al., also probed several alkyl amine-containing frameworks using multicomponent adsorption. For every amine-containing MOF studied, the decreases in the CO₂ adsorption capacities are minimal in the presence of water (Figure 1.5). Even in some cases, a slight increase can be observed upon the introduction of water.

Recently, an alternative strategy for achieving water stability was reported by Cohen et al., who introduced polyMOFs, which are constructed by ligands with long hydrophobic polymeric chains. Some of these polyMOF materials are shown to exhibit relatively high CO₂ sorption with minimal N₂ sorption, making them promising materials for CO₂/N₂ separations. Although the parent MOFs are generally unstable to water, the polyMOFs demonstrated excellent water stability due to the hydrophobic polymer, as well as the cross-linking of the polymer chains within the MOF. Further, the polyMOFs exhibit minimal change in their CO₂ adsorption properties before and after water exposure [239]. While many of the studies focused on enhancing water stability and assessing the performance of MOFs in wet environments are still in their infancy, this work has already led to significant improvements in materials performance providing optimism toward the eventual implementation of MOFs in various energy-relevant gas separations.

1.4 MOFs FOR PRE-COMBUSTION CAPTURE

1.4.1 Advantages of Pre-combustion Capture

Pre-combustion capture, which primarily involves the separation of CO_2 from H_2 and a few other impurities, has several advantages over other carbon-capture technologies. First, the separation is carried out at high pressure ranging from 5 to 40 bar [81] with much higher CO_2 concentrations. As a result, it will be less energy intensive to regenerate the material. The high pressure allows implementation of a PSA-type regeneration process where the pressure is simply dropped to atmospheric, eliminating the need to heat the material through a temperature swing process, as in post-combustion capture. Further, the actual separation of CO_2 from H_2 is significantly easier due to much larger disparities in their chemical properties such as polarizability and quadrupole moment for CO_2/H_2 compared to CO_2/N_2 and O_2/N_2 in post-combustion and oxy-fuel processes (Table 1.2). These differences provide much higher selectivity for CO_2 over H_2 in solid adsorbents allowing the separation to be done using a purely physisorptive process. All of these added benefits could allow a more rapid development of separation materials and their subsequent implementation into industrial separations.

Currently, the separation of CO_2 and H_2 is already carried out on extremely large scales worldwide, 50 million tons per year, for the purification of H_2 which is used primarily in the production of ammonia and various hydrocarbons [240]. This process is typically carried out via PSA with solid adsorbents such as activated carbons or zeolites [84]. While the process is still too energetically inefficient to make pre-combustion capture economically viable, significant improvements in the efficiency of solid adsorbents for the separation of CO_2/H_2 could render the technology workable on a large scale or provide further energy savings in existing hydrogen purification infrastructure worldwide. It is projected that a 10% energy savings in already implemented hydrogen purification industries would be the equivalent of closing 18 coal-fired power plants [88]. The already existing infrastructure for hydrogen purification and the scale with which this separation is already carried out, implies that the implementation of pre-combustion capture could be expedited relative to post-combustion and oxy-fuel technologies.

1.4.2 Necessary Framework Properties for CO₂ Capture

Most of the energy expended in the separation of CO_2 and H_2 is related to mass transport of the gas and PSA regeneration process. As such, much energy savings could be realized through an improvement in the selectivity and working capacity of the solid adsorbent. Working capacity is defined as the difference between the amount of gas adsorbed at the flue gas stream pressure and the amount of gas adsorbed at the regeneration pressure. High gravimetric and volumetric working capacity lowers the amount of material required and/or size of the fixed bed for the separation and hence also lowers the overall energy input for the PSA regeneration process.

Other factors to be considered when selecting materials for pre-combustion capture should include their long-term stability and that their separation properties are maintained in the presence of other minor impurities in a flue gas stream such as CO, H_2O , and H_2S . While there are many studies assessing the hydrolytic stability of MOFs previously mentioned, little is known about their behavior in H_2S . Only a few studies are included in the literature; in one of these Eddaoudi et al. show that SIFSIX-3-Ni (SIFSIX = hexafluorosilicate) MOF has high selectivity for CO_2 and is stable in the presence of H_2S [241]. Further, De Weireld et al. have studied H_2S adsorption in a series of MIL-frameworks. They show that two MOFs, including MIL-53(Al, Cr) and MIL-47(V), maintain their methane adsorption properties after H_2S treatment, whereas MIL-100 and MIL-101 show significant decreases in their CH_4 adsorption capacities [242].

Considering our limited ability to tune the pore size, pore shape, and surface functionality of activated carbons and zeolites, it is expected that only minor improvements can be made regarding their efficiency of the separation could be realized. Indeed, MOFs already offer record-breaking capacity for CO₂ adsorption in the pressure regime of interest for pre-combustion capture [85, 105, 243–245]. To date, the highest high pressure carbon dioxide adsorption belongs to NU-11 with the absolute uptake of 856 cm³ per gram of MOF at 30 bar and 25°C. Further, the

facile structural tunability of MOFs can allow significant improvements in binding strength of CO₂ and hence the selectivity of CO₂ over H₂. Last, their unprecedented internal surface areas, a factor of strong importance for high-pressure separations, offer significant promise with regard to this separation [88, 246–250].

1.4.3 Potential MOF Candidates for CO₂/H₂ Separations

To date, while there are a number of studies looking at high-pressure CO_2 adsorption (up to 50 bar) in MOFs, there are very few studies focused specifically on assessing their properties for hydrogen purification or pre-combustion capture. Currently, more work is needed to assess the properties of existing frameworks and in turn gain more insight into the structural features that give rise to enhanced separation ability of CO_2/H_2 in MOFs. For the most part, current CO_2/H_2 studies are limited to a few frameworks and are based on the use of single-component CO_2 and H_2 adsorption isotherms to estimate the separation ability of the MOFs in question.

The first experimental study of MOFs for CO₂:H₂ separations by PSA was carried out by Herm et al. This work features single-component adsorption isotherms for a series of 5 MOFs, which are further compared to state of the art separation materials including zeolite 13X and activated carbon JX101 [88]. The MOF series were comprised of two frameworks with OMCs and modest surface areas, i.e. Mg₂(dobdc) (1800 m² g⁻¹) [62] and Cu-BTTri (1750 m² g⁻¹) [151], two frameworks with high surface areas and no polarizing functionality, i.e. MOF-177 (4690 m² g⁻¹) [245] and Be-BTB (4400 m² g⁻¹, BTB = benzene-1,3,5 tribenzoate) [42], and one flexible framework, Co-BDP (2030 m² g⁻¹, BDP = 1,4benzenedipyrozolate) [251]. Single-component adsorption isotherms were collected for H₂ and CO₂ at pressures up to 40 bar and 40°C and then IAST was used to estimate the materials behaviors in a binary mixtures of 80:20 or 60:40 H₂:CO₂. It was revealed that the materials with highly polarizing functionality on their internal surface such as the OMC-containing MOFs and zeolite 13X yielded much higher selectivities, between 75 and 859. This was also true for the activated carbon and was rationalized based on the small pores and overlapping van der Waals potential. Although the MOFs with high surface areas and no polarizing functionality show appreciable CO₂ uptake at high pressures compared to the other materials assessed, they have shown inadequate selectivities of significantly less than 10 (Figure 1.23a), limiting their performance in an actual separation process. In addition to selectivities, the gravimetric and volumetric working capacities were also estimated from IAST (Figures 1.23b and 1.23c). Further, if we consider the MOF with the highest selectivity among those tested in this work (Figure 1.23a) Mg₂(dobdc), the gravimetric and volumetric working capacities can even climb up to 6.4 and 5.9 mol per kg or mol per Liter, respectively. It is suggested that if the separations are carried out in the high pressure regime with Mg₂(dobdc) replacing zeolite 13X, then the mass and volume of the required adsorbent would be decreased by a factor of 2 and 2.7, respectively. This study shows while materials with high surface areas can have high adsorption capacities, adsorbents with polarizing functional groups lend to higher

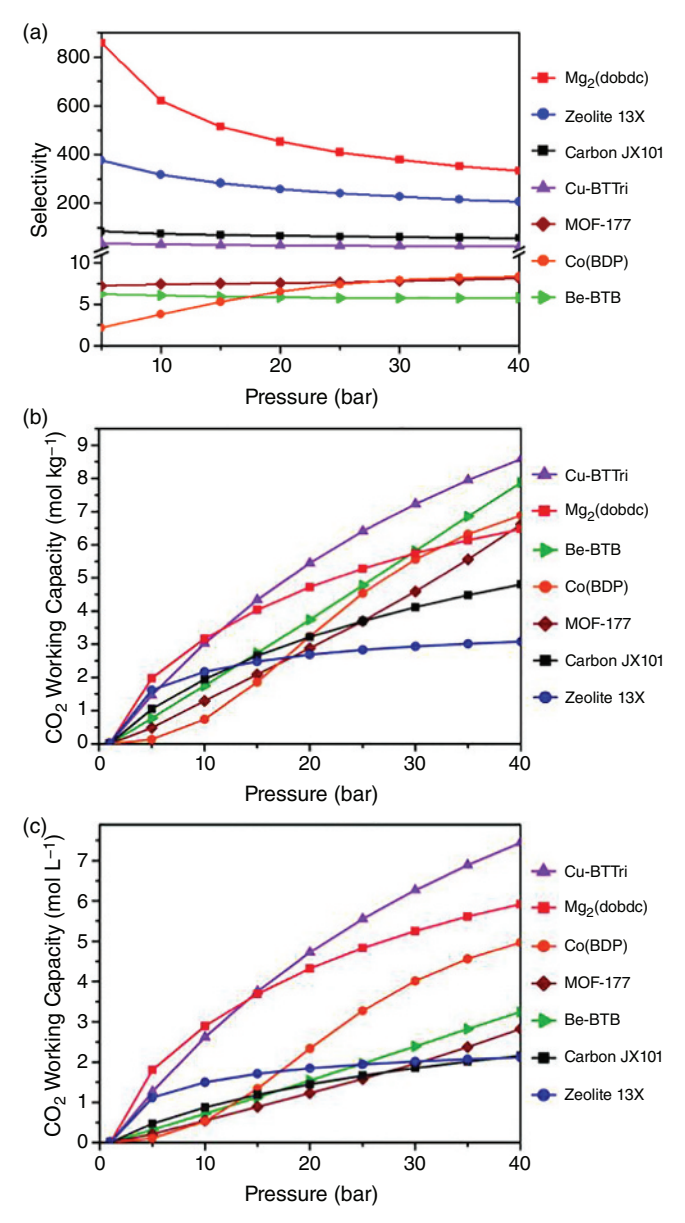


Figure 1.23 IAST-calculated (a) selectivity, (b) gravimetric, and (c) volumetric CO_2 working capacities for an 80:20 H_2/CO_2 mixture at 40°C for the metal-organic frameworks MOF-177, Be-BTB, Co(BDP), Cu-BTTri, and Mg_2 (dobdc), the activated Carbon JX101 and zeolite 13X. Source: Herm et al. 2011 [88]. Reproduced with permission of American Chemical Society.

CO₂:H₂ selectivities and enhanced performance with regard to working capacity. This study is further the proof of the concept that MOFs can indeed potentially outperform the state of the art materials [88].

In light of the previous work, Vaidhzanathan et al. began working with small framework ligands for the synthesis of ultramicroporous MOFs [250]. They were inspired by the knowledge that OMCs are susceptible to poisoning by even trace amounts of water. As such, they began to look at a small pore material without OMCs, Ni-(4-pyridylcarboxzlate)₂ (Figure 1.24a) that might lend to overlapping van der Waals potential and hence high selectivities as in the case of the aforementioned carbon. This Ni-MOF exhibits a cubic framework with ultramicropores ranging

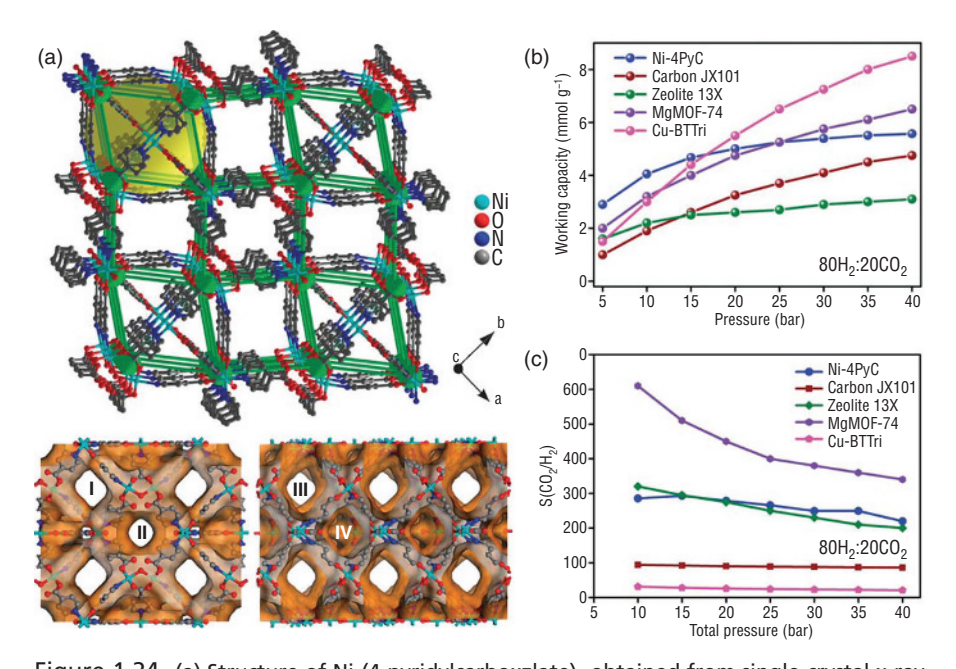


Figure 1.24 (a) Structure of Ni-(4-pyridylcarboxzlate)₂ obtained from single-crystal x-ray structure green, Ni dimers reduced to one node. The green cones trace the six-connected distorted cubic arrangement formed by collapsing the Ni dimers to nodes and the PyC linkers as lines. The yellow ball represents the cages in the structure. Below the structure is the Connolly surface diagram. The channels labeled I and III are interconnected and run along the a and c axes, respectively, whereas the channel labeled II propogate along the c axis. IV represents the cages, which are lined with terminal water molecules in addition to the ligand groups. (b) IAST working capacities and (c) selectivity characteristics from a 20:80 mixture of CO_2 : CO_2 : CO_3 at CO_4 : CO_4 at CO_4 : CO_4 :

from 3.5 to 4.8 Å, labeled I–IV in Figure 1.24a. High pressure adsorption isotherms, collected up to 10 bar at 40°C, were used to calculate the IAST selectivities and capacities for a 1–10 bar PSA process. The results show that the selectivities of the material is 285 and 230 for 20:80 and 40:60 CO₂:H₂ mixtures, respectively, and despite a modest surface area (945 m² g⁻¹), the gravimetric capacity is relatively high, 3.95 mmol per gram of MOF (Figure 1.24b). While the selectivities are lower than Mg₂(dobdc), they are similar to those observed for zeolite 13X. Further, the gravimetric working capacity bests all materials analyzed by Herm et al. (at 10 bar) and more importantly Ni-(4-pyridylcarboxzlate)₂ is shown to retain its CO₂ adsorption properties after exposure to H₂O. Last, the CO₂ self-diffusivities (3 × 10⁻⁹ m² s⁻¹) were determined to be as much as two times higher than zeolite 13X and comparable to the top performing CO₂ adsorbing MOFs [250].

Other experimental studies have included one by Chen et al. that form a NbO-type MOF referred to as UTSA-40 (1630 m² g⁻¹, also known as $[Cu_2(L)(H_2O)_2] \cdot 6DMF \cdot 2H_2O$ where L = 6,6-dichloro-2,2-diethoxy-1,1-binaphthyl-4,4-di(5-isophthalic acid)) that consists of a tetracarboxylate ligand and dicopper paddlewheel cluster. The authors found that the material outperforms several traditional zeolites, and while the performance is lower than two OMC-containing MOFs, including $Mg_2(dobdc)$ [62] and Cu-TDPAT [148], this framework has a significantly lower energy cost for regeneration [238].

One weakness in many of the aforementioned studies is the lack of assessment of the materials performance in the presence of other impurities in the flue gas stream such as H₂O, H₂S, CO, and CH₄ (the latter in the case of methane reforming). The adsorption behavior of each impurity can vary widely in MOFs as it is dictated by the pore size, shape, and surface functionalization. It is expected, for instance, that H₂O, H₂S, and/or CO could poison the OMCs and block the adsorption of CO₂. While most of the water could be removed by condensation or other adsorbents placed in route to the fixed bed intended for CO₃/H₂ separation, it is likely that all of these impurities cannot be removed from the flue gas stream. As such, a more thorough assessment of materials performance in multicomponent streams is needed. Ideally a study would include both the adsorption properties in the multicomponent gas stream containing all potential impurities. The best way to test these properties is via experimental or simulated breakthrough curves. Because experimental breakthrough analysis containing very minor impurities or mixtures of more than two or three components can be extremely time-consuming or in some cases experimentally intractable, Krishna et al. have used computational methods to simulate breakthrough curves for a number of MOFs, zeolites, and carbons in the tertiary mixture, CO₂/CH₄/H₂ and their binary combinations [252]. Their study revealed the utility of breakthrough simulations for MOFs and further implied that Mg₂(dbodc) was the top performer of the materials tested under dry conditions. As such, this work was followed by an experimental one of Herm et al. for validation of the computational methods [253]. For this, breakthrough curves were generated for Mg₂(dobdc) in several multicomponent streams including CO₂/CH₄, CH₄/H₂, and CO₂/CH₄/H₂ [253]. The experiment not only validated the aforementioned simulations, but also showed that this MOF additionally outperformed zeolite 13X for all three-gas mixtures. Later, Wu et al. simulated several MOFs and zeolites in quaternary mixtures including CO₂/CO/CH₄/H₂ and identified a new pre-combustion capture candidate, Cu-TDPAT [254] and then Banu et al. carried out simulations for a quinary mixture including CO₂/CO/CH₄/H₂/N₂ for a series of four Zr-containing MOFs [255].

The results of these studies suggest that MOFs with small pores and open metal-sites, or other sources of charged functionality could be used to achieve both high selectivity and working capacity necessary to improve the efficiency of the CO₂:H₂ separation. However, considering the few number of data points, more work is needed to screen a large number of existing MOFs with varying structural features to gain more clarity related to their structure-derived function. Studies of this kind will provide insight into how to find the intricate balance between strength of CO₂ adsorption and high working capacity. Additionally, while it is clear that MOFs have a high potential to outperform the state of the art zeolites or activated carbons, more understanding of MOF properties in flue gas mixtures containing minor impurities must be obtained.

1.5 MOFs FOR OXY-FUEL COMBUSTION CAPTURE

1.5.1 Necessary Framework Properties for O₂/N₂ Separations

The implementation of oxy-fuel combustion in the power industry is limited by an adequate, low-cost gas separation technology for the separation of O₂ from air. Currently, air purification, which predominately involves the separation of O₂ from N₂, is most widely carried out via cryogenic distillation; while it provides high purity O₂ (99%), due to very low boiling points of O₂ and N₂ (-196°C and -183°C for N2 and O2, respectively), it also poses a large energy and economic cost for execution on the scale that is necessary for CCS. As such, other technologies have been studied; these included various adsorbents like zeolites and activated carbons and membrane-based separations. All of these aforementioned technologies can be implemented; they are limited to processes that can utilize O₂ at a purity level that is less than 94%, a direct result of limited selectivity for N₂ over O₂ [84]. The development of adsorbent materials that exhibit higher selectivities (lending to O₂ purity levels >95%) and are also operational at ambient temperature and pressure could afford significant energy savings. Compared to post-combustion and pre-combustion technologies, the capture step for an oxy-fuel process is relatively easy, using existing condensation protocol to isolate CO₂ (55–65 wt%) from water (25–35 wt%) after the combustion process [256]. As such, existing power plants could be easily retrofitted to accommodate this process, which has shown capture rates of CO₂ on the order of 95%, a value significantly higher than pre- or post-combustion capture technologies [257]. In addition to easy implementation, the O_2 stream used for combustion in an oxy-fuel process is first diluted with CO_2 to a partial pressure of approximately 0.21 bar to control the flame temperature, an act that limits the formation of NO_x impurities [258].

The most energy consuming part of the oxy-fuel process is generating large quantities of nearly pure O₂ [259] from air whose main component is N₂. As such, separation materials must show high selectivities and capacities for O2 in the pressure and temperature regime of interest, which is approximately 0.2 bar and 25°C. The modularity of MOFs makes them ideal candidates for this separation; however, compared to CO_2 and N_2 discussed in the previous section, O_2 and N_2 have even smaller disparities in their physical properties including kinetic diameter, quadrupole moment, polarizability, and boiling point, creating a challenge for the design of adsorbents. Looking at Table 1.2, the polarizability and quadrupole moment of N_2 is slightly higher than O₂, making most framework materials like MOFs and zeolites with highly polarizing adsorption sites only slightly more selective for N₂ over O₂. This will cause the selectivities and hence resulting O₂ purity to be quite low. As such, recent efforts in MOF chemistry are instead focused on the differences in the chemical properties of O₂ and N₂. Of these two small molecules, O₂ exhibits a significantly higher electron affinity than N₂ making redox active MOFs that might give rise to a reversible electron transfer to O₂ of great interest for oxy-fuel combustion.

1.5.2 Biological Inspiration for O₂/N₂ Separations in MOFs

Knowledge of the reactivity of O₂ with transition metal complexes is not new as this property is exploited in heme containing metaloproteins that are responsible for transport and storage of O2 in mammalian systems. Heme species, also known as porphyrins, are a group of heterocycles composed of four modified pyrrole subunits with Fe²⁺ bound in the center (Figure 1.25a). Much research has been dedicated to producing synthetic molecular complexes that can mimic the reversible O₂ binding observed in nature; [84] however, these molecular species have a strong propensity to react and combine upon formation of the metal-O₂ complex making them highly difficult to isolate [260]. The instability of the mononuclear species has prompted the development of porphyrin-based supports that provide isolation of the reactive species to inhibit their decomposition and allow experimental observation of the porphyrin-O₂ adduct [29]. While observation of this species has been limited to spectroscopic evidence at low temperature, recent work of Harris et al. used a heme-based Zr-MOF, PCN-224 [261], to give the first crystallographic evidence of a five-coordinate heme-O₂ adduct (Figure 1.25b) [262]. Relative to their molecular counterparts, MOFs contain immobilized, separated active sites and offer facile structural tunability, allowing control over important metrics such as binding enthalpy and adsorption capacity for O₂ and regeneration conditions. Further, given their highly crystalline nature, crystallography techniques can be used to unveil their structure-derived function. As such, MOFs provide an ideal platform to study O₂ adsorption and separation.

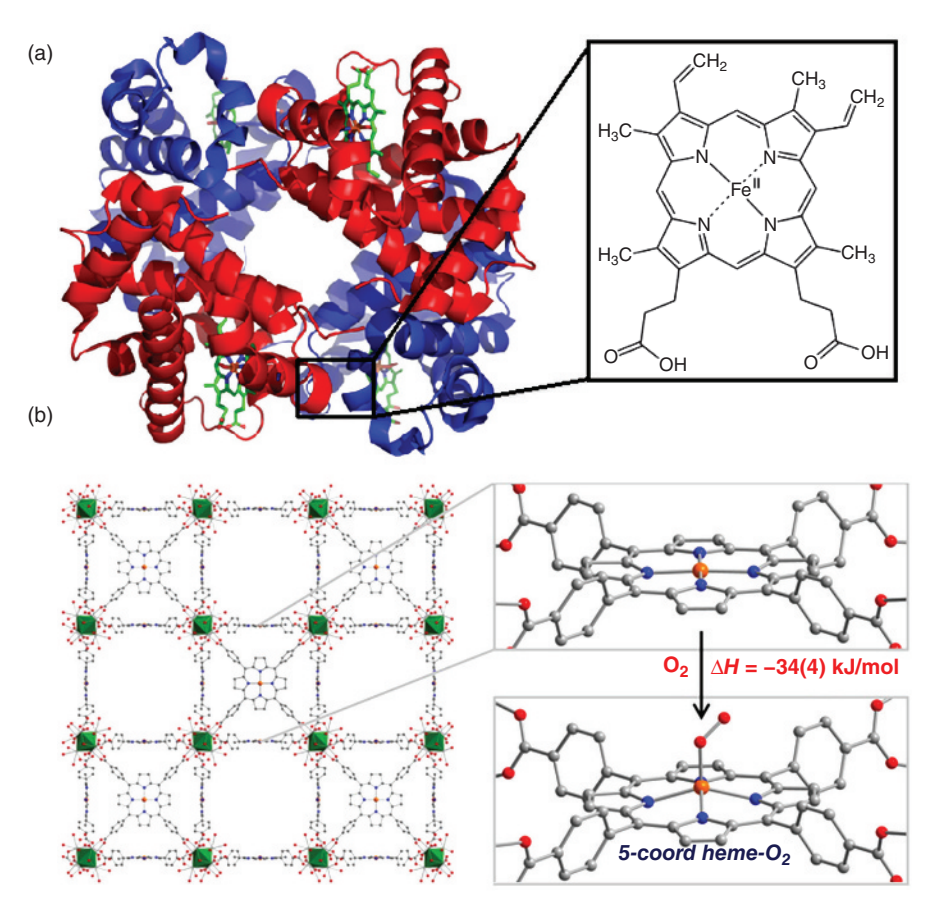
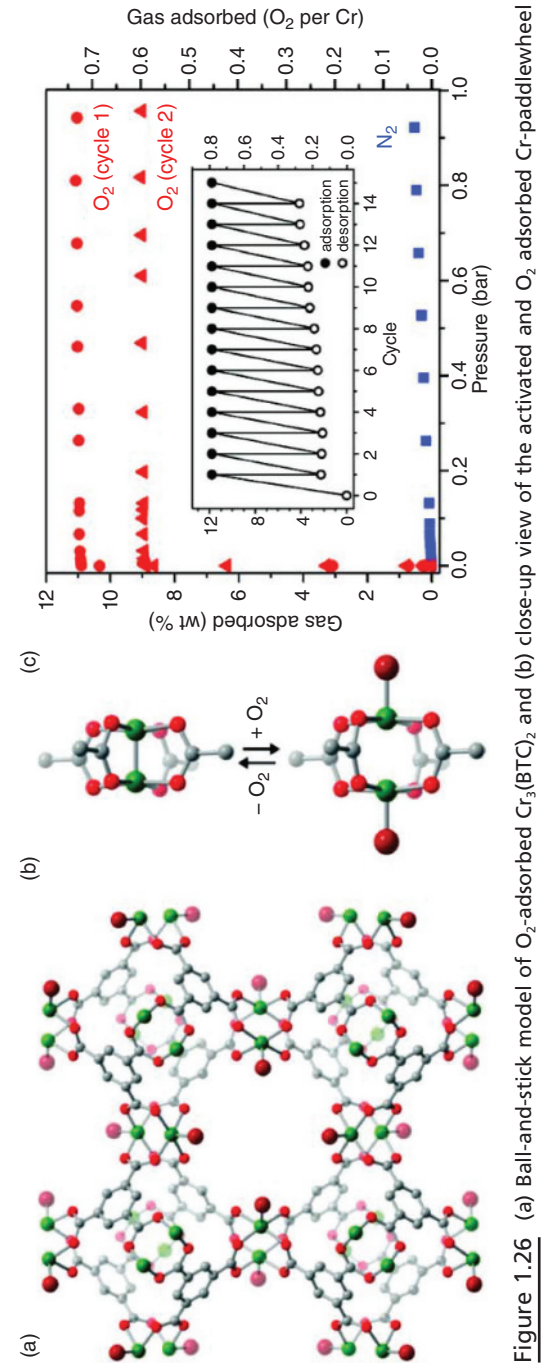


Figure 1.25 (a) Heme-based metaloprotein and (b) PCN-224-Fe (*left*), which forms PCN-224-Fe- O_2 at -78° C (*right*). The structure consists of Zr₆ clusters interlinked by TCPP ligands (where TCPP = tetrakis(4-carboxyphenyl)porphyrin. Green octahedra represent Zr atoms; Fe, N, O, and C atoms are represented by orange, blue, red, and gray spheres, respectively. The distances and angles for PCN-224-Fe- O_2 are Fe-O 1.79(1), O-O 1.15(4), Fe-··N₄ plane 0.526(2), Fe-O-O 118(4), N-Fe-O 104(1). *Source:* Anderson et al. 2014 [262]. Reproduced with permission of American Chemical Society.

1.5.3 Potential MOF Candidates for O₂/N₂ Separations

While studies related to O_2 adsorption are still limited, over the last few years, there have been several reports that show O_2 adsorption in redox active OMC-containing MOFs. These materials are thus far limited to a few SBUs constructed by metals such as Cr^{2+} , Fe^{2+} , and Ti^{3+} , all of which have a propensity to undergo redox activity in the presence of oxygen. One of the first studies of O_2/N_2 adsorption in a redox active MOF was carried out on $Cr_3(BTC)_2$ ($BTC^{3-} = 1,3,5$ benzenetri-carboxylate) (Figures 1.26a and 1.26b) [203]. The material, which is isostructural with the



where the large red spheres represent bound O₂ molecules. The structures were obtained from Rietveld refinement of powder neutron Upon evacuation, the O_2 isotherms reveal reduced capacity. The inset shows O_2 adsorption in $Cr_3(BTC)_2$ over 15 consecutive cycles at 25°C. Desorption was carried out by heating at 50°C under vacuum for 48 h. *Source:* Murray et al. 2010 [203]. Reproduced with permission of diffraction data. (c) Uptake of O_2 and N_2 by $Cr_3(BTC)$, at 298 K. The compound saturates with O_2 at ~ 2 mbar but shows little affinity for N_2 . American Chemical Society.

aforementioned HKUST-1 and has a BET surface area of $1810 \text{ m}^2 \text{ g}^{-1}$, displayed both a high O_2 loading capacity and high selectivity, ≈ 22 , for binding O_2 (0.73 mmol per gram O_2 at 0.21 bar) over O_2 (0.033 mmol per gram O_2 at 0.78 bar) at 25°C; however, the material showed a significant loss in capacity with cycling (Figure 1.26c) [203].

More recently, this same group studied O₂ and N₂ adsorption in a redox active Fe₂(dobdc) [82] (Figure 1.27a), which has a BET surface area of 1360 m² g⁻¹ and features a hexagonal array of one-dimensional channels lined with coordinatively unsaturated Fe²⁺ OMCs. Single-component gas adsorption isotherms collected at 298 K indicate that this framework binds O₂ preferentially over N₂ (Figure 1.27c); however there is an irreversible capacity of 9.3 wt%, corresponding to the adsorption of 0.5 O₂ molecule per Fe²⁺-OMC. Upon cooling the material to 211 K, O₂ uptake becomes fully reversible and the capacity increases to 18.2 wt%, a value that corresponds to the adsorption of one O₂ molecule per Fe²⁺-OMC. Several techniques, including Mössbauer spectroscopy, infrared spectroscopy, and neutron powder diffraction were used to investigate this crossover from the physisorption (211 K) to the chemisorption regime where O₂ adsorption becomes irreversible. All characterization pointed to a partial charge transfer from Fe²⁺ to O₂ at low temperature and a complete charge transfer to form Fe3+ and O22- at room temperature. Rietveld analysis of powder neutron diffraction data confirms this interpretation, revealing O₂ bound to Fe in a symmetric side-on configuration with an O-O distance of 1.25(1) Å at low tempearture, labeled as site I in Figure 1.27b. This value is only slightly elongated compared to the distance found in a free O₂ species (1.2071(1) Å) [263]. Neutron diffraction carried out after the exposure of Fe₂(dobdc) to O₂ at room temperature reveals a different structure with the O₂ species in a slipped side-on mode with O-O distance of 1.6(1) Å (Figure 1.27b), a value that is consistent with a two electron reduction of O₂ to a peroxide species. These measurements also unveiled two secondary adsorption sites at low temperatures labeled as II and III in Figure 1.27a. Simulated breakthrough curves, which were calculated via single-component gas adsorption isotherms and IAST, indicate that the material should be capable of the high-capacity separation of O₂ from air at temperatures as high as 226 K, well above the current temperatures employed in cryogenic distillation [82].

 $Cr_3(BTC)_2$ and $Fe_2(dobdc)$, are representative members of large isostructural framework families that have been synthesized with a wide number of transition metal cations $(M_3(btc)_2$ where M = Cr, Fe, Ni, Cu, Zn, Mo, or Ru [201–206] and $M_2(dobdc)$ where M = Mg, Mn, Fe, Co, Ni, Cu, or Zn [99, 105, 112, 113, 135, 194–196]). Despite this, no other material in the framework families has shown utility in the separation of O_2 from N_2 . As such, recent work of Bloch et al. have explored a new framework family known as M-BTT with the sodalite-type structure, $M_3[(M_4 Cl)_3(BTT)_8]_2$. While the aforementioned MOF family has also been synthesized with a variety of M^{2+} OMCs (M-BTT) where M = Mn, Fe, Co, Cu, Cd); only the most recently synthesized Cr^{2+} analog (with a BET surface area of 2300 m² g⁻¹) shows

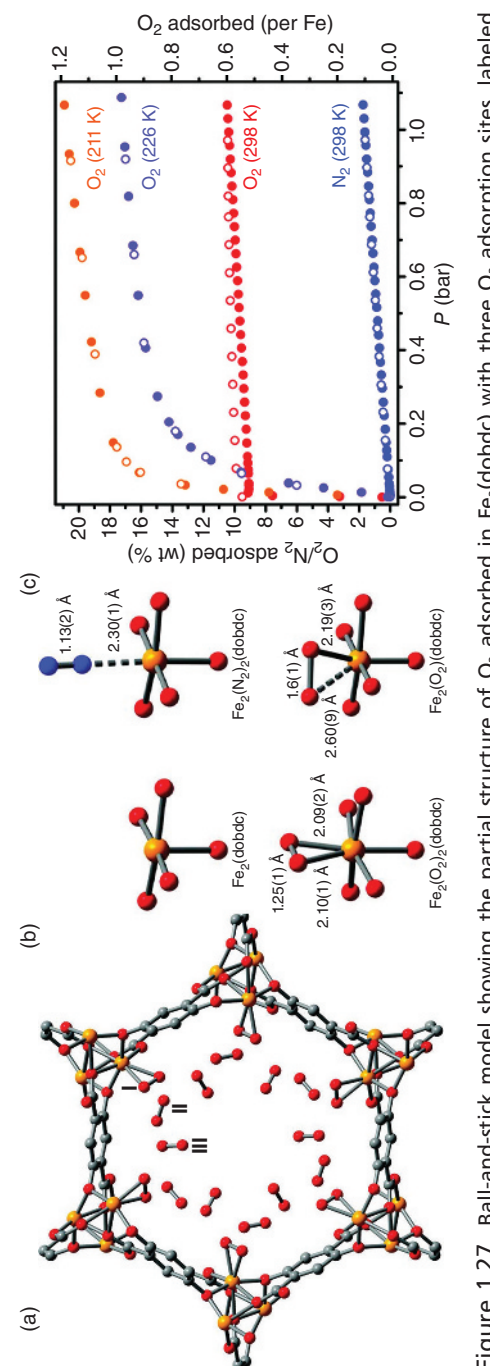


Figure 1.27 Ball-and-stick model showing the partial structure of O₂ adsorbed in Fe₂(dobdc) with three O₂ adsorption sites, labeled as I-III. Site I is bound in a side-on fashion to the Fe-OMC. (b) A close-up view of the Fe-OMC after activation and then after dosing with N, and O₂. The structures are for samples under vacuum (*upper left*), dosed with N, at 100 K (*upper right*), dosed with O, at 100 K (*lower* (eft), and dosed with O₂ at 298 K (Jower right). All structures were determined via Rietveld analysis of neutron powder diffraction data. Orange, blue, and red spheres represent Fe, N, and O atoms, respectively. All diffraction data were collected below 10 K. (c) Adsorption isotherms collected for Fe, (dobdc) at 211 (orange), 226 (purple), 298 K (red), and N, adsorption at 298 K (blue). Filled and open circles represent adsorption and desorption, respectively. Source: Bloch et al. 2011 [82]. Reproduced with permission of American Chemical Society.

utility in O_2/N_2 separations (Figure 1.28a) [133]. The single-component adsorption isotherms indicated a high selectivity for O_2 over N_2 as the material has a reasonably high O_2 uptake of 7.01 wt% at 0.2 bar and 298 K and a low adsorption capacity for N_2 , which is less than 0.6 wt% at 0.8 bar and 298 K (Figure 1.28b). Consistent

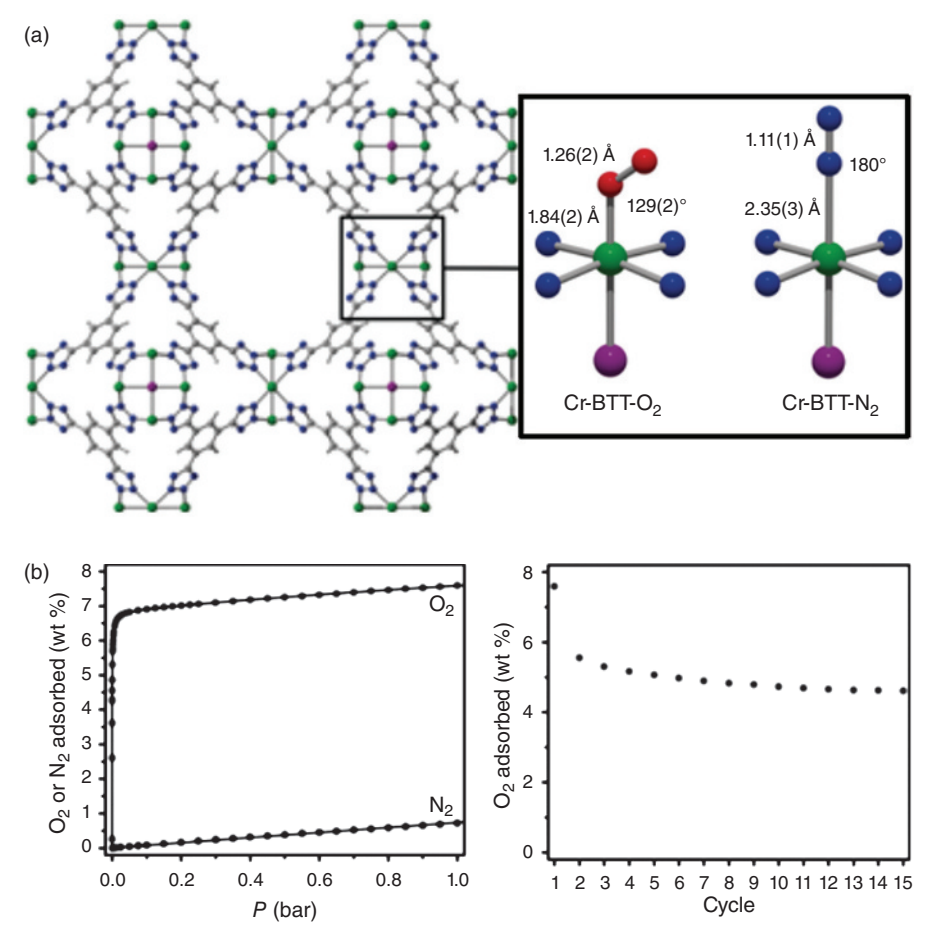


Figure 1.28 (a) Ball-and-stick model of Cr-BTT and the first coordination spheres for the Cr centers within O₂- and N₂-dosed Cr-BTT as determined from Rietveld analysis of powder neutron diffraction data. Atom colors: Cr dark green, Cl purple, O red, N blue. Values in parenthesis give the estimated standard deviation in the final digit of the number. (b) Excess O₂ and N₂ adsorption isotherms collected for Cr-BTT at 298 K; the solid lines represent Langmuir–Freundlich fits to the data. *Bottom*: Uptake of O₂ at 200 mbar in Cr-BTT over 15 cycles at 298 K. Adsorption experiments were performed over 30 min and desorption was carried out by placing the sample under a dynamic vacuum at 423 K for 30 min. *Source*: Bloch et al. 2016 [133]. Reproduced with permission of John Wiley & Sons.

with the significantly higher O₂ capacity compared to N₂, the material exhibits an isosteric heat of -65 kJ mol⁻¹ and -15.3 kJ mol⁻¹ for O₂ and N₂, respectively. IAST calculations reveal that the material has a selectivity factor greater than 2500 under conditions necessary for O₂ separation from air. As shown in Figure 1.28b, Cr-BTT displays only a moderate capacity loss after the first adsorption/desorption cycle, with a decreased uptake from 7.01 wt% to 5.6 wt%. After the second cycle, the capacity drops a bit further to 4.6 wt%, but then appears to plateau for the next 13 consecutive cycles. Despite this slight loss in capacity, the material shows rapid adsorption/desorption and a reversible capacity of 4.6 wt%. While the capacity loss is not yet fully understood, several in situ techniques were employed to understand the O₂ binding mechanism. Infrared spectroscopy and neutron diffraction were again used to show experimental evidence of the electron transfer to form a Cr³⁺ superoxo species. The diffraction data are consistent with what was observed in the IR spectrum, showing an end-on coordination of the guest species and a Cr-O₂ distance of 1.84(2) Å, a value that is in excellent agreement with other previously reported Cr³⁺-superoxo species (1.876(4) Å) [264]. As observed in the case of Fe₂(dobdc), the O-O distance is slightly elongated to 1.26(2) compared to free O_2 , consistent with the formation of a superoxo. Further, Cr-N and Cr-Cl distances decrease from 2.064(3) Å and 2.57(2) Å to 2.026(4) Å and 2.52(2) Å, upon oxidation from Cr²⁺ to Cr³⁺, respectively [133].

All of the aforementioned work demonstrates the importance of having redox active OMCs in MOFs for selective separations of O_2 over N_2 . While this work is dependent on existing framework families that can undergo metal substitution, there is a lot of room for further MOF development for air purification through the use of (i) metaloligands, which may offer a way to post-synthetically decorate MOF surfaces with under coordinated metals or (ii) through the infusion or appendage of other metal-containing small moleucles on the internal surface of MOFs. A proof of concept for redox active MOF-composites was highlighted by Zhange et al., which infused a well-known Cr-MIL-101 with the redox active Fe²⁺ containing ferrocene molecule [265]. Heating the material above 350°C led to a transformation of the ferrocene into maghemite nanoparticles rendering a composite MOF materials that exhibited a high selectivity for O₂ over N₂. Experimental breakthrough obtained using a custom-built apparatus equipped with a residual gas analyzer (in a gas mixture of 0.21% O₂ and 0.79% N₂) showed N₂ breakthrough within 1 min, while O₂ required 40 min. At any rate, MOFs offer an unprecedented opportunity to tailor-make materials with controlled capacities, selectivities, and regeneration energies [265].

1.6 FUTURE PERSPECTIVES AND OUTLOOK

The previous sections have highlighted some of the recent progress made in the advancement of MOFs toward carbon-capture applications. While we have confirmed that there are a number of frameworks currently available for the efficient

separation of CO₂/N₂, O₂/N₂, and CO₂/H₂, there are still a number of factors that need to be addressed for their eventual implementation. More understanding of how MOF materials function in wet environments and in the presence of other minor impurities present in gas streams is a necessity. To achieve this, it will require experimentalists to characterize the materials in more application-relevant environments as in multicomponent adsorption and breakthrough analysis. Further, ongoing work should pay more attention to the temperatures and pressures necessary for the varying applications as these two factors vary a great deal throughout the literature, making it difficult on some occasions to gain an accurate comparison between two differing materials. Also, there are a number of reports that show disparities in measured values for various properties ranging from surface areas, adsorption capacities, selectivities, and isosteric heats. As such, more emphasis should be placed on sample quality and efforts should be made to understand how varying reaction conditions affect the crystallization and hence subsequent framework properties.

Once the more fundamental problems are addressed, it is expected that MOF chemistry will naturally gravitate away from the synthesis of new materials and look toward addressing more engineering-related issues. Some of these areas include: (i) material scale-up and cost analysis, (ii) nanostructuring materials for pelletization, (iii) the impact of pelletization on MOF performance, (iv) assessing their performance over many adsorption/desorption cycles, and (v) accurate determination of the energy penalty associated with MOF regeneration. While we know that the parasitic energy cost of liquid amine scrubbers is approximately 30%, to the best of our knowledge, there are no thorough studies addressing the energy penalty and economic cost related to MOF adsorbents and so it is a necessity for the future. It is assumed throughout the literature that these materials will have better performance due to lower heats capacities, but a number of factors must be considered. For instance, there is not a lot of information pertaining to MOF thermal conductivity [266], a parameter that dictates the efficiency of the adsorbent bed and the duration of the regeneration cycle of a TSA capture process. In the same regard, there are few studies addressing the desorption of CO₂ via PSA in any great detail either.

While it is not discussed to a large extent throughout this chapter, it should be noted that there are a number of developing computational tools that might allow accurate structure and property prediction in MOFs [267]. Advancements in this area could provide experimentalists with target frameworks that will perform well in predefined gas mixtures and hence deliver these materials more rapidly to industry [268]. Though progress has been made through cooperative work between theoreticians and experimentalists to understanding MOF–small molecule interactions, the rate at which theoretical tools are being actively used to provide optimized MOF targets remains slow. One challenge, for instance, is the difficulty of developing synthetic pathways toward a specific structure containing the desired building blocks or the inability to predict structural changes that occur with adsorption. While these challenges are large, the partnership between experimentalists and theoreticians is

becoming more prevalent throughout the literature and hence significant progress has been made in the area [83]. As such, we are confident that computational tools, including high throughput screening methods, could push MOF chemistry past the era of largely serendipitous discoveries and allow for engineering porous media for solving specific problems.

Given the huge scientific progress made in the last 10 years within MOF research, we have an optimistic outlook on MOF chemistry for their eventual implementation in a wide number of energetically relevant gas separations. Unprecedented internal surface areas, facile structural tunability, and the ease with which MOFs readily undergo post-synthetic modification clearly distinguish this class of materials from other porous counterparts. It is demonstrated throughout the literature that MOFs offer a unique opportunity for controlled design, allowing one to find the intricate balance necessary between a variety of properties such as selectivity, gravimetric and volumetric working capacity, regeneration energy, and framework stability, making them likely candidates for future carbon-capture technologies.

ACKNOWLEDGMENTS

This work was supported by the Swiss National Science Foundation under Grant PYAPP2_160581 and the Swiss Commission for Technology and Innovation (CTI).

REFERENCES

- McConnaughey, T.A., et al., Carbon isotopes in biological carbonates: respiration and photosynthesis. *Geochimica et Cosmochimica Acta*, 1997, 61(3):611–622.
- 2. Pierrehumbert, R.T., High levels of atmospheric carbon dioxide necessary for the termination of global glaciation. *Nature*, 2004, **429**(6992):646–649.
- 3. Victor, D.G., et al., *Mitigation of Climate Change*. Contribution of Working Group III to the Fifth Assessment Report of the Intergovernmental Panel on Climate Change. Cambridge University Press, New York, 2014.
- Culp, J.T., Flexible solid sorbents for CO₂ capture and separation. Novel Materials for Carbon Dioxide Mitigation Technology, 2015, 149.
- 5. Schultz, H., Climate change and viticulture: a European perspective on climatology, carbon dioxide and UV-B effects. *Australian Journal of Grape and Wine Research*, 2000, **6**(1):2–12.
- Sims, R.E., et al., Energy supply, in *Climate Change 2007: Mitigation*. Contribution of Working Group III to the Fourth Assessment Report of the Intergovernmental Panel on Climate Change. Cambridge University Press, 2007.
- 7. Eggleton, T., A Short Introduction to Climate Change, Cambridge University Press, 2012.
- Ritter, S.K., Global CO₂ breaches 400 ppm, American Chemical Society, Washington, DC, 2015.
- Greenhouse Gas Bulletin No. 8, World Meteorological Organization, Geneva, 2012, 1–3.

- 10. Birol, F. (ed.), CO₂ Emissions from Fuel Combustion, IEA Publications, Paris, France, 2015.
- 11. Metz, B., et al., *IPCC Special Report on Carbon Dioxide Capture and Storage*, Cambridge University Press, Cambridge, 2005.
- 12. Rochelle, G.T., Amine scrubbing for CO₂ capture. *Science*, 2009, **325**(5948):1652–1654.
- 13. Awais, M., Determination of the mechanism of the reaction between CO₂ and alkanolamines, MS thesis. Institutt for kjemisk prosessteknologi, 2013.
- 14. Yu, C.-H., C.-H. Huang, and C.-S. Tan, A review of CO₂ capture by absorption and adsorption. *Aerosol Air Qual. Res*, 2012, **12**(5):745–769.
- 15. Kohl, A.L. and R. Nielsen, Gas Purification, Gulf Professional Publishing, 1997.
- 16. Yang, J., et al., CO₂ capture by dry alkanolamines and an efficient microwave regeneration process. *Journal of Materials Chemistry A*, 2015, **3**(12):6440–6446.
- Strelzoff, S. and W.W. Shen, Separation of carbon dioxide from ammonia. Google Patents, 1957.
- Laroche, C.R. and J.R. Dowdle, Process for the removal of acid gases from gaseous mixtures using an aqueous solution of 2-dimethylamino-2-hydroxymethyl-1, 3-propanediol. Google Patents, 2016.
- Songolzadeh, M., et al., Carbon dioxide separation from flue gases: a technological review emphasizing reduction in greenhouse gas emissions. *Scientific World Journal*, 2014. 2014: Article ID 828131.
- 20. Stylianou, K.C. and W.L. Queen, Recent advances in carbon capture with metal—organic frameworks. *Chimia International Journal for Chemistry*, 2015, **69**(5):274–283.
- 21. Liu, Y., Z.U. Wang, and H.C. Zhou, Recent advances in carbon dioxide capture with metal–organic frameworks. *Greenhouse Gases: Science and Technology*, 2012, **2**(4):239–259.
- Mohanned, M., et al., Review of Recent Developments in CO₂ Capture Using Solid Materials: Metal Organic Frameworks (MOFs), Greenhouse Gases Bernardo Llamas, IntechOpen, 2016. DOI: 10.5772/62275.
- D'Alessandro, D.M., B. Smit, and J.R. Long, Carbon dioxide capture: prospects for new materials. Angewandte Chemie International Edition, 2010, 49(35):6058–6082.
- 24. Songolzadeh, M., M.T. Ravanchi, and M. Soleimani, Carbon dioxide capture and storage: a general review on adsorbents. *World Academy of Science, Engineering and Technology*, 2012, **70**:225–232.
- Kearley, G.J. and V.K. Peterson, Neutron Applications in Materials for Energy, Springer, 2015.
- 26. Li, H., et al., Establishing microporosity in open metal—organic frameworks: gas sorption isotherms for Zn(BDC) (BDC= 1, 4-benzenedicarboxylate). *Journal of the American Chemical Society*, 1998, **120**(33):8571–8572.
- 27. Li, H., et al., Design and synthesis of an exceptionally stable and highly porous metalorganic framework. *Nature*, 1999, **402**(6759):276–279.
- Janiak, C., Demonstration of permanent porosity in flexible and guest-responsive organic zeolite analogs (now called MOFs). *Chemical Communications*, 2013, 49(62):6933–6937.
- 29. Gallagher, A.T., et al., Dioxygen binding at a four-coordinate cobaltous porphyrin site in a metal–organic framework: structural, EPR, and O₂ adsorption analysis. *Inorganic Chemistry Frontiers*, 2016, **3**(4):536–540.

30. Farha, O.K., et al., Metal–organic framework materials with ultrahigh surface areas: is the sky the limit? *Journal of the American Chemical Society*, 2012, **134**(36):15016–15021.

- 31. Farrusseng, D., Metal–Organic Frameworks: Applications from Catalysis to Gas Storage, John Wiley & Sons, 2011.
- 32. Czaja, A.U., N. Trukhan, and U. Müller, Industrial applications of metal–organic frameworks. *Chemical Society Reviews*, 2009, **38**(5):1284–1293.
- 33. Lu, W., et al., Porous polymer networks: synthesis, porosity, and applications in gas storage/separation. *Chemistry of Materials*, 2010, **22**(21):5964–5972.
- 34. Schröder, M., Functional Metal—Organic Frameworks: Gas Storage, Separation and Catalysis, vol. 293, Springer, 2010.
- 35. Mueller, U., et al., Metal–organic frameworks—prospective industrial applications. *Journal of Materials Chemistry*, 2006, **16**(7):626–636.
- Li, J.-R., R.J. Kuppler, and H.-C. Zhou, Selective gas adsorption and separation in metal–organic frameworks. *Chemical Society Reviews*, 2009, 38(5):1477–1504.
- 37. Chang, Z., et al., Microporous organic polymers for gas storage and separation applications. *Physical Chemistry Chemical Physics*, 2013, **15**(15):5430–5442.
- 38. Lee, J., et al., Metal–organic framework materials as catalysts. *Chemical Society Reviews*, 2009, **38**(5):1450–1459.
- 39. Gascon, J., et al., Metal organic framework catalysis: Quo vadis? *ACS Catalysis*, 2013, 4(2):361–378.
- 40. Kuppler, R.J., et al., Potential applications of metal–organic frameworks. *Coordination Chemistry Reviews*, 2009, **253**(23):3042–3066.
- 41. Liu, J., et al., Progress in adsorption-based CO₂ capture by metal–organic frameworks. *Chemical Society Reviews*, 2012, **41**(6):2308–2322.
- Sumida, K., et al., Synthesis and hydrogen storage properties of Be₁₂(OH)₁₂(1,3,5-benzenetribenzoate)₄. *Journal of the American Chemical Society*, 2009, 131(42): 15120–15121.
- 43. Peng, Y., et al., Methane storage in metal–organic frameworks: current records, surprise findings, and challenges. *Journal of the American Chemical Society*, 2013, **135**(32):11887–11894.
- 44. Furukawa, H., et al., Ultrahigh porosity in metal–organic frameworks. *Science*, 2010, **329**(5990):424–428.
- 45. Tranchemontagne, D.J., J.R. Hunt, and O.M. Yaghi, Room temperature synthesis of metal–organic frameworks: MOF-5, MOF-74, MOF-177, MOF-199, and IRMOF-0. *Tetrahedron*, 2008, **64**(36):8553–8557.
- Bae, Y.J., et al., Transparent metal–organic framework/polymer mixed matrix membranes as water vapor barriers. ACS Applied Materials and Interfaces, 2016, 8(16):10098–10103.
- 47. Sanchez-Sanchez, M., et al., Synthesis of metal–organic frameworks in water at room temperature: salts as linker sources. *Green Chemistry*, 2015, **17**(3):1500–1509.
- 48. Khan, N.A. and S.H. Jhung, Synthesis of metal—organic frameworks (MOFs) with microwave or ultrasound: rapid reaction, phase-selectivity, and size reduction. *Coordination Chemistry Reviews*, 2015, **285**:11–23.
- Friscic, T., Supramolecular concepts and new techniques in mechanochemistry: cocrystals, cages, rotaxanes, open metal—organic frameworks. *Chemical Society Reviews*, 2012, 41(9):3493–3510.

- 50. Crawford, D., et al., Synthesis by extrusion: continuous, large-scale preparation of MOFs using little or no solvent. *Chemical Science*, 2015, **6**(3):1645–1649.
- 51. Rubio-Martinez, M., et al., Versatile, high quality and scalable continuous flow production of metal–organic frameworks. *Scientific Reports*, 2014, **4**:5443.
- 52. Bayliss, P.A., et al., Synthesis of metal–organic frameworks by continuous flow. *Green Chemistry*, 2014, **16**(8):3796–3802.
- 53. Carné-Sánchez, A., et al., A spray-drying strategy for synthesis of nanoscale metalorganic frameworks and their assembly into hollow superstructures. *Nat Chem*, 2013, **5**(3):203–211.
- 54. Jasuja, H., Developing design criteria and scale up methods for water-stable metalorganic frameworks for adsorption applications. *DTIC Document*, 2014.
- 55. Peplow, M., The hole story. *Nature*, 2015, **520**(7546):148–150.
- 56. Peplow, M., Materials science: the hole story. *Nature, News Feature*, 2015, **520**(7546):148–150.
- 57. Furukawa, H., BASF develops method for industrial-scale MOF synthesis: trials underway in natural gas vehicle tanks. *Green Car Congress*, 2010.
- Dhakshinamoorthy, A., M. Alvaro, and H. Garcia, Commercial metal-organic frameworks as heterogeneous catalysts. *Chemical Communications*, 2012, 48(92):11275–11288.
- 59. Parkes, M.V., et al., Screening metal–organic frameworks for selective noble gas adsorption in air: effect of pore size and framework topology. *Physical Chemistry Chemical Physics*, 2013, **15**(23):9093–9106.
- Deniz, E., et al., A combined computational and experimental study of high pressure and supercritical CO₂ adsorption on Basolite MOFs. *Microporous and Mesoporous Materials*, 2013, 175:34–42.
- 61. Yilmaz, B., N. Trukhan, and U. MüLLER, Industrial outlook on zeolites and metal organic frameworks. *Chinese Journal of Catalysis*, 2012, **33**(1):3–10.
- 62. Mason, J.A., et al., Evaluating metal–organic frameworks for post-combustion carbon dioxide capture via temperature swing adsorption. *Energy & Environmental Science*, 2011, **4**(8):3030–3040.
- 63. Queen, W.L., et al., Comprehensive study of carbon dioxide adsorption in the metalorganic frameworks M_2 (dobdc) (M = Mg, Mn, Fe, Co, Ni, Cu, Zn). *Chemical Science*, 2014, 5(12):4569–4581.
- 64. Hoeven, M.V. (ed.), CO₂ Emissions from Fuel Combustion, IEA Publications, Paris Cedex, France, 2012.
- Singh, S., How long will fossil fuels last? Business Standard Ltd, India. 2015. Available from: http://www.business-standard.com/article/punditry/how-long-will-fossil-fuels-last-115092201397_1.html
- Clemente, J. How much oil does the world have left? 2015. Available from: http:// www.forbes.com/sites/judeclemente/2015/06/25/how-much-oil-does-the-world-have-left/#13416d395dc5.
- 67. World Energy Day 2014: How much oil is left and how long will it last? International Bussiness Times, UK, 2014.
- 68. Xu, X., et al., Separation of CO₂ from power plant flue gas using a novel CO₂ 'molecular basket' adsorbent. *ACS Division of Fuel Chemistry, Preprints*, 2003, **48**(1):162–163.
- 69. Goldthorpe, S. (ed.), Study on carbon capture and storage in natural gas-based power plants, Beijing, China, 2014.

- 70. CO₂ Capture Technologies, Global CCS Institute, Canberra, Australia, 2011, 16.
- 71. Feron, P., Absorption-Based Post-Combustion Capture of Carbon Dioxide, Elsevier Science, 2016.
- 72. Zevenhoven, R. and P. Kilpinen, *Control of Pollutants in Flue Gases and Fuel Gases*, Helsinki University of Technology Espoo, Finland, 2001.
- 73. Granite, E.J. and H.W. Pennline, Photochemical removal of mercury from flue gas. *Industrial & Engineering Chemistry Research*, 2002, **41**(22):5470–5476.
- 74. Yang, S.-I., et al., Hydrogen separation by multi-bed pressure swing adsorption of synthesis gas. *Adsorption*, 2008, **14**(4):583–590.
- Cormos, C.-C., et al., Innovative concepts for hydrogen production processes based on coal gasification with capture. *International Journal of Hydrogen Energy*, 2008, 33(4):1286–1294.
- 76. J. Yan, Handbook of Clean Energy Systems, 6 Volume Set, Wiley, 2015.
- 77. Brimblecombe, P., *Air Composition and Chemistry*, Cambridge University Press, 1996.
- Rao, A.B. and E.S. Rubin, A technical, economic, and environmental assessment of amine-based CO₂ capture technology for power plant greenhouse gas control. *Environmental Science & Technology*, 2002, 36(20):4467–4475.
- 79. Lu, W., et al., Building multiple adsorption sites in porous polymer networks for carbon capture applications. *Energy & Environmental Science*, 2013, **6**(12):3559–3564.
- 80. Leung, D.Y., G. Caramanna, and M.M. Maroto-Valer, An overview of current status of carbon dioxide capture and storage technologies. *Renewable and Sustainable Energy Reviews*, 2014, **39**:426–443.
- 81. Yang, H. and J.-R. Li, Metal–organic frameworks (MOFs) for CO₂ capture, in *Porous Materials for Carbon Dioxide Capture*, Springer, 2014, 79–113.
- 82. Bloch, E.D., et al., Selective binding of O₂ over N₂ in a redox–active metal–organic framework with open iron(II) coordination sites. *Journal of the American Chemical Society*, 2011, **133**(37):14814–14822.
- Lee, J.S., et al., Understanding small-molecule interactions in metal-organic frameworks: coupling experiment with theory. *Advanced Materials*, 2015, 27(38):5785–5796.
- 84. Sumida, K., et al., Carbon dioxide capture in metal—organic frameworks. *Chemical Reviews*, 2011, **112**(2):724–781.
- 85. Millward, A.R. and O.M. Yaghi, Metal—organic frameworks with exceptionally high capacity for storage of carbon dioxide at room temperature. *Journal of the American Chemical Society*, 2005, **127**(51):17998–17999.
- 86. Myers, A. and J.M. Prausnitz, Thermodynamics of mixed-gas adsorption. *AIChE Journal*, 1965, **11**(1):121–127.
- Mason, J.A., et al., Application of a high-throughput analyzer in evaluating solid adsorbents for post-combustion carbon capture via multicomponent adsorption of CO₂, N₂, and H₂O. *Journal of the American Chemical Society*, 2015, 137(14):4787–4803.
- 88. Herm, Z.R., et al., Metal—organic frameworks as adsorbents for hydrogen purification and precombustion carbon dioxide capture. *Journal of the American Chemical Society*, 2011, **133**(15):5664–5667.
- Krishna, R. and J.M. van Baten, In silico screening of metal–organic frameworks in separation applications. *Physical Chemistry Chemical Physics*, 2011, 13(22):10593–10616.

- 90. Krishna, R. and J.M. van Baten, Investigating the potential of MgMOF-74 membranes for CO₂ capture. *Journal of Membrane Science*, 2011, **377**(1):249–260.
- 91. Krishna, R. and J.M. van Baten, Maxwell–Stefan modeling of slowing-down effects in mixed gas permeation across porous membranes. *Journal of Membrane Science*, 2011, **383**(1):289–300.
- 92. Cessford, N.F., N.A. Seaton, and T. Düren, Evaluation of ideal adsorbed solution theory as a tool for the design of metal–organic framework materials. *Industrial & Engineering Chemistry Research*, 2012, **51**(13):4911–4921.
- 93. Queen, W.L., et al., Hydrogen adsorption in the metal–organic frameworks Fe₂ (dobdc) and Fe₂ (O₂)(dobdc). *Dalton Transactions*, 2012, **41**(14):4180–4187.
- 94. Ruthven, D.M., Fundamentals of adsorption equilibrium and kinetics in microporous solids, in *Adsorption and Diffusion*, Springer, 2006, 1–43.
- 95. Carrington, K.R., et al., Recommended best practices for the characterization of storage properties of hydrogen storage materials. U.S. Department of Energy—Office of Energy Efficiency & Renewable Energy, 2012.
- 96. Farrusseng, D., et al., Heats of adsorption for seven gases in three metal–organic frameworks: systematic comparison of experiment and simulation. *Langmuir*, 2009, **25**(13):7383–7388.
- 97. Wang, Q.M., et al., Metallo-organic molecular sieve for gas separation and purification. *Microporous and Mesoporous Materials*, 2002, **55**(2):217–230.
- 98. Britt, D., et al., Highly efficient separation of carbon dioxide by a metal–organic framework replete with open metal sites. *Proceedings of the National Academy of Sciences*, 2009, **106**(49):20637–20640.
- 99. Caskey, S.R., A.G. Wong-Foy, and A.J. Matzger, Dramatic tuning of carbon dioxide uptake via metal substitution in a coordination polymer with cylindrical pores. *Journal of the American Chemical Society*, 2008, **130**(33):10870–10871.
- Hamon, L., et al., Co-adsorption and separation of CO₂–CH₄ mixtures in the highly flexible MIL-53(Cr) MOF. *Journal of the American Chemical Society*, 2009, 131(47):17490–17499.
- 101. Ferey, G., et al., Hydrogen adsorption in the nanoporous metal-benzenedicarboxylate M(OH)(O₂C-C₆H₄-CO₂) (M = Al3+, Cr3+), MIL-53. *Chemical Communications*, 2003(24):2976–2977.
- 102. Mollmer, J., et al., Pure and mixed gas adsorption of CH₄ and N₂ on the metal–organic framework Basolite® A100 and a novel copper-based 1,2,4-triazolyl isophthalate MOF. *Journal of Materials Chemistry*, 2012, 22(20):10274–10286.
- 103. Xu, J., et al., Fast and highly efficient SO₂ capture by TMG immobilized on hierarchical micro-meso-macroporous AlPO-5/cordierite honeycomb ceramic materials. Chemical Communications, 2016, 52(38):6367–6370.
- 104. Plaza, M.G., et al., Experimental and simulation study of adsorption in postcombustion conditions using a microporous biochar. 1. CO₂ and N₂ adsorption. *Industrial & Engineering Chemistry Research*, 2016, 55(11):3097–3112.
- 105. Dietzel, P.D., V. Besikiotis, and R. Blom, Application of metal—organic frameworks with coordinatively unsaturated metal sites in storage and separation of methane and carbon dioxide. *Journal of Materials Chemistry*, 2009, 19(39):7362–7370.
- 106. Kizzie, A.C., A.G. Wong-Foy, and A.J. Matzger, Effect of humidity on the performance of microporous coordination polymers as adsorbents for CO₂ capture. *Langmuir*, 2011, 27(10):6368–6373.

107. Bhatt, P.M., et al., A fine-tuned fluorinated MOF addresses the needs for trace CO₂ removal and air capture using physisorption. *Journal of the American Chemical Society*, 2016, 138(29):9301–9307.

- 108. Fracaroli, A.M., et al., Metal–organic frameworks with precisely designed interior for carbon dioxide capture in the presence of water. *Journal of the American Chemical Society*, 2014, 136(25):8863–8866.
- 109. Coelho, J.A., et al., Stability of an al-fumarate MOF and its potential for CO₂ capture from wet stream. *Industrial & Engineering Chemistry Research*, 2016, **55**(7):2134–2143.
- Nakagawa, K., et al., Enhanced selectivity of CO₂ from a ternary gas mixture in an interdigitated porous framework. *Chemical Communications*, 2010, 46(24):4258–4260.
- 111. Mason, J., et al., Evaluating metal—organic frameworks for post-combustion carbon dioxide capture via temperature swing adsorption. *Energy & Environmental Science*, 2011, 4:3030; (b) Perry, J.J., J.A. Perman, and M.J. Zaworotko. Design and synthesis of metal—organic frameworks using metal—organic polyhedra as supermolecular building blocks. *Chemical Society Reviews*, 2009, 38:1400.
- 112. Dietzel, P.D., et al., An in situ high-temperature single-crystal investigation of a dehydrated metal–organic framework compound and field-induced magnetization of one-dimensional metal–oxygen chains. *Angewandte Chemie*, 2005, 117(39):6512–6516.
- 113. Dietzel, P.D.C., et al., Adsorption properties and structure of CO₂ adsorbed on open coordination sites of metal–organic framework Ni₂(dhtp) from gas adsorption, IR spectroscopy and X-ray diffraction. *Chemical Communications*, 2008 (41):5125–5127.
- Llewellyn, P.L., et al., High Uptakes of CO₂ and CH₄ in mesoporous metal organic frameworks MIL-100 and MIL-101. *Langmuir*, 2008, 24(14):7245–7250.
- 115. Valenzano, L., et al., Structure–activity relationships of simple molecules adsorbed on CPO-27-Ni metal–organic framework: in situ experiments vs. theory. *Catalysis Today*, 2012, **182**(1):67–79.
- Kontos, A.G., et al., CO₂ captured in zeolitic imidazolate frameworks: raman spectroscopic analysis of uptake and host–guest interactions. *ChemSusChem*, 2014, 7(6):1696–1702.
- 117. McDonald, T.M., et al., Cooperative insertion of CO₂ in diamine-appended metalorganic frameworks. *Nature*, 2015, **519**(7543):303–308.
- 118. Kong, X., et al., CO₂ dynamics in a metal-organic framework with open metal sites. *Journal of the American Chemical Society*, 2012, **134**(35):14341–14344.
- 119. Lin, L.C., et al., Understanding CO₂ dynamics in metal–organic frameworks with open metal sites. *Angewandte Chemie International Edition*, 2013, **52**(16):4410–4413.
- Drisdell, W.S., et al., Probing adsorption interactions in metal-organic frameworks using X-ray spectroscopy. *Journal of the American Chemical Society*, 2013, 135(48):18183–18190.
- 121. Dietzel, P.D., et al., Interaction of hydrogen with accessible metal sites in the metalorganic frameworks M 2 (dhtp)(CPO-27-M; M = Ni, Co, Mg). *Chemical Communications*, 2010, **46**(27):4962–4964.
- 122. Yan, Y., et al., Metal-organic polyhedral frameworks: high H₂ adsorption capacities and neutron powder diffraction studies. *Journal of the American Chemical Society*, 2010, 132(12):4092–4094.
- 123. Yazaydın, A.O., et al., Enhanced CO₂ adsorption in metal–organic frameworks via occupation of open-metal sites by coordinated water molecules. *Chemistry of Materials*, 2009, 21(8):1425–1430.

- 124. Sumida, K., et al., Hydrogen storage properties and neutron scattering studies of Mg 2 (dobdc)—a metal–organic framework with open Mg 2+ adsorption sites. Chemical Communications, 2011, 47(4):1157–1159.
- 125. Salles, F., et al., Adsorption and diffusion of H₂ in the MOF type systems MIL-47 (V) and MIL-53 (Cr): a combination of microcalorimetry and QENS experiments with molecular simulations. *Journal of Physical Chemistry C*, 2009, 113(18):7802–7812.
- 126. Chapman, K.W., G.J. Halder, and P.J. Chupas, Guest-dependent high pressure phenomena in a nanoporous metal—organic framework material. *Journal of the American Chemical Society*, 2008, **130**(32):10524–10526.
- Chapman, K.W., G.J. Halder, and P.J. Chupas, Guest-dependent high pressure phenomena in a nanoporous metal—organic framework material. *Journal of the American Chemical Society*, 2008, 130(32):10524–10526.
- 128. Xiao, D.J., et al., Oxidation of ethane to ethanol by N₂O in a metal-organic framework with coordinatively unsaturated iron(II) sites. *Nature Chemistry*, 2014, **6**(7):590–595.
- 129. Bloch, E.D., et al., Reversible CO binding enables tunable CO/H₂ and CO/N₂ separations in metal–organic frameworks with exposed divalent metal cations. *Journal of the American Chemical Society*, 2014, **136**(30):10752–10761.
- 130. Wu, H., et al., Adsorption sites and binding nature of CO₂ in prototypical metal–organic frameworks: a combined neutron diffraction and first-principles study. *Journal of Physical Chemistry Letters*, 2010, **1**(13):1946–1951.
- 131. Serre, C., et al., An explanation for the very large breathing effect of a metal–organic framework during CO₂ adsorption. *Advanced Materials*, 2007, **19**(17):2246–2251.
- 132. Furukawa, H., et al., Water adsorption in porous metal–organic frameworks and related materials. *Journal of the American Chemical Society*, 2014, **136**(11):4369–4381.
- 133. Bloch, E.D., et al., Hydrogen storage and selective, reversible O₂ adsorption in a metal–organic framework with open chromium(II) sites. *Angewandte Chemie International Edition*, 2016, **55**(30):8605–8609.
- 134. Kitaura, R., et al., Formation of a one-dimensional array of oxygen in a microporous metal–organic solid. *Science*, 2002, **298**(5602):2358–2361.
- 135. Bloch, E.D., et al., Gradual release of strongly bound nitric oxide from Fe₂(NO)₂ (dobdc). *Journal of the American Chemical Society*, 2015, **137**(10):3466–3469.
- 136. Gygi, D., et al., Hydrogen storage in the expanded pore metal–organic frameworks M₂(dobpdc) (M = Mg, Mn, Fe, Co, Ni, Zn). *Chemistry of Materials*, 2016, **28**(4):1128–1138.
- 137. Queen, W.L., et al., Hydrogen adsorption in the metal–organic frameworks Fe₂(dobdc) and Fe₂(O₂)(dobdc). *Dalton Transactions*, 2012, **41**(14):4180–4187.
- 138. Bourrelly, S., et al., Different adsorption behaviors of methane and carbon dioxide in the isotypic nanoporous metal terephthalates MIL-53 and MIL-47. *Journal of the American Chemical Society*, 2005, **127**(39):13519–13521.
- Loiseau, T., et al., A rationale for the large breathing of the porous aluminum terephthalate (MIL-53) upon hydration. *Chemistry—A European Journal*, 2004, 10(6): 1373–1382.
- 140. Llewellyn, P.L., et al., How hydration drastically improves adsorption selectivity for CO₂ over CH₄ in the flexible chromium terephthalate MIL-53. *Angewandte Chemie*, 2006, 118(46):7915–7918.

141. Plonka, A.M., et al., Mechanism of carbon dioxide adsorption in a highly selective coordination network supported by direct structural evidence. *Angewandte Chemie International Edition*, 2013, **52**(6):1692–1695.

- 142. Kwon, H.T. and H.-K. Jeong, In situ synthesis of thin zeolitic–imidazolate framework ZIF-8 membranes exhibiting exceptionally high propylene/propane separation. *Journal of the American Chemical Society*, 2013, **135**(29):10763–10768.
- 143. Nijem, N., et al., Molecular hydrogen "pairing" interaction in a metal organic framework system with unsaturated metal centers (MOF-74). *Journal of the American Chemical Society*, 2010, 132(42):14834–14848.
- 144. Yao, Y., et al., Analyzing the frequency shift of physiadsorbed CO₂ in metal organic framework materials. *Physical Review B*, 2012, **85**(6):064302.
- 145. Schloss, J.M., Infrared spectroscopy of trapped gases in metal–organic frameworks. Oberlin College Honors Theses, 2011.
- 146. Valenzano, L., et al., Computational and experimental studies on the adsorption of CO, N₂, and CO₂ on Mg-MOF-74. *Journal of Physical Chemistry C*, 2010, 114(25):11185–11191.
- 147. Zhang, Z., Z. Li, and J. Li, Computational study of adsorption and separation of CO₂, CH₄, and N₂ by an rht-type metal–organic framework. *Langmuir*, 2012, 28(33): 12122–12133.
- 148. Li, B., et al., Enhanced binding affinity, remarkable selectivity, and high capacity of CO₂ by dual functionalization of a rht-type metal—organic framework. *Angewandte Chemie International Edition*, 2012, **51**(6):1412–1415.
- 149. Li, B., et al., Enhanced binding affinity, remarkable selectivity, and high capacity of CO₂ by dual functionalization of a rht-type metal—organic framework. *Angewandte Chemie International Edition*, 2012, **51**(6):1412–1415.
- Chen, Y., et al., In situ spectroscopy studies of CO₂ adsorption in a dually functionalized microporous metal–organic framework. *Journal of Materials Chemistry A*, 2015, 3(9):4945–4953.
- 151. Demessence, A., et al., Strong CO₂ binding in a water-stable, triazolate-bridged metal-organic framework functionalized with ethylenediamine. *Journal of the American Chemical Society*, 2009, 131(25):8784–8786.
- 152. McDonald, T.M., et al., Enhanced carbon dioxide capture upon incorporation of *N*,*N'*-dimethylethylenediamine in the metal–organic framework CuBTTri. *Chemical Science*, 2011, **2**(10):2022–2028.
- 153. Huck, J.M., et al., Evaluating different classes of porous materials for carbon capture. *Energy & Environmental Science*, 2014, **7**(12):4132–4146.
- 154. Greenaway, A., et al., In situ synchrotron IR microspectroscopy of CO₂ adsorption on single crystals of the functionalized MOF Sc₂(BDC-NH₂)₃. Angewandte Chemie International Edition, 2014, 53(49):13483–13487.
- 155. Yang, S., et al., Selectivity and direct visualization of carbon dioxide and sulfur dioxide in a decorated porous host. *Nature Chemistry*, 2012, **4**(11):887–894.
- 156. Stallmach, F., et al., NMR studies on the diffusion of hydrocarbons on the metalorganic framework material MOF-5. *Angewandte Chemie International Edition*, 2006, **45**(13):2123–2126.
- 157. Gassensmith, J.J., et al., Strong and reversible binding of carbon dioxide in a green metal–organic framework. *Journal of the American Chemical Society*, 2011, 133(39):15312–15315.

- 158. Lopez, M.G., P. Canepa, and T. Thonhauser, NMR study of small molecule adsorption in MOF-74-Mg. *Journal of Chemical Physics*, 2013, **138**(15):154704.
- 159. Lucier, B.E.G., et al., Grasping hydrogen adsorption and dynamics in metal—organic frameworks using 2H solid-state NMR. *Chemical Communications*, 2016, **52**(48): 7541–7544.
- 160. Horike, S., et al., Motion of methanol adsorbed in porous coordination polymer with paramagnetic metal ions. *Chemical Communications*, 2004(19):2152–2153.
- 161. Sutrisno, A., et al., Characterization of Zn-containing metal–organic frameworks by solid-state 67Zn NMR spectroscopy and computational modeling. *Chemistry—A European Journal*, 2012, **18**(39):12251–12259.
- 162. Peterson, G.W., et al., Ammonia vapor removal by Cu(3)(BTC)(2) and its characterization by MAS NMR. *Journal of Physical Chemistry C*, 2009, 113(31): 13906–13917.
- Stallmach, F., et al., NMR studies on the diffusion of hydrocarbons on the metalorganic framework material MOF-5. *Angewandte Chemie International Edition*, 2006, 45(13):2123–2126.
- 164. Wehring, M., et al., Self-diffusion studies in CuBTC by PFG NMR and MD simulations. *Journal of Physical Chemistry C*, 2010, **114**(23):10527–10534.
- Hoffmann, H.C., et al., Solid-state NMR spectroscopy of metal-organic framework compounds (MOFs). *Materials*, 2012, 5(12):2537–2572.
- 166. Klein, N., et al., Monitoring adsorption-induced switching by 129Xe NMR spectroscopy in a new metal—organic framework Ni2(2,6-ndc)2(dabco). *Physical Chemistry Chemical Physics*, 2010, 12(37):11778–11784.
- 167. Hoffmann, H., et al., Solid-State NMR spectroscopy of metal–organic framework compounds (MOFs). *Materials*, 2012, **5**(12):2537–2572.
- 168. Rosenbach, N., et al., Quasi–elastic neutron scattering and molecular dynamics study of methane diffusion in metal organic frameworks MIL-47(V) and MIL-53(Cr). *Angewandte Chemie International Edition*, 2008, **47**(35):6611–6615.
- 169. Salles, F., et al., Experimental evidence supported by simulations of a very high H₂ diffusion in metal organic framework materials. *Physical Review Letters*, 2008, 100(24):245901.
- 170. Salles, F., et al., Self and transport diffusivity of CO₂ in the metal–organic framework MIL-47(V) explored by quasi-elastic neutron scattering experiments and molecular dynamics simulations. *ACS Nano*, 2010, **4**(1):143–152.
- 171. Vieira Soares, C., et al., Adsorption of small molecules in the porous zirconium-based metal organic framework MIL-140A (Zr): a joint computational-experimental approach. *Journal of Physical Chemistry C*, 2016, **120**(13):7192–7200.
- 172. Prakash, M., et al., Diffusion of H₂, CO₂, and their mixtures in the porous zirconium based metal–organic framework MIL-140A(Zr): combination of quasi-elastic neutron scattering measurements and molecular dynamics simulations. *Journal of Physical Chemistry C*, 2015, **119**(42):23978–23989.
- 173. Tan, K., et al., Competitive coadsorption of CO₂ with H₂O, NH₃, SO₂, NO, NO₂, N₂, O₂, and CH₄ in M-MOF-74 (M = Mg, Co, Ni): the role of hydrogen bonding. *Chemistry of Materials*, 2015, **27**(6):2203–2217.
- 174. Yang, S., et al., Selectivity and direct visualization of carbon dioxide and sulfur dioxide in a decorated porous host. *Nature Chemistry*, 2012, **4**(11):887–894.

175. Wang, Q., et al., Finely tuning MOFs towards high-performance post-combustion CO₂ capture materials. *Chemical Communications*, 2016, **52**(3):443–452.

- 176. Poloni, R., et al., Understanding trends in CO₂ adsorption in metal–organic frameworks with open-metal sites. *Journal of Physical Chemistry Letters*, 2014, **5**(5):861–865.
- 177. Vaidhyanathan, R., et al., An amine-functionalized metal organic framework for preferential CO₂ adsorption at low pressures. *Chemical Communications*, 2009(35):5230–5232.
- 178. Couck, S., et al., An amine-functionalized MIL-53 metal—organic framework with large separation power for CO₂ and CH₄. *Journal of the American Chemical Society*, 2009, **131**(18):6326–6327.
- Arstad, B., et al., Amine functionalised metal organic frameworks (MOFs) as adsorbents for carbon dioxide. *Adsorption*, 2008, 14(6):755–762.
- 180. Gascon, J., et al., Amino-based metal-organic frameworks as stable, highly active basic catalysts. *Journal of Catalysis*, 2009, **261**(1):75–87.
- 181. Landa, H.O.R., D. Flockerzi, and A. Seidel-Morgenstern, A method for efficiently solving the IAST equations with an application to adsorber dynamics. *AIChE Journal*, 2013, **59**(4):1263–1277.
- 182. Keskin, S., T.M. van Heest, and D.S. Sholl, Can metal—organic framework materials play a useful role in large-scale carbon dioxide separations? *ChemSusChem*, 2010, **3**(8):879–891.
- 183. Bae, Y.S. and R.Q. Snurr, Development and evaluation of porous materials for carbon dioxide separation and capture. *Angewandte Chemie International Edition*, 2011, **50**(49):11586–11596.
- 184. Lin, Y., et al., Enhanced selective CO₂ adsorption on polyamine/MIL-101(Cr) composites. *Journal of Materials Chemistry A*, 2014, **2**(35):14658–14665.
- 185. McDonald, T.M., et al., Capture of carbon dioxide from air and flue gas in the alkylamine-appended metal—organic framework mmen-Mg2(dobpdc). *Journal of the American Chemical Society*, 2012, **134**(16):7056–7065.
- 186. Hu, Y., et al., Alkylamine-Tethered stable metal–organic framework for CO₂ capture from flue gas. *ChemSusChem*, 2014, **7**(3):734–737.
- 187. Wu, D., et al., Direct calorimetric measurement of enthalpy of adsorption of carbon dioxide on CD-MOF-2, a green metal—organic framework. *Journal of the American Chemical Society*, 2013, 135(18):6790–6793.
- 188. Li, T., et al., Systematic modulation and enhancement of CO₂: N₂ selectivity and water stability in an isoreticular series of bio-MOF-11 analogues. *Chemical Science*, 2013, 4(4):1746–1755.
- 189. Min Wang, Q., et al., Metallo-organic molecular sieve for gas separation and purification. *Microporous and Mesoporous Materials*, 2002, **55**(2):217–230.
- Choi, J.-S., et al., Metal-organic framework MOF-5 prepared by microwave heating: factors to be considered. *Microporous and Mesoporous Materials*, 2008, 116(1–3):727–731.
- 191. Zhang, Z., et al., Enhancement of CO₂ adsorption and CO₂/N₂ selectivity on ZIF-8 via postsynthetic modification. *AIChE Journal*, 2013, **59**(6):2195–2206.
- 192. Liu, Y., et al., Increasing the density of adsorbed hydrogen with coordinatively unsaturated metal centers in metal–organic frameworks. *Langmuir*, 2008, **24**(9):4772–4777.
- Shultz, A.M., et al., A catalytically active, permanently microporous MOF with metalloporphyrin struts. *Journal of the American Chemical Society*, 2009, 131(12): 4204–4205.

- 194. Rosi, N.L., et al., Rod packings and metal—organic frameworks constructed from rod-shaped secondary building units. *Journal of the American Chemical Society*, 2005, 127(5):1504–1518.
- 195. Dietzel, P.D., et al., Hydrogen adsorption in a nickel based coordination polymer with open metal sites in the cylindrical cavities of the desolvated framework. *Chemical Communications*, 2006(9):959–961.
- 196. Zhou, W., H. Wu, and T. Yildirim, Enhanced H₂ adsorption in isostructural metal—organic frameworks with open metal sites: strong dependence of the binding strength on metal ions. *Journal of the American Chemical Society*, 2008, 130(46):15268–15269.
- Dincă, M., et al., Hydrogen storage in a microporous metal-organic framework with exposed Mn2+ coordination sites. *Journal of the American Chemical Society*, 2006, 128(51):16876–16883.
- Dincă, M., et al., Observation of Cu2+–H2 interactions in a fully desolvated sodalitetype metal–organic framework. *Angewandte Chemie International Edition*, 2007, 46(9):1419–1422.
- 199. Sumida, K., et al., Hydrogen storage and carbon dioxide capture in an iron-based sodalite-type metal—organic framework (Fe-BTT) discovered via high-throughput methods. *Chemical Science*, 2010, **1**(2):184–191.
- 200. Biswas, S., et al., Fuel purification, Lewis acid and aerobic oxidation catalysis performed by a microporous Co-BTT (BTT³⁻ = 1,3,5-benzenetristetrazolate) framework having coordinatively unsaturated sites. *Journal of Materials Chemistry*, 2012, **22**(20):10200–10209.
- 201. Chui, S.S.-Y., et al., A chemically functionalizable nanoporous material $[Cu_3(TMA)_2 (H_2O)_3]_n$. Science, 1999, **283**(5405):1148–1150.
- Kramer, M., U. Schwarz, and S. Kaskel, Synthesis and properties of the metalorganic framework Mo₃(BTC)₂ (TUDMOF-1). *Journal of Materials Chemistry*, 2006, 16(23):2245–2248.
- 203. Murray, L.J., et al., Highly-Selective and reversible O₂ binding in Cr₃(1,3,5-benzenetri-carboxylate)₂. *Journal of the American Chemical Society*, 2010, **132**(23):7856–7857.
- 204. Feldblyum, J.I., et al., Reconciling the discrepancies between crystallographic porosity and guest access as exemplified by Zn-HKUST-1. *Journal of the American Chemical Society*, 2011, 133(45):18257–18263.
- Kozachuk, O., et al., Solvothermal growth of a ruthenium metal—organic framework featuring HKUST-1 structure type as thin films on oxide surfaces. *Chemical Communications*, 2011, 47(30):8509–8511.
- 206. Wade, C.R. and M. Dincă, Investigation of the synthesis, activation, and isosteric heats of CO₂ adsorption of the isostructural series of metal–organic frameworks M₃ (BTC)₂ (M = Cr, Fe, Ni, Cu, Mo, Ru). *Dalton Transactions*, 2012, 41(26):7931–7938.
- Queen, W.L., et al., Site-specific CO₂ adsorption and zero thermal expansion in an anisotropic pore network. *Journal of Physical Chemistry C*, 2011, 115(50):24915–24919.
- 208. Yu, D., et al., A combined experimental and quantum chemical study of CO₂ adsorption in the metal–organic framework CPO-27 with different metals. *Chemical Science*, 2013, **4**(9):3544–3556.
- 209. Zhang, Zhangjing, et al. "Perspective of microporous metal-organic frameworks for CO₂ capture and separation." *Energy & Environmental Science* 7.9 (2014): 2868–2899.

210. Morris, W., et al., A combined experimental–computational investigation of carbon dioxide capture in a series of isoreticular zeolitic imidazolate frameworks. *Journal of the American Chemical Society*, 2010, 132(32):11006–11008.

- 211. An, J., S.J. Geib, and N.L. Rosi, High and selective CO₂ uptake in a cobalt adeninate metal–organic framework exhibiting pyrimidine-and amino-decorated pores. *Journal of the American Chemical Society*, 2009, **132**(1):38–39.
- 212. Chen, Y. and J. Jiang, A bio-metal-organic framework for highly selective CO₂ capture: a molecular simulation study. *ChemSusChem*, 2010, **3**(8):982–988.
- 213. Vaidhyanathan, R., et al., Direct observation and quantification of CO₂ binding within an amine-functionalized nanoporous solid. *Science*, 2010, **330**(6004):650–653.
- Vaidhyanathan, R., et al., An amine-functionalized metal organic framework for preferential CO₂ adsorption at low pressures. *Chemical Communications*, 2009(35):5230–5232.
- 215. House, K.Z., et al., The energy penalty of post-combustion CO₂ capture and storage and its implications for retrofitting the US installed base. *Energy & Environmental Science*, 2009, 2(2):193–205.
- 216. Hwang, Y.K., et al., Amine grafting on coordinatively unsaturated metal centers of MOFs: consequences for catalysis and metal encapsulation. *Angewandte Chemie International Edition*, 2008, **47**(22):4144–4148.
- 217. Lee, W.R., et al., Diamine-functionalized metal-organic framework: exceptionally high CO₂ capacities from ambient air and flue gas, ultrafast CO₂ uptake rate, and adsorption mechanism. *Energy & Environmental Science*, 2014, 7(2):744–751.
- 218. Ciferno, J., et al., DOE/NETL carbon dioxide capture and storage RD&D roadmap. *National Energy Technology Laboratory*, 2010, **13**: 2011.
- 219. McDonald, T.M., et al., Capture of carbon dioxide from air and flue gas in the alkylamine-appended metal–organic framework mmen-Mg₂ (dobpdc). *Journal of the American Chemical Society*, 2012, **134**(16):7056–7065.
- 220. Song, H.-J., et al., Simplified estimation of regeneration energy of 30 wt% sodium glycinate solution for carbon dioxide absorption. *Industrial & Engineering Chemistry Research*, 2008, **47**(24): 9925–9930.
- 221. McDonald, T.M., et al., Cooperative insertion of CO₂ in diamine-appended metalorganic frameworks. *Nature*, 2015, **519**(7543): 303–308.
- 222. Wu, D., et al., Direct calorimetric measurement of enthalpy of adsorption of carbon dioxide on CD-MOF-2, a green metal–organic framework. *Journal of the American Chemical Society*, 2013, **135**(18): 6790–6793.
- Bosch, M., M. Zhang, and H.-C. Zhou, Increasing the stability of metal-organic frameworks. Advances in Chemistry, 2014, 2014: 8.
- 224. Lee, K.B. and S. Sircar, Removal and recovery of compressed CO₂ from flue gas by a novel thermal swing chemisorption process. *AIChE Journal*, 2008, **54**(9):2293–2302.
- 225. Huang, X.C., et al., Ligand-directed strategy for zeolite-type metal-organic frame-works: zinc(II) imidazolates with unusual zeolitic topologies. *Angewandte Chemie*, 2006, 118(10):1587–1589.
- Park, K.S., et al., Exceptional chemical and thermal stability of zeolitic imidazolate frameworks. *Proceedings of the National Academy of Sciences*, 2006, 103(27):10186–10191.
- 227. DeCoste, J.B., et al., Stability and degradation mechanisms of metal–organic frameworks containing the Zr₆O₄(OH)₄ secondary building unit. *Journal of Materials Chemistry A*, 2013, **1**(18):5642–5650.

- 228. Colombo, V., et al., High thermal and chemical stability in pyrazolate-bridged metal—organic frameworks with exposed metal sites. *Chemical Science*, 2011, **2**(7):1311–1319.
- 229. Clingerman, D.J., et al., Stabilization of a highly porous metal–organic framework utilizing a carborane-based linker. *Chemical Communications*, 2015, **51**(30): 6521–6523.
- Decoste, J.B., et al., Enhanced stability of Cu-BTC MOF via perfluorohexane plasmaenhanced chemical vapor deposition. *Journal of the American Chemical Society*, 2012, 134(3):1486–1489.
- 231. Yang, S.J. and C.R. Park, Preparation of highly moisture-resistant black-colored metal organic frameworks. *Advanced Materials*, 2012, **24**(29):4010–4013.
- Carné-Sánchez, A., et al., Protecting metal—organic framework crystals from hydrolytic degradation by spray-dry encapsulating them into polystyrene microspheres.
 Advanced Materials, 2015, 27(5): 869–873.
- 233. Shearer, G.C., et al., Stability vs. reactivity: understanding the adsorption properties of Ni₃ (BTP)₂ by experimental and computational methods. *Dalton Transactions*, 2013, 42(18):6450–6458.
- 234. Wu, T., et al., Enhancing the stability of metal—organic frameworks in humid air by incorporating water repellent functional groups. *Chemical Communications*, 2010, 46(33):6120–6122.
- 235. Jasuja, H., Y.-g. Huang, and K.S. Walton, Adjusting the stability of metal—organic frameworks under humid conditions by ligand functionalization. *Langmuir*, 2012, **28**(49):16874–16880.
- 236. Padial, N.M., et al., Highly hydrophobic isoreticular porous metal—organic frameworks for the capture of harmful volatile organic compounds. *Angewandte Chemie International Edition*, 2013, **52**(32):8290–8294.
- 237. Singh, M.P., et al., Influence of water on the chemistry and structure of the metal–organic framework Cu₃(btc)₂. *Journal of Physical Chemistry C*, 2016, **120**(31):17323–17333.
- 238. Lin, Y., et al., Polyethyleneimine incorporated metal–organic frameworks adsorbent for highly selective CO₂ capture. *Scientific Reports*, 2013, **3**:1859.
- 239. Zhang, Z., et al., Polymer–metal–organic frameworks (polyMOFs) as water tolerant materials for selective carbon dioxide separations. *Journal of the American Chemical Society*, 2016, **138**(3):920–925.
- 240. Lipman, T., An overview of hydrogen production and storage systems with renewable hydrogen case studies. *Clean Energy States Alliance*, 2011.
- 241. Shekhah, O., et al., A facile solvent-free synthesis route for the assembly of a highly CO₂ selective and H₂S tolerant NiSIFSIX metal—organic framework. *Chemical Communications*, 2015, **51**(71):13595–13598.
- 242. Hamon, L., et al., Comparative study of hydrogen sulfide adsorption in the MIL-53(Al, Cr, Fe), MIL-47(V), MIL-100(Cr), and MIL-101(Cr) metal–organic frameworks at room temperature. *Journal of the American Chemical Society*, 2009, **131**(25):8775–8777.
- 243. Peng, Y., et al., Simultaneously high gravimetric and volumetric methane uptake characteristics of the metal–organic framework NU-111. *Chemical Communications*, 2013, 49(29):2992–2994.
- 244. Grünker, R., et al., Dye encapsulation inside a new mesoporous metal–organic framework for multifunctional solvatochromic-response function. *Chemistry—A European Journal*, 2012, **18**(42):13299–13303.

245. Cui, P., et al., Multipoint interactions enhanced CO₂ uptake: a zeolite-like zinc-tetrazole framework with 24-nuclear zinc cages. *Journal of the American Chemical Society*, 2012, 134(46): 18892–18895.

- 246. Rowsell, J.L., et al., Hydrogen sorption in functionalized metal–organic frameworks. *Journal of the American Chemical Society*, 2004, **126**(18):5666–5667.
- Farha, O.K. and J.T. Hupp, Rational design, synthesis, purification, and activation of metal-organic framework materials. *Accounts of Chemical Research*, 2010, 43(8):1166–1175.
- 248. Han, S.S., D.-H. Jung, and J. Heo, Interpenetration of metal organic frameworks for carbon dioxide capture and hydrogen purification: good or bad? *Journal of Physical Chemistry C*, 2012, **117**(1):71–77.
- Kang, Z., et al., Mixed matrix membranes (MMMs) comprising exfoliated 2D covalent organic frameworks (COFs) for efficient CO₂ separation. *Chemistry of Materials*, 2016, 28(5):1277–1285.
- Nandi, S., et al., A single-ligand ultra-microporous MOF for precombustion CO₂ capture and hydrogen purification. Science Advances, 2015, 1(11):e1500421.
- 251. Choi, H.J., M. Dinca, and J.R. Long, Broadly hysteretic H₂ adsorption in the microporous metal–organic framework Co(1,4-benzenedipyrazolate). *Journal of the American Chemical Society*, 2008, **130**(25):7848–7850.
- 252. Krishna, R. and J.R. Long, Screening metal–organic frameworks by analysis of transient breakthrough of gas mixtures in a fixed bed adsorber. *Journal of Physical Chemistry C*, 2011, **115**(26):12941–12950.
- 253. Herm, Z.R., R. Krishna, and J.R. Long, Reprint of: CO₂/CH₄, CH₄/H₂ and CO₂/CH₄/H₂ separations at high pressures using Mg₂(dobdc). *Microporous and Mesoporous Materials*, 2012, **157**:94–100.
- 254. Wu, H., et al., Cu-TDPAT, an rht-type dual-functional metal—organic framework offering significant potential for use in H₂ and natural gas purification processes operating at high pressures. *Journal of Physical Chemistry C*, 2012, **116**(31):16609–16618.
- 255. Banu, A.-M., et al., A multiscale study of MOFs as adsorbents in H₂ PSA purification. *Industrial & Engineering Chemistry Research*, 2013, **52**(29):9946–9957.
- 256. Kakaras, E., et al., Oxyfuel boiler design in a lignite-fired power plant. *Fuel*, 2007, **86**(14):2144–2150.
- Rezvani, S., et al., Comparative assessment of sub-critical versus advanced super-critical oxyfuel fired PF boilers with CO₂ sequestration facilities. *Fuel*, 2007, 86(14):2134–2143.
- 258. Buhre, Bart JP, et al. "Oxy-fuel combustion technology for coal-fired power generation." Progress in energy and combustion science 31.4 (2005): 283–307.
- 259. Zheng, Chuguang, et al. "Fundamental and technical challenges for a compatible design scheme of oxyfuel combustion technology." Engineering 1.1 (2015): 139–149.
- 260. Hoffman, A., et al., Crystal structure and molecular stereochemistry of μ-oxo-bis[α,β,γ,δ-tetraphenylporphinatoiron(III)]. *Journal of the American Chemical Society*, 1972, **94**(10):3620–3626.
- Feng, D., et al., Construction of ultrastable porphyrin Zr metal–organic frameworks through linker elimination. *Journal of the American Chemical Society*, 2013, 135(45):17105–17110.
- Anderson, J.S., et al., A five-coordinate heme dioxygen adduct isolated within a metal-organic framework. *Journal of the American Chemical Society*, 2014, 136(47):16489–16492.

- 263. Babcock, H.D. and L. Herzberg, Fine structure of the red system of atmospheric oxygen bands. *Astrophysical Journal*, 1948, **108**:167.
- 264. Cho, J., J. Woo, and W. Nam, An "end-on" chromium (III)-superoxo complex: crystal-lographic and spectroscopic characterization and reactivity in C–H bond activation of hydrocarbons. *Journal of the American Chemical Society*, 2010, 132(17):5958–5959.
- 265. Zhang, W., et al., Redox-Active metal–organic composites for highly selective oxygen separation applications. *Advanced Materials*, 2016, **28**(18):3572–3577.
- 266. Mu, B. and K.S. Walton, Thermal analysis and heat capacity study of metal—organic frameworks. *Journal of Physical Chemistry C*, 2011, **115**(46):22748–22754.
- 267. Colon, Y.J. and R.Q. Snurr, High-throughput computational screening of metal–organic frameworks. *Chemical Society Reviews*, 2014, **43**(16):5735–5749.
- 268. Wilmer, C.E., et al., Large-scale screening of hypothetical metal–organic frameworks. *Nature Chemistry*, 2012, **4**(2):83–89.